Assessing the Impact of Climate Change on Intensity-Duration-Frequency (IDF) Curves in Manitoba

by

Tultul Saha

A Thesis submitted to the Faculty of Graduate Studies of

The University of Manitoba

in partial fulfillment of the requirements of the degree of

MASTER OF SCIENCE

Department of Civil Engineering

University of Manitoba

Winnipeg

Abstract

Global climate models predict changes in precipitation patterns in many areas of the world. Extreme precipitation in particular is poorly represented in climate models and there are significant difficulties involved in assessing the frequency and severity of future extreme precipitation events. In this study, several methods have been reviewed and compared for estimating projected changes in Intensity-Duration-Frequency (IDF) curves, commonly used in urban hydrology. A theoretical approach based on geostatistical considerations is employed to derive reasonable areal-reduction factors that make it possible to compare gridded model data with observations.

The mean value method and QQ-mapping have been used to remove biases from modeled data. A simple scaling model has been developed to construct IDF curves using the bias-corrected modeled data for the control and future climate. To investigate uncertainties in predicted changes, different simulations from the North American Regional Climate Change Assessment Program (NARCCAP) have been analyzed.

Acknowledgements

First and foremost, all praises go to God for the strengths and His blessings in completing this thesis. Special appreciation goes to my supervisor, Dr. Peter Rasmussen, for his continuous guidance and constant support. It would be impossible to finish this thesis without his guidance and help. He is not only my supervisor but also like my guardian in Winnipeg. He is not only very friendly but also inspirational. His encouragement and inspiration helped me to complete this research successfully. I am deeply indebted to my supervisor whose help, simulating suggestions, knowledge and experience helped me in all the times of study and analysis in the pre and post research period.

I would like to thank Manitoba Hydro and the Natural Sciences and Engineering Research Council of Canada (NSERC) for their financial contribution which enabled me to undertake a good proportion of my research and to successfully complete my studies.

Sincere thanks to Hassan, Reza, Andrea, and others with whom I have worked closely over the years for their kindness and moral support during studies. Thanks for the friendship and memories.

I am not forgetting my loving husband, Sabyasachi Gupta, who helped me during the final stage of M.Sc and his support is greatly appreciated. I would like to thank my beloved parents for all their love and encouragement. Their continuous mental support has helped me to complete this master's program. Last but not least, I would like to thank my parents in law who always encouraged me in my studies. Thank you all.

To my parents Radha Rani Saha and Dulal Chandra Saha and my husband

Sabyasachi Gupta

Contents

Abstract **i**

Acknowledgements **ii**

1 Introduction **1**

1.1 Background 1

1.2 Objectives 13

2 Study area and Data **15**

2.1 Station data 15

2.2 Canadian Regional Climate Model data 17

2.3 The North American Regional Climate Change Assessment Program (NARCCAP) 19

3 Areal Reduction Factor **21**

3.1 Analytical derivation of Areal Reduction Factors 22

3.1.1 Parent distribution of point rainfall 22

3.1.2 Areal averaging of point rainfall 24

3.1.3 Estimation of variance reduction factor 26

3.1.4 Parent distribution of areal average rainfall 29

3.1.5 Distribution of maximum annual point and areal precipitation 30

3.1.6 An example application 32

3.1.7 Estimation of the coefficient of variation of maximum annual areal rainfall 34

3.1.8 Estimation of Areal Reduction Factor 37

4 IDF curves at the grid box scale 40

4.1 Estimation of maximum annual rainfalls at the station scale 44

4.1.1 Constant ARF approach 44

4.1.2 Δ-approach for future prediction 49

4.2 Comparison between constant ARF and Δ-method 51

5 Scaling models for IDF curves 54

5.1 Regionalization 54

5.2 Generalized extreme value distribution 56

5.3 Mean values bias correction 57

5.4 QQ bias correction 59

5.5 Scaling method 59

5.5.1 Simple scaling GEV model 60

5.5.2 Log-normal multiscaling model 61

5.6 Development of regional IDF curves 64

5.7 Development of regional IDF scaling model 66

6 Results and Evaluation 67

6.1 Mean value bias correction 67

6.2 Δ- method 71

6.3 Scaling method 71

6.4 Quantile-Quantile mapping 81

6.5 Summary 83

6.6 Comparison of IDF curves from observations and CRCM data 85

6.6.1 Region 1 85

6.6.2 Region 2 89

6.6.3 Region 3 93

6.6.4 Region 4 94

7 Uncertainty analysis 98

8 Summary and Conclusion 109

8.0.5 Recommendation 112

8.0.6 Future work 113

Bibliography 115

Appendix

A 120

B **126**

List of Tables

1.1 Observed and simulated mean annual maximum precipitation (mm) at Brandon, MB. 3

2.1 Stations used in the analysis. 17

2.2 NARCCAP simulations used in the present study 19

4.1 Relative changes (percentage) in the future climate from the constant ARF method and the Δ-method. 53

5.1 Grouping according to geographical location. 55

6.1 Scaling exponents from observed, control simulated, and future simulated data 68

6.2 t-test results; p-value, statistics. 79

7.1 ARF from NARCCAP simulations for Region 2. 101

7.2 Relative changes in percent in future from NARCCAP simulations for Region 2. 103

7.3 ARF from NARCCAP different simulations for Region 3. 104

7.4 Relative changes (percent) in future from NARCCAP simulations for Region 3. 105

7.5 ARF from NARCCAP simulations for Region 4. 107

7.6 Relative changes (percent) in future from NARCCAP simulations for Region 4. 107

List of Figures

1.1 Intensity-Duration-Frequency curves 6

2.1 Location of stations 16

3.1 Plot of the cumulative probability distribution function of daily precipitation greater than zero for the Brandon raingauge station. 23

3.2 Spatial correlation versus inter-station distance based on daily data where both stations in a pair record precipitation. 25

3.3 Spatial correlation versus inter-station distance based on all daily data including zeros. 25

3.4 Spatial correlation versus inter-station distance based on daily data where at least one station record precipitation. 25

3.5 Variance reduction factor versus non dimensional catchment area $\frac{A}{\lambda^2}$. The catchment area is approximated by a square and the correlogram is exponential. 28

3.6 Fitted Gumbel parameters along with approximations for $\alpha_{np}(d)$ and $u_{np}(d)$ given in Equations (3.26a) and (3.26b). 33

3.7 Point IDF curves for the Flin Flon station. 35

3.8 Areal IDF curves for the Flin Flon station for $\frac{A}{\lambda^2} = 0.32$. 35

3.9 Areal IDF curves for the Flin Flon station for $\frac{A}{\lambda^2} = 1$. 36

3.10 Areal IDF curves for the Flin Flon station for $\frac{A}{\lambda^2} = 25$. 36

3.11 Coefficient of variation of areal maximum extreme rainfall intensities for 24-hr duration 38

3.12 Areal reduction factor at the Flin Flon station for 24-hr precipitation 39

3.13 Areal reduction factor versus return period. 39

4.1 IDF curves for control and future climate at the Flin Flon station . . 41

4.2 Ratio of future and control climate of simulated data at the Flin Flon station. 42

4.3 Comparison of IDF curves of areal and CRCM precipitation for 24-hr duration at the Flin Flon station. 42

4.4 Cumulative probability curves for the control and the future climate for each duration at the grid box scale. 43

4.5 ARF's derived analytically from observations versus ARF's defined as the ratio of CRCM quantiles and observed quantiles. Data are from the Flin Flon station. 46

4.6 Comparison of IDF curves of the control and future climate at the station scale for the Flin Flon station 48

4.7 Comparison of IDF curves estimated from areal data for the control and future climate at the Flin Flon station 48

4.8 Cumulative probability curves for 1-hr and 24-hr duration for the present climate. 49
4.9 Cumulative probability curves at the Glenlea station for 24-hr duration. 50
4.10 Cumulative probability curves at the Gillam station for 24-hr duration. 50
4.11 Cumulative probability curves at the Lynnlake station for 24-hr duration. 50
4.12 IDF curves at the Flin Flon station using Δ-method 52
4.13 IDF curves for areally averaged rainfall intensity at the Flin Flon station using Δ-method 52
4.14 IDF curves at the grid box scale for the Flin Flon station 52
4.15 Comparison between observed, CRCM, and estimated areal rainfall intensity at the Flin Flon station. 53

5.1 Cumulative probability distribution for each region for 24-hr duration annual extreme rainfall. 55
5.2 Relationship between the skewness coefficient and κ for the GEV distribution. 58
5.3 Box plot of precipitation depth for observations at The Pas station. . 65
5.4 Box plot of precipitation depth for simulations at The Pas station. . 65

6.1 δ versus duration at the Brandon station 68

6.2 δ versus duration at the Brandon station. $\delta_{\lambda d}$ is determined from (6.9). 71

6.3 Δ versus duration at the Brandon station 72

6.4 IDF curves for future prediction using the GEV distribution at the Brandon station 73

6.5 IDF curves for future prediction using future CRCM simulation along with scaling laws 75

6.6 IDF curves for future prediction for Δ-method quantiles along with scaling laws 75

6.7 IDF curves from corrected CRCM data and future observed data for future prediction using scaling laws 76

6.8 Quantile-Quantile plot for 24-hr duration after correcting the control run by the δ-method. 76

6.9 IDF curves for observations 77

6.10 IDF curves for the corrected control simulation run 77

6.11 Comparison between observations and control simulation run using the GEV scaling model 78

6.12 Comparison between ensemble member 1 and member 5. 79

6.13 Comparison between observations and control simulation run (ensemble member 5) using GEV scaling model 80

6.14 IDF curves for future prediction (using ensemble 5) using scaling laws 80

6.15 Quantile-Quantile plot for 1-hr duration for the control climate after applying QQ mapping. 81
6.16 Future IDF curves by applying QQ mapping to the future simulation run 82
6.17 Future IDF curves by correcting future simulation run (ensemble member 5) by QQ mapping 82
6.18 Cumulative probability distribution at the Churchill station. 86
6.19 IDF curves for the control climate for observed data at the Churchill station 87
6.20 IDF curves for the control climate for the CRCM simulation at the Churchill station 87
6.21 IDF curves for the future climate for the CRCM simulation at the Churchill station 88
6.22 IDF curves for the future climate for observations at the Churchill station 88
6.23 Comparison of IDF curves for future climate and control climate at the Churchill station 89
6.24 IDF curves from observed data for the control climate for Region 2 . 90
6.25 IDF curves from corrected CRCM data for the control climate for Region 2 90
6.26 Comparison of IDF curves for control climate for Region 2 91

6.27 Comparison of IDF curves from observed and corrected CRCM data for the future climate for Region 2 92
6.28 Relative changes between control and future climate for Region 2. . . 92
6.29 Comparison of simple scaling GEV model from observed and corrected CRCM for the control climate for Region 3 94
6.30 IDF curves from simple scaling GEV model for corrected CRCM for the future climate for Region 3 95
6.31 IDF curves for the corrected CRCM data for Region 3 95
6.32 Relative changes between control and future climate for Region 3. . 96
6.33 IDF curves for the bias corrected CRCM data for Region 4 97
6.34 Relative changes between control and future climate for Region 4. . 97

7.1 Cumulative probability plots for five regional climate models from NARCCAP simulations at the Thompson station for the 24-hr duration. 99
7.2 Boxplot of precipitation depth for NARCCAP simulations at the Thompson station. 99
7.3 DDF curves from the simple scaling GEV model and the GEV distribution for the CRCM-CGCM3 for the control climate for Region 2 102
7.4 DDF curves from simple scaling GEV model and the GEV distribution for the CRCM-CGCM3 for the future climate for Region 2 102

7.5 ARFs versus return period for Region 2 using CRCM-CGCM3 simulations 103

7.6 ARFs versus return period for Region 3 using CRCM-CGCM3 simulations 104

7.7 IDF curves from the simple scaling GEV model and the GEV distribution for the CRCM-CGCM3 simulation for the control climate for Region 4 106

7.8 IDF curves from the simple scaling GEV model and the GEV distribution for the CRCM-CGCM3 simulation for the future climate for Region 4 106

7.9 Relative changes for the model NARCCAP CRCM-CGCM3 at Region 4. 108

A.1 Comparison of IDF curves of areal and CRCM precipitation for each duration. 121

A.2 Cumulative probability curves for each duration. 121

A.3 Quantile-Quantile plot for each duration after correcting the control simulation by the δ-method. 122

A.4 Moments versus durations for observations. 123

A.5 Scaling exponent versus NCM order for observations. 123

A.6 Moments versus durations for control simulation run. 123

A.7 Scaling exponent versus NCM order for control simulation run. 123

A.8 Quantile-Quantile plot for each duration control climate after mapping the control simulation run by QQ mapping. 124
A.9 Quantile-Quantile plot for each duration future climate after mapping the future simulation run based on future observations by QQ mapping 125

B.1 IDF curves from observed data for the future climate at Region 2. . . 127
B.2 IDF curves from corrected CRCM data for the future climate at Region 2. 127
B.3 IDF curves from simple scaling GEV model for observed data for the control climate for Region 3. 128
B.4 IDF curves from simple scaling GEV model for corrected CRCM data for the control climate for Region 3. 128
B.5 IDF curves for the corrected CRCM data for Region 4 for the control climate. 129
B.6 IDF curves for the observed data for Region 4 for the control climate. 129
B.7 IDF curves for the corrected CRCM data for Region 4 for the future climate. 130
B.8 IDF curves for the observed data for Region 4 for the future climate. 130
B.9 Comparison of IDF curves for Region 4 for the future climate between observed data and corrected CRCM data. 130
B.10 DDF curves from simple scaling GEV for the CRCM-CCSM for the control climate at Region 2. 131

B.11 DDF curves from simple scaling GEV for the CRCM-CCSM for the future climate at Region 2. 131

B.12 DDF curves from simple scaling GEV for the MM5I-CCSM for the control climate at Region 2. 131

B.13 DDF curves from simple scaling GEV for the MM5I-CCSM for the future climate at Region 2. 131

B.14 DDF curves from simple scaling GEV for the HRM3-GFDL for the control climate at Region 2. 132

B.15 DDF curves from simple scaling GEV for the HRM3-GFDL for the future climate at Region 2. 132

B.16 DDF curves from simple scaling GEV for the HRM3-HADCM3 for the control climate at Region 2. 132

B.17 DDF curves from simple scaling GEV for the HRM3-HADCM3 for the future climate at Region 2. 132

Chapter 1

Introduction

1.1 Background

The 21^{st} century will face many challenges and one of them is a changing climate. Climate change affects the economy, infrastructure, health, and wildlife. Hence climate change has become one of the most important issues in the world as natural calamities, global warming, and extreme events appear to increase in frequency day by day. Climate change is measured by the change of temperature, wind, precipitation, sea level and snow cover. According to the IPCC report 2007, increased levels of Carbon-di-oxide, Methane, Ozone, Halocarbon, and Nitrous oxide contribute to the global warming. The report concludes that human activities are responsible for much of the warming. In Canada the mean temperature has increased about 1.3^0C over the past century (www.nrcan.gc.ca). In the future, the snow cover will be reduced, sea ice will continue to shrink, and heat waves and extreme precipitation events will occur with increasing frequency.

The climatic system is complex and the factors contributing to climate change are not working individually. Climate change can involve both changes in average conditions and changes in extreme conditions. Greenhouse gas is the primary cause of climate change. In Canada, 80 percent of total greenhouse gas emissions are associated with the production or consumption of fossil fuels. Globally, Canada accounts for about two percent of total annual greenhouse gas emissions (www.climatechange.gc.ca). Measures to reduce greenhouse gas are being introduced in Canada but additional climate change is unavoidable and will have significant negative economic, social and environmental impacts on Canadian communities.

Over the last several decades many studies have been conducted to assess climate change. Most of the studies have focused on average conditions of climate, not extreme events. The Canadian Centre for Climate Modelling and Analysis has developed a number of climate models to assess future climate change and variability, resulting from projected scenarios of greenhouse gas emissions and aerosol forcing. Future weather and climate extremes are predicted by comparing the control climate model simulations to simulations of the future. The earlier climate models focused only on the mean climate change (*Houghton et al.*, 1990), but now climate modelers have started to look at the weather and climate extremes. In recent years, climate models have been improved enough to simulate more complex features. There is increasing confidence that climate models can provide projections of changes more

Table 1.1: Observed and simulated mean annual maximum precipitation (mm) at Brandon, MB.

	1hr	2hr	6hr	12hr	24hr
Observed	19	24	36	42	48
CRCM	5	8	16	22	29

accurately, but there is still problems with the prediction of extreme precipitation. Global climate models predict changes in precipitation patterns in many areas of the world. GCM's have coarse resolution and for most practical applications must be combined with downscaling techniques designed to resolve sub-grid variability and remove biases. Extreme precipitation in particular is poorly represented in climate models and even when combined with traditional downscaling methods, there are significant difficulties involved in assessing the frequency and severity of future extreme precipitation events.

Table 1.1 shows the mean annual maxima for durations of 1-hr, 2-hr, 6-hr, 12-hr and 24-hr for the raingauge at Brandon, along with corresponding values simulated by the Canadian Regional Climate Model (CRCM). There is a considerable difference between observed and simulated extreme precipitation statistics. Evidently, climate models do not represent maximum precipitations very well. At the same time, this type of information is important for the design of urban drainage systems that typically have long design lives and performance that will be affected by future climate change.

Climate models attempt to represent the real climate but in practice, biases and coarse spatial resolution of global models limit their direct use. Hence, it is necessary to apply two additional steps to regional and local impact studies : downscaling and bias removal. According to the IPCC fourth assessment report, the uncertainty in regional climate model projections is still large in spite of increasing horizontal resolution. An ensemble RCM projections over North America from North American Regional Climate Change Assessment Program (NARCCAP) are available which makes it possible to compare the results from different climate models and investigate the uncertainties involved in future predictions.

Downscaling is required to overcome the limitations of coarse spatial resolution in the global models. In mountainous terrain, a single grid box will consider only mean elevation. In reality, the conditions at the mountaintop and valley locations will be much different. Such processes as local snow pack accumulation and melting cannot be studied accurately with direct model output. The typical resolution cannot represent the conditions of small scale processes clearly, especially for precipitation. The occurrence of heavy rainfall is an important climate feature but an area the size of a grid box may experience heavy rains at some points while others receive no rain at all. For this reason, the largest grid box values typically are smaller than those observed at the local scale.

Bias removal is often done by the Δ-method. Change amounts are determined by comparing the climate model output for current and future climates, typically a difference for temperature and a percentage change for precipitation. Then these changes are applied to observed climate data to construct input to impact models. The Δ-method assumes that future model biases for both mean and variability will be the same as those in present-day simulations, and that the future frequency and magnitude of extreme weather events are the same relative to the mean climate of the future as they are in present-day climate.

Extreme rainfall characteristics are often required for the design of hydraulic structures. Information about extreme rainfall can be expressed by Intensity-Duration-Frequency (IDF) curves. The establishment of IDF curves for extreme rainfall is a common task in risk analysis of natural hazards. In design problems, it is necessary to know the storm duration and intensity for different return periods and IDF curves provide this information.

IDF curves are widely used as hydrological tools in engineering applications. IDF curves are most often used for design of infrastructure that includes minimum capacity in terms of rainfall return periods. For example, in Canada storm sewers are typically designed to carry a 5-year storm. There are a number of ways to establish IDF curves. For example, the relationship between intensity, duration and return period may be expressed by (*Subramanya*, 1984)

$$i = \frac{KT^x}{(D+a)^n} \tag{1.1}$$

where K, a, x and n are constants for a given catchment and i is the average of intensity of a storm event with duration D and return period T. The steps involved in the typical establishment of IDF curves are the following:

- For each duration, fit a probability distribution function to the series of maxi-

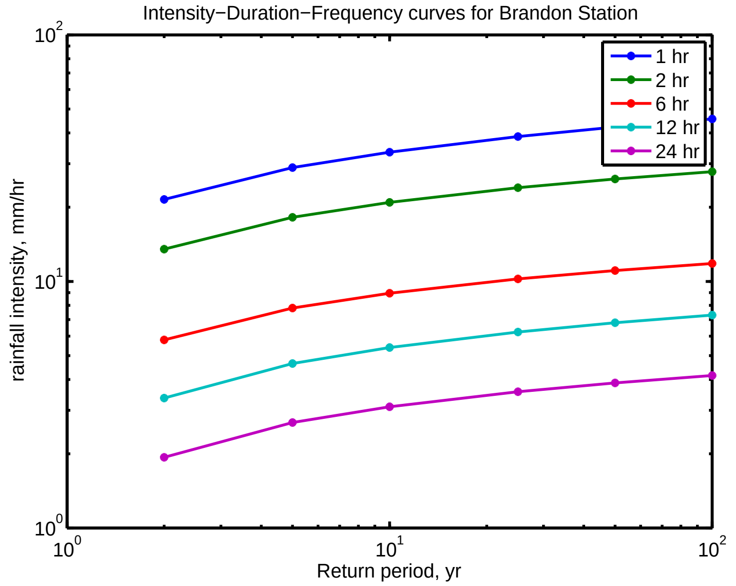

Figure 1.1: Intensity-Duration-Frequency curves

mum annual values.

- Calculate rainfall intensities for specific durations and specific return periods, using the probability distribution functions derived in the first step.

- Fit an empirical formula such as (1.1) to the quantiles from the previous step. The least squares method can be used to determine parameters of the empirical IDF equation that is used to represent the Intensity-Duration relationships.

An example of IDF curves is shown in Figure 1.1. Here the IDF curves have been established using the generalized extreme value (GEV) distribution. The curves were estimated by fitting probability distributions for several pre-determined rainfall durations.

In urban hydrology, knowledge of short-duration rainfall events is needed. Short temporal rainfall data are often not available or the period of record may be too short for analysis (*Aronica and Freni*, 2005). One way to overcome this problem is to make use of scale invariance theory. The advantage of using scaling laws is that quantiles for any duration rainfall can be determined by this theory. The basic theoretical framework of scaling theory has been investigated by many authors. Scaling models can be used to transfer results between different temporal or spatial scales and thereby overcome the difficulty of inadequate data (*Nhat et al.*, 2007). If $H(d)$ and $H(\lambda d)$ are random variables at two distinct time or spatial scales d and λd, respectively, then the definition of scaling is given by

$$H(d) \stackrel{dist}{=} \lambda^{-\beta} H(\lambda d) \tag{1.2}$$

where the equality sign represents the identity of probability distributions, λ is the scale factor, and β is the scaling exponent. In simple scaling laws, the scaling exponent is proportional to the order of moments. When analyzing extreme rainfall events, it is possible that the scaling exponent is not proportional to the order of moment and in such cases, multiple scaling theory may be used.

Aronica and Freni (2005) estimated sub-hourly depth-duration-frequency (DDF) curves using the scaling properties of hourly and sub-hourly data at partially gauged sites. *Menabde et al.* (1999) identified simple scaling properties for annual maxima series by examining moment and parameter scaling of an extreme value distribution fitted to the data. *Burlando and Rosso* (1996) employed scaling and multiscaling models to develop depth-duration-frequency curve for storm precipitation and showed that most of the observed data follow simple scaling laws. However, the model performance in some cases can be improved by using a multiple scaling approach.

One of the major problems in climate studies is the temporal and spatial scale mismatch between the outputs of climate models and station data, as station observations are point data and model values are areal data. Areal IDF curves are flatter in appearance than point IDF curves because of the smoothing associated with the spatial averaging of rainfall over the area. In order to transform the point rainfall intensity to areal average rainfall intensity, hydrologists use so-called areal reduction factors (ARF). An areal reduction factor is simply a ratio of catchment rainfall intensity for a specific duration and return period and point rainfall intensity for the same duration and return period. Areal IDF curves can be obtained by multiplying the rainfall intensity obtained from point IDF curves by the ARF. For very small catchments, the ARF tends to unity. There are two kinds of ARF presently in use (*Sivapalan and Bloschl*, 1998):

- Fixed-area ARFs describe rainfall at an arbitrary point. Point rainfall quantiles are estimated and then averaged over a catchment which is fixed in space.
- Storm-centered ARFs which refer to a given storm. Storm-centered ARFs are determined as the ratio of the average rainfall depth over an area and maximum rainfall depth for the storm.

Storm-centered ARFs are usually smaller than fixed area ARFs. Storm-centered ARFs are used in the probable maximum flood estimation and Fixed-area ARFs are used in the design of hydraulic structures like bridges, culverts and drainage pipes. In this study, fixed area ARFs have been estimated to develop areal IDF curves.

In the past 15-20 years, research on rainfall processes has been dominated by stochastic modeling of rainfall fields in time and space (e.g *Waymire et al.* (1984);*Sivapalan and Wood* (1987)). Several empirical models have been proposed to transform point rainfall depths to average areal rainfall. For example, the U.S Weather Bureau developed the following equation (*Leclerc and Schaake* (1972))

$$ARF = 1 - \exp(-1.1d^{1/4}) + \exp(-1.1d^{1/4} - 0.01A) \tag{1.3}$$

where d is the duration in hours and A is the area in square miles. The shortcomings of this formula is that storm magnitude is not considered. *Roche* (1963) presented a theoretical basis to transform point rainfall to areal rainfall. This method was technically correct but cumbersome and difficult to apply in a practical manner. *Rodriguez-Iturbe and Mejia* (1974) used the spatial correlation structure of rainfall fields to approximate rainfall fields as a zero mean Gaussian process. The areal averaging resulted in variance reduction factors which were a function of the assumed spatial correlation structure and the size and shape of the catchment area. They argued that the variance reduction factors can be interpreted as ARFs but these ARFs only refer to the parent rainfall intensities, not extreme rainfalls. *Yoo and*

Ha (2007) discussed the definition of spatial correlation, specifically whether dry days should be included in the determination of spatial correlation of precipitation. Their results show that the effect of including dry days is significant during the wet season where the inter-station correlations are significantly lower than those estimated during the dry season. The consideration of zeros always yields high inter-station correlation coefficients than when only wet days are considered. Areal reduction factors are necessary tools in climate change studies as they provide the link between observed point precipitation and simulated grid precipitation that represents areally averaged values.

There are many ways to estimate the future change of climate and among them two methods are described in this section. Theses methods are explained in *Mailhot et al.* (2007).

- Intensity-dependent ARF approach

  According to the hypothesis, ARFs for rainfall of a given intensity and duration in the future climate will be the same as for rainfall with same intensity and duration in the control climate. Only the probability of occurrence of these events will change. This hypothesis can be expressed in mathematical form as

$$ARF_f(x_f^{(g)}) = \frac{x_f^{(g)}}{x_p^{(s)}\left[F_p^{(g)}(x_f^{(g)})\right]} \tag{1.4}$$

  where $x_f^{(g)}$ is the future annual maximum estimates at the grid box scale, $x_p^{(s)}$ is the control annual maximum rainfall estimates at the station scale, $F_p^{(g)}(x_f^{(g)})$ is the corresponding probability of non exceedance at the grid box scale, and brackets indicate that $x_p^{(s)}$ is a function of $F_p^{(g)}(x_f^{(g)})$.

- Constant ARF approach

  In this method, to generate IDF curves at the station scale, the rainfall depths for a given duration and for a given return period at the grid box scale are used to estimate the rainfall depths at the station scale for the future climate. The assumption is

$$ARF_f = ARF_p \tag{1.5}$$

  The rainfall depths can be written mathematically

$$x_f^{(s)} = x_p^{(s)} \frac{x_f^{(g)}}{x_p^{(g)}} \tag{1.6}$$

  where $x_p^{(s)}$ is the rainfall depths at the station scale for the control climate, $x_f^{(g)}$ is the rainfall depths at the grid box scale for the future climate, and $x_p^{(g)}$ is the rainfall depths at the grid box scale for the control climate.

Another way to compare observed and model data is statistical downscaling. Statistical downscaling can be done at the monthly or daily timescales. The most common downscaled variables are precipitation and temperature. There are several approaches to statistical downscaling, described in the following (*Walsh*, 2011);

- Delta method: In this method, differences between the GCM future and historical periods are superimposed on historical monthly or daily observations.

- Bias correction method: In this method, the differences between observed climatological mean values and corresponding simulated GCM mean values for the reference period are used to correct future GCM simulations.

- Statistical downscaling: In this method, a statistical relationship is established between large scale predictors and local predictands based on multiple linear regression.

Willems and Vrac (2011) used a quantile perturbation-based downscaling method. The quantile perturbation basically involves the estimation of the change factor in daily precipitation for a specific month and a specific empirical probability. *Mavromatis and Jones* (1999) used daily outputs from HadCM2 GCM as input to CERES-Wheat for studying the potential impact of climate change on wheat in France and their conclusion was that the daily GCM cannot represent the year-to-year variability adequately.

Challinor et al. (2005) found that to get good predictions with GCMs, it is necessary to calibrate the model to observed district yield because of GCM biases. *Ines and Hansen* (2006) proposed a two-step bias correction to correct GCM rainfall. The procedure involves truncating the GCM rainfall at a point so that it can reproduce the observed wet-dry day probabilities and then mapping the truncated GCM precipitation distribution onto a gamma distribution fitted to observed intensity distribution. Corrected GCM output is calculated by (*Ines and Hansen*, 2006)

$$x'_i = F^{-1}_{I,obs}(F_{I,GCM}(x_i)) \tag{1.7}$$

where $F_{I,GCM}(x_i)$ is the cumulative distribution function (CDF) of daily rainfall amounts above the threshold and $F^{-1}_{I,obs}$ is the inverse of the observed intensity distribution.

1.2 Objectives

The overall objective of this thesis is to apply and evaluate methods for estimating changes in IDF-curves resulting from climate change. Specific objectives are

1. To identify and compare methodologies for predicting changes in IDF curves and derivation of areal reduction factors allowing for comparison of observed point precipitation and modeled grid precipitation at short temporal scales.

2. To find a relationship between CRCM data and station data by using scale invariance theory. Two methods for future prediction will be examined - 1) bias correction for each duration (either δ-factor correction or QQ mapping) and 2) bias correction for the reference duration and the use of scaling laws estimated from observed data to obtain results for all other durations.

3. To assess changes in IDF curves for Manitoba for a selected future climate scenario (A2).

4. To investigate the uncertainties in regional projections of the future climate by using different simulations from the North American Regional Climate Change Assessment Program (NARCCAP).

Chapter 2

Study area and Data

The province of Manitoba was selected as the study area for this research. Rainfall data from 19 raingauge stations in Manitoba (Figure 2.1) were used in the study.

2.1 Station data

From December to April, most precipitation in Manitoba falls as snow. Due to the cold weather, tipping bucket raingauge stations are inoperative during these months, but the exact period of operation varies from year to year and from station to station. Maximum annual precipitation values from April to November were considered in this study. This is also the period of the year where the annual maxima usually occur. The data are provided by Environment Canada from the Canadian Daily Climate Data (CDCD). Manitoba has a total of 31 weather stations. Most stations are located in the southern part of the province, whereas there are a few weather

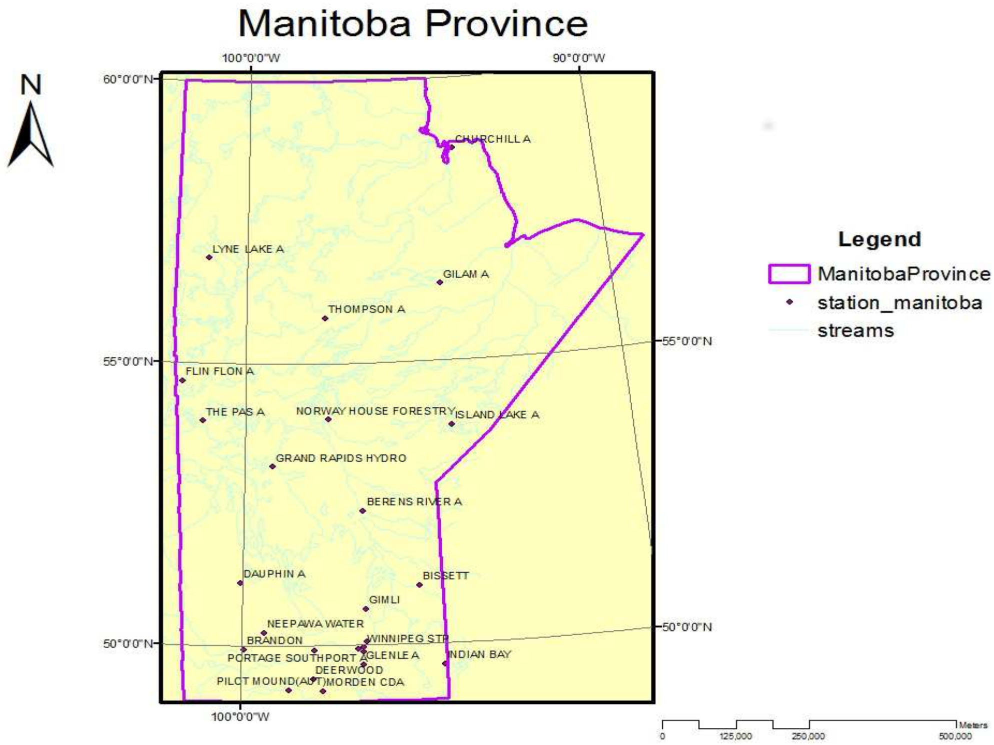

Figure 2.1: Location of stations

stations in the north. Very few weather stations have long-term records, and therefore large temporal gaps exist across the province. Stations in the southern portion of the province generally has the longest records with some extending back to the 1870's, while in the north, records do not extend further back than 1950's. This temporal gap make climate change analysis more difficult. In this study, a total of 19 stations were considered, selected on the basis of data availability and record length. Rainfall stations with less than 20 years of record were discarded from the study.

An analysis was performed on the annual maximum rainfall series from the 19 rainfall stations for durations of 1-hr, 2-hr, 6-hr, 12-hr, and 24-hr. The record lengths range from 25 to 38 years. The raingauge stations have data for nine durations: 5-

Table 2.1: Stations used in the analysis.

name	latitude	longitude	elevation (m)	Records	Mean AM rainfall (24-hr,mm)
BRANDON A	49.92	-99.95	409	1970-2006	48
DEERWOOD	49.40	-98.32	338	1951-1995	49
GLENLEA	49.65	-97.12	234	1967-2000	55
LYNN LAKE A	56.86	-101.08	356	1969-2005	40
GILLAM	56.36	-94.71	145	1970-2006	37
PORTAGE SOUTHPORT A	49.90	-98.27	269	1964-1991	53
FLIN FLON A	54.68	-101.68	303	1968-2006	41
BISSETT	51.03	-95.70	259	1968-1997	53
BRANDON CDA	49.92	-99.95	363	1941-2006	52
CHURCHILL A	58.74	-94.06	28	1943-2006	31
DAUPHIN A	51.10	-100.05	304	1942-2006	52
INDIAN BAY	49.62	-95.20	326	1915-2006	53
ISLAND LAKE A	53.85	-94.65	236	1970-2006	43
MORDEN CDA	49.18	-98.08	297	1918-1998	56
NEEPAWA WATER	50.22	-99.47	358	1969-2006	52
NORWAY HOUSE FORESTRY	54.00	-97.80	217	1970-2000	41
PILOT MOUND	49.20	-98.90	270	1943-2006	45
THOMPSON A	55.80	-97.87	222	1967-2006	41

min, 10-min, 15-min, 30-min, 1-hr, 2-hr, 6-hr, 12-hr, and 24-hr. In this study the durations ranging from 1-hr to 24-hr were considered as these durations are also available from the Canadian Regional Climate Model (CRCM). Table 2.1 lists the raingauge stations. The last column shows the mean of annual maximum 24-hr rainfall.

2.2 Canadian Regional Climate Model data

Regional climate models (RCMs) increase the resolution of the GCM in a local area of interest. They allow for better representation of the underlying topography within the model domain and are also able to resolve atmospheric processes based on the model resolution. The results of *LaPrise et al.* (1998) demonstrate the great potential of continuous multi-year nested regional climate model simulations using the Canadian RCM (CRCM) at 45km resolution. RCMs are able to evaluate the effect of a variety of forcings upon the regional climate that cannot be obtained from GCMs.

The Canadian Regional Climate Model simulations were used in this study. The CRCM's grid size resolution is 45km-by-45km. The CRCM data were provided by the Ouranos Climate Simulation Team as a part of the Canadian Regional Climate Projections program. The following three experiments were used in this study:

- Experiment version aev: Based on CRCM model version MRCC 4.2.3, ensemble 5, covering the period from 1961-2100.
- Experiment version aey: Based on CRCM model version MRCC 4.2.3, ensemble 1, covering the period from 1961-2000.
- Experiment version aew: Based on CRCM model version MRCC 4.2.3, ensemble 5, covering the period from 2041-2070.

The CRCM simulations are driven by data from the CGCM3.1. In this study, the T47 version was used which has a spatial resolution of roughly 3.75 degrees lat/lon and 31 levels in the vertical (*Flato and Boer* (2001), *Kim et al.* (2002), *Kim et al.* (2003)). A single emission scenario is used: the SRES A2 which is characterized by economical development, technological development, energy use, population change, and land use change. The A2 scenario is at the higher end of the SRES emission

Table 2.2: NARCCAP simulations used in the present study

RCM	GCM
HRM3	GFDL (Geophysical Fluid Dynamics Laboratory GCM)
CRCM	CCSM (Community climate system model)
CRCM	CGCM3 (The third generation coupled global climate model)
HRM3	HADCM3 (Hadley centre coupled model, version3)
MM5I	CCSM (Community climate system model)

scenarios. This was preferred for the development of the methodology but ideally other scenarios should be considered as well.

2.3 The North American Regional Climate Change Assessment Program (NARCCAP)

The North American Regional Climate Change Assessment Program (NARCCAP) is an international initiative that provides high resolution climate scenarios for the United States, Canada and Northern Mexico using regional climate models coupled with global climate models. NARCCAP provides high resolution climate change simulations that are useful for investigating uncertainties in regional scale projections of future climate.

Different GCMs have been forced with the SRES A2 emission scenario for the 21st century (*Mearns*, 2007, updated 2011). Simulations with the models were also produced for the current (historical) period. The RCMs are nested within the GCMs for the current period 1968-2000 and for the future period 2041-2070. NARCCAP data are stored in NetCDF format and distributed via the Earth System Grid website.

NARCCAP data are provided at a 50km horizontal resolution. The data are at a 3-hr resolution, and 3-hr, 6-hr, 12-hr, 18-hr, and 24-hr precipitation depths were extracted from NARCCAP. Table 2.2 shows the different simulations from NARCCAP that are used in this study.

Chapter 3

Areal Reduction Factor

In this chapter, a methodology is employed to derive areal reduction factors (ARFs) analytically to construct Intensity-Duration-Frequency (IDF) curves for large areas. This is a necessary step in order to compare model data that represent grid averages with observations at a point in space. Two experiments from the CRCM were used to make comparison between estimated areal rainfall from observations and CRCM rainfall intensities.The methodology here is based on *Sivapalan and Bloschl* (1998). ARFs were derived based on the spatial correlation structure of rainfall. To determine the spatial correlation structure, daily precipitation values were used in this study. These data were obtained from Environment Canada's web site for the period of 1970-1979. The following steps were involved:

- First, the parent distribution of areal daily rainfall depth was derived from point rainfall depth.

- The parent distribution was then transformed to an extreme value distribution.
- The parameters of the extreme value distribution for areal rainfalls were determined.
- The new areal IDF curves were then produced using these parameters and ARFs were estimated by the ratio of grid box rainfall intensity at a specific duration and a specific return period and the point rainfall intensity at the same duration and the same return period.

Analytically computed ARFs depend on the catchment area, the spatial correlation structure, and the return period. The methodology is described in details in the following sections.

3.1 Analytical derivation of Areal Reduction Factors

3.1.1 Parent distribution of point rainfall

Daily precipitation P has a mixed distribution and it is assumed that the parent distribution of daily precipitation at a point in space is exponential for $P > 0$ as several studies indicate that the exponential distribution represents a good approximation of the rainfall process [*Eagleson* (1972); *Warrilow et al.* (1986)]. The exponential

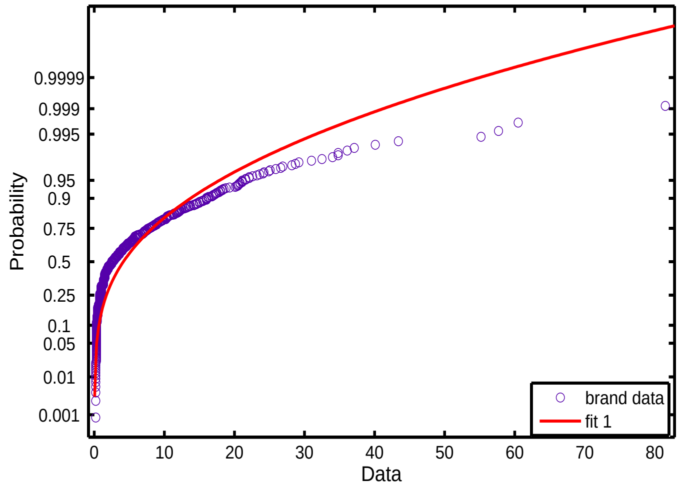

Figure 3.1: Plot of the cumulative probability distribution function of daily precipitation greater than zero for the Brandon raingauge station.

probability density function can be written as

$$f_{Ip}(i_p) = \frac{1}{\beta_p} \exp\left(-i_p/\beta_p\right), \quad i_p \geq 0 \tag{3.1}$$

where i_p is the daily rainfall intensity on wet days and β_p is the exponential parameter. The index p is used to indicate that this parameter is for point precipitation. Figure 3.1 shows an example of an exponential distribution fitted to daily precipitation data at the Brandon station. The mean and the variance are

$$\mu_p = \beta_p \tag{3.2a}$$

$$\sigma_p^2 = \beta_p^2 \tag{3.2b}$$

An assumption is made that the spatial correlogram for daily point precipitation is isotropic and of the exponential type [*Rodriguez-Iturbe and Mejia* (1974); *Wood and Hebson* (1986)], i.e.

$$\rho_p(r) = \exp\left(-r/\lambda\right) \tag{3.3}$$

where r is the distance between two stations and λ is the spatial correlation length defined by

$$\lambda = \int_0^\infty \rho_p(r)dr \tag{3.4}$$

Spatial correlograms were developed for three different cases. In the first case, correlations were based on cases where both stations record rain (Figure 3.2). The second case considered all cases, including zeros (Figure 3.3). And the third case considered days where at least one station in a pair record rain (Figure 3.4). The inter-stations correlations are significantly lower when only jointly wet days are considered. To develop IDF curves for catchments, only the first case is of practical interest. The correlogram in Figure 3.2 has a spatial correlation length of 116 km.

3.1.2 Areal averaging of point rainfall

The assumption made in this study is that the spatial random field of point rainfall intensities is stationary. The areally averaged rainfall intensity over the area A is defined by

$$i_A = \frac{1}{A}\int_A i_p(\mathbf{x})d\mathbf{x} \tag{3.5}$$

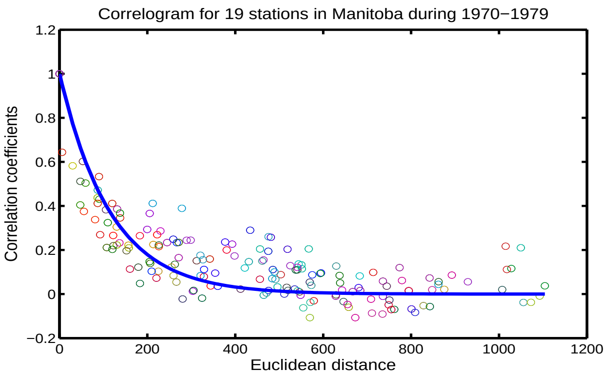

Figure 3.2: Spatial correlation versus inter-station distance based on daily data where both stations in a pair record precipitation.

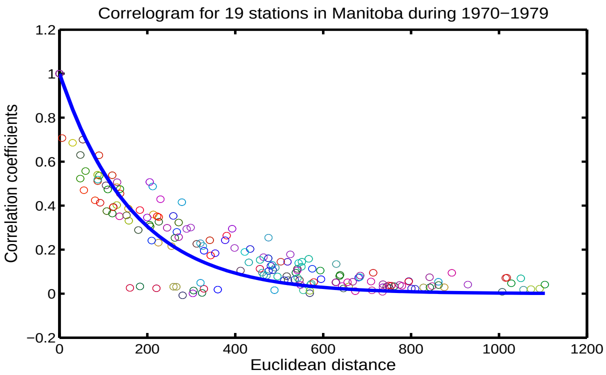

Figure 3.3: Spatial correlation versus inter-station distance based on all daily data including zeros.

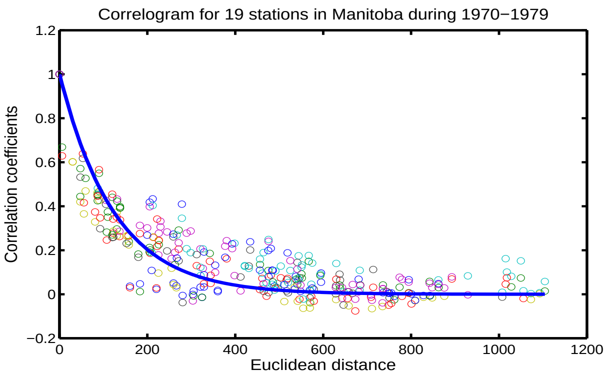

Figure 3.4: Spatial correlation versus inter-station distance based on daily data where at least one station record precipitation.

where $\mathbf{x}$ is a vector of coordinates inside the area. As it is assumed that the spatial random field is stationary, the mean of i_A will be the same as the mean of i_P:

$$\mu_A = \mu_P \tag{3.6}$$

Due to smoothing involved in the spatial integration, the variance of the areally averaged process, σ_A^2, is less than the variance of the point rainfall process, σ_P^2. The ratio of σ_A^2/σ_P^2 is called the variance reduction factor, denoted ν^2. The variance of daily areal precipitation can be written as

$$\sigma_A^2 = \sigma_P^2 \nu^2 \tag{3.7}$$

3.1.3 Estimation of variance reduction factor

The variance reduction factor depends on the correlation structure of the rainfall field and the size and the shape of the area. *Rodriguez-Iturbe and Mejia* (1974) expressed ν^2 for a stationary isotropic spatial random field by

$$\nu^2 = E[\rho_p(|\mathbf{x}_2 - \mathbf{x}_1|)] \tag{3.8}$$

which is the expected value of the spatial correlation coefficient between any two points $\mathbf{x}_1$ and $\mathbf{x}_2$ randomly chosen within the catchment domain of size A and $|.|$ represents the Euclidean distance between them. In other words, the above equation can be written as

$$\nu^2 = \int_0^{R_{max}} \rho_p(r) f_R(r) dr \tag{3.9}$$

where R is the Euclidean distance between randomly selected two points within the area, R_{max} is the maximum distance between two points within the area, and f_R is the pdf of the random variable R. This PDF can be estimated numerically for any shape of catchment area. In the present application, it is appropriate to assume that the area is square and the pdf of R for this case has been derived by *Ghosh* (1951). The probability density function of R, the random distance between two independent points in a square of side length a, was given by *Ghosh* (1951):

$$f_R(r) = \frac{4r}{a^4}\phi(r) \tag{3.10}$$

where for the range of $r = 0$ to $r = a$,

$$\phi(r) = \frac{1}{2}\pi a^2 - 2ar + \frac{1}{2}r^2 \tag{3.11}$$

and for the range of $r = a$ to $r = \sqrt{2}a$,

$$\phi(r) = a^2(\sin^{-1}\frac{a}{r} - \cos^{-1}\frac{a}{r}) + 2a\sqrt{r^2 - a^2} - \frac{1}{2}(r^2 + 2a^2) \tag{3.12}$$

Equation (3.9) can be integrated analytically and the result of (3.9) is presented in Figure 3.5. The figure is identical to the variance reduction factor obtained by

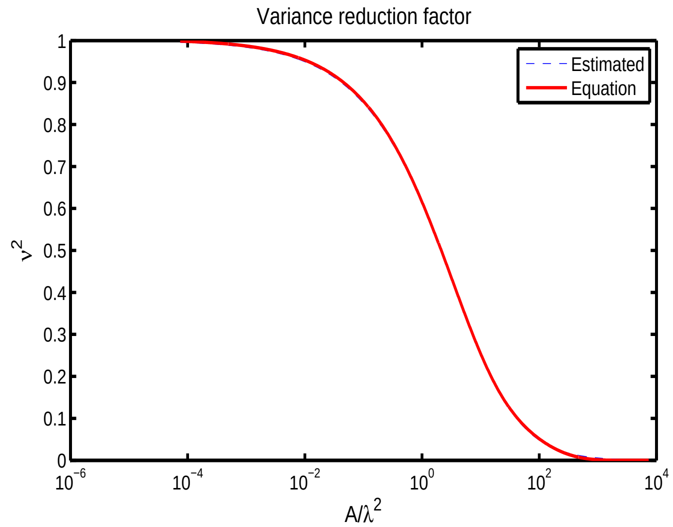

Figure 3.5: Variance reduction factor versus non dimensional catchment area $\frac{A}{\lambda^2}$. The catchment area is approximated by a square and the correlogram is exponential.

Rodriguez-Iturbe and Mejia (1974) in their figure 5. From Figure 3.5, it is found that when the area tends to zero, the variance reduction factor goes to 1 as one should expect. The variance reduction factor decreases with the increase of area. More specifically, $\nu^2 \to 0$ when $A \to \infty$. An accurate approximation of the curve in Figure 3.5 can be written as

$$\nu^2 = 0.75 \exp(\frac{-0.63\sqrt{A}}{\lambda}) + 0.25 \exp(\frac{-0.16\sqrt{A}}{\lambda}) \tag{3.13}$$

Equation (3.13) is a function of a square catchment area and the spatial correlation length, λ.

3.1.4 Parent distribution of areal average rainfall

When the point rainfall is exponentially distributed, the areal averaged rainfall will be approximately Gamma distributed [*Wood and Hebson* (1986);*Hebson and Wood* (1986);*Sivapalan et al.* (1990)]. The Gamma probability density function with parameters k_A and β_A is

$$f_{I_A}(i_A) = \frac{(\frac{i_A}{\beta_A})^{k_A-1} \exp\left(-\frac{i_A}{\beta_A}\right)}{\beta_A \Gamma(k_A)} \tag{3.14}$$

where index A indicate that the parameters pertain to the areal distribution. The mean and variance of the Gamma distribution are

$$\mu_A = k_A \beta_A \tag{3.15a}$$

$$\sigma_A^2 = k_A \beta_A^2 \tag{3.15b}$$

and from (3.2a), (3.2b), (3.6), and (3.7) it is found that

$$k_A \beta_A = \beta_p \tag{3.16}$$

$$k_A \beta_A^2 = \beta_p^2 \nu^2 \tag{3.17}$$

where ν^2 is the variance reduction factor estimated from (3.9) or (3.13) for a square area. From (3.16) and (3.17), the areal distribution parameters k_A and β_A can be expressed in terms of the point distribution parameters as:

$$k_A = \nu^{-2} \tag{3.18a}$$

$$\beta_A = \beta_p \nu^2 \tag{3.18b}$$

Equations (3.18a) and (3.18b) describe the change of parameters of the parent distribution of the areally-averaged rainfall with catchment area A.

3.1.5 Distribution of maximum annual point and areal precipitation

The discussion so far has focused on the distribution of daily precipitation on wet days. In the context of IDF curves, the main interest is in extreme values, i.e. the largest value in a calendar year. From extreme value theory it is known that the largest value of n exponentially distributed variables has an extreme value type I, also called Gumbel distribution. The same is true for the largest of n Gamma distributed variables. The Gumbel distribution has the form

$$F(i) = \exp\left[-\exp\left\{-\alpha_n(i-u_n)\right\}\right] \tag{3.19}$$

Assuming there are n wet days in a year, one can establish the following relationship between parent and extreme value distribution: For point rainfall

$$\alpha_{np} = \frac{1}{\beta_p} \tag{3.20a}$$

$$u_{np} = \beta_p \log(n) \tag{3.20b}$$

For areal rainfall

$$\alpha_{nA} = \frac{f_1(k_A)}{\beta_A} \tag{3.21a}$$

$$u_{np} = f_2(k_A)\beta_A \log(n) \tag{3.21b}$$

where f_1 and f_2 are functional approximations derived by *Sivapalan and Bloschl* (1998). These approximations are given by:

$$f_1(k_A) = 1 - 0.17l \log(k_A) \tag{3.22a}$$

$$f_2(k_A) = 0.39 + 0.61(k_A)^{0.8} \tag{3.22b}$$

In the case of point precipitation, the relationship between the Gumbel parameters and the exponential parameters is exact. For areal precipitation, the relationship between Gumbel parameters and Gamma parameters is an approximation. It should be noted that the approximations for f_1 and f_2 do not depend on data. Noting that $k_A\beta_A = \beta_p$ and $k_A = \nu^{-2}$, the relationship between the parameters of extreme point and areal rainfall can be written:

$$\frac{\alpha_{nA}}{\alpha_{np}} = \frac{f_1(k_A)/\beta_A}{1/\beta_p} = \frac{f_1(\nu^{-2})}{\nu^2} \tag{3.23a}$$

$$\frac{u_{nA}}{u_{np}} = \frac{f_2(k_A)\beta_A \log k_A}{\beta_p \log k_A} = \nu^2 f_2(\nu^{-2}) \tag{3.23b}$$

The usefulness of (3.23a) and (3.23b) is that these formulas provide a simple means of obtaining the parameters for the distribution of annual maximum areal rainfall from point (station) information.

3.1.6 An example application

To illustrate the methodology, IDF curves were developed for the Flin Flon station. It is assumed that the Gumbel distribution is appropriate for all durations, i.e.

$$F(i) = \exp\left[-\exp\left\{-\alpha_{np}(d)(i - u_{np}(d))\right\}\right] \tag{3.24}$$

where the notation $\alpha_{np}(d)$ and $u_{np}(d)$ highlights the dependence of the Gumbel parameters on durations. Precipitation quantiles can be found by inverting the CDF:

$$i = -\frac{\log(-\log(F))}{\alpha_{np}(d)} + u_{np}(d) \tag{3.25}$$

The Gumbel parameters were estimated using point rainfall intensity for durations of 1-hr, 2-hr, 6-hr, 12-hr, and 24-hr. Estimated parameters were then plotted against

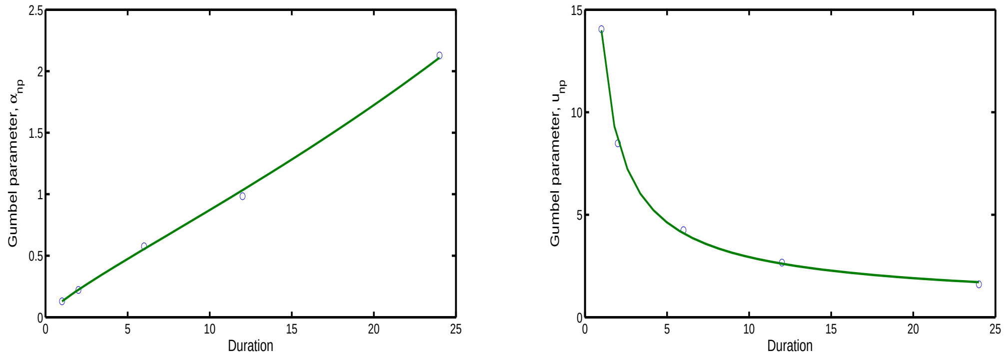

Figure 3.6: Fitted Gumbel parameters along with approximations for $\alpha_{np}(d)$ and $u_{np}(d)$ given in Equations (3.26a) and (3.26b).

durations to establish empirical relationships between the parameters and duration. The following empirical relationships were obtained for the Flin Flon station:

$$\alpha_{np}(d) = -0.2366 + 7.9986d^{-0.7618} \tag{3.26a}$$

$$u_{np}(d) = 0.3130 + 13.6862d^{-0.7183} \tag{3.26b}$$

Equations (3.26a) and (3.26b) are site-specific and must be obtained for each station. The fitted curves are presented in Figure 3.6. To get the Gumbel parameters for the areal averaged rainfall α_{np} and u_{np} were replaced in (3.23a) and (3.23b) by $\alpha_{np}(d)$ and $u_{np}(d)$ respectively resulting in

$$\alpha_{nA} = \alpha_{np}(d)\frac{f_1(\nu^{-2})}{\nu^2} \tag{3.27a}$$

$$u_{nA} = u_{np}(d)\nu^2 f_2(\nu^{-2}) \tag{3.27b}$$

Equations (3.27a) and (3.27b) give the general Gumbel parameters for the areally averaged extreme rainfall intensity, taking into account the effects of the catchment area and the correlation structure of rainfall. For point rainfall, IDF curves are shown in Figure 3.7. For a catchment area of 45 km by 45 km, corresponding to a CRCM grid cell IDF curves are presented in Figure 3.8. To illustrate the importane of catchment area, areal IDF curves were constructed for $A/\lambda^2 = 1$ and $A/\lambda^2 = 25$ and presented in Figures 3.9 and 3.10. The figures show that both the mean and standard deviation for extreme rainfall intensities decrease with the increase of catchment area but at different rates which implies that the coefficient of variation will change with catchment area.

With the increase of the area, IDF curves become flatter in appearance. When the area tends to zero, the curves approach the point IDF curves.

3.1.7 Estimation of the coefficient of variation of maximum annual areal rainfall

The mean and the standard deviation of maximum areal precipitation are related to the Gumbel parameters as follows:

$$\mu_A = u_{nA} + 0.5772/\alpha_{nA} \tag{3.28a}$$

$$\sigma_A = \frac{\pi}{\sqrt{6}\alpha_{nA}} \tag{3.28b}$$

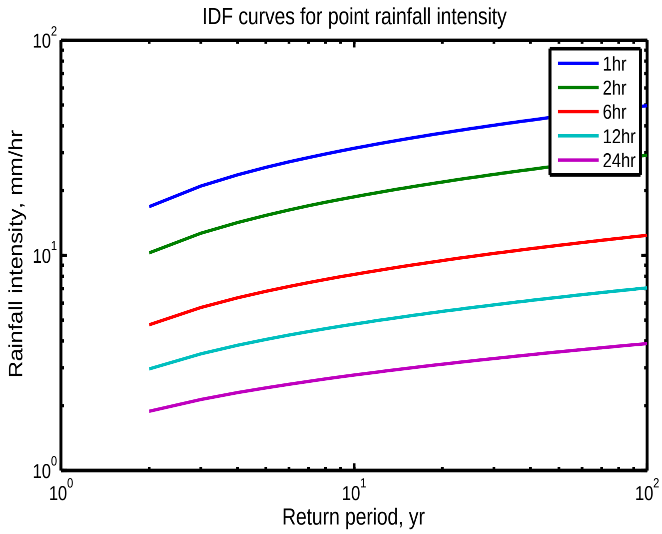

Figure 3.7: Point IDF curves for the Flin Flon station.

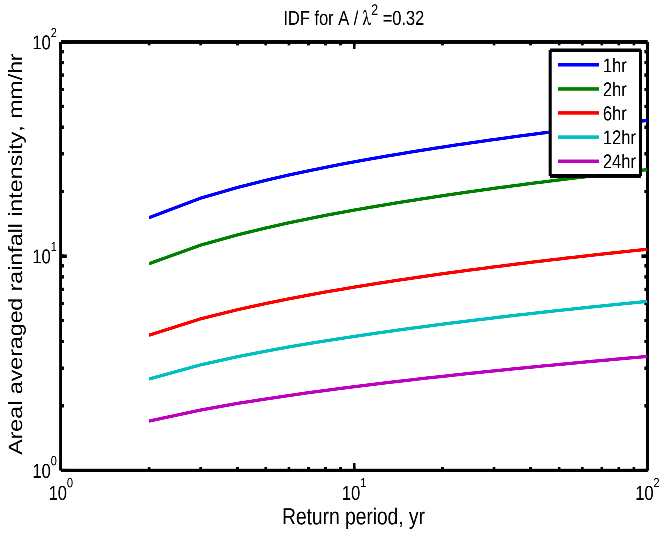

Figure 3.8: Areal IDF curves for the Flin Flon station for $\frac{A}{\lambda^2} = 0.32$.

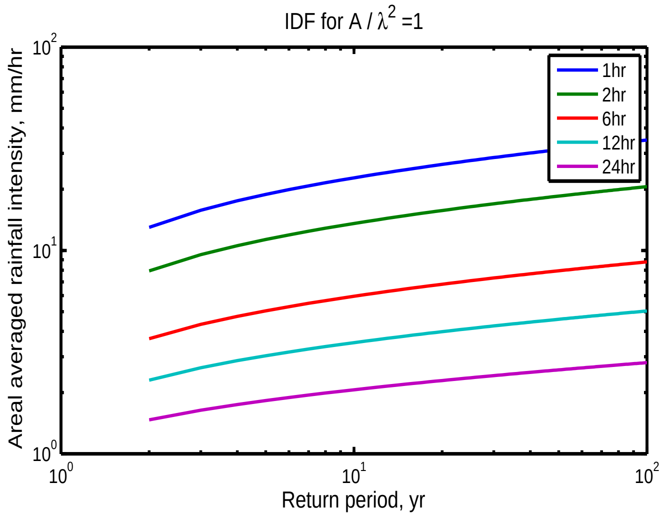

Figure 3.9: Areal IDF curves for the Flin Flon station for $\frac{A}{\lambda^2} = 1$.

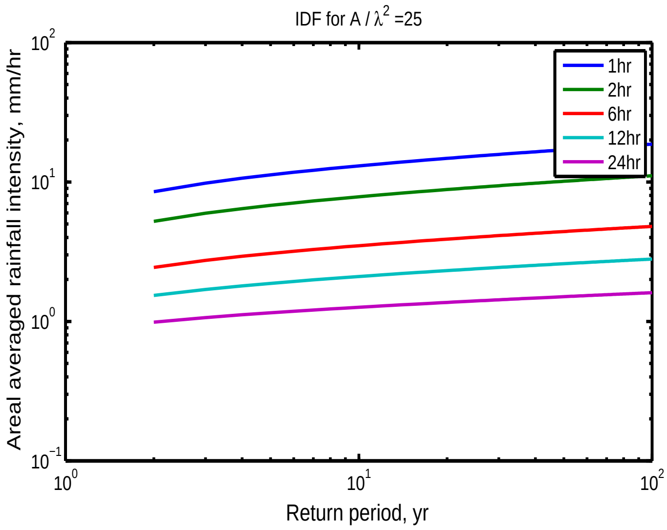

Figure 3.10: Areal IDF curves for the Flin Flon station for $\frac{A}{\lambda^2} = 25$.

Using (3.27a) and (3.27b), (3.28a) and (3.28b) can be expanded as

$$\mu_A = \nu^2 \left(u_{np}(d) f_2(\nu^{-2}) + \frac{0.5772}{\alpha_{np}(d) f_1(\nu^{-2})} \right) \tag{3.29a}$$

$$\sigma_A = \nu^2 \frac{\pi}{\sqrt{6}\alpha_{np}(d) f_1(\nu^{-2})} \tag{3.29b}$$

Combining (3.29a) and (3.29b), we have

$$CV_A = \frac{\sigma_A}{\mu_A} = \frac{\pi/\sqrt{6}}{0.5772 + \alpha_{np}(d) u_{np}(d) f_1(\nu^{-2}) f_2(\nu^{-2})} \tag{3.30}$$

For the point rainfall $\nu^2 = 1$ and substituting this value into (3.30) yields the coefficient of variation for the point extreme rainfall.

$$CV_p = \frac{\pi/\sqrt{6}}{0.5772 + \alpha_{np}(d) u_{np}(d)} \tag{3.31}$$

Figure 3.11 represents the coefficient of variation estimated using (3.30) and (3.31) for 24-hr duration rainfall. The coefficient of variation decreases with increase in catchment area.

3.1.8 Estimation of Areal Reduction Factor

The areal reduction factor is simply the ratio of $i_{A,d}(T)/i_{p,d}(T)$ and generally depends on duration and return period. ARFs can be obtained by the proposed method using the distributions of point and areal IDF curves. Quantiles $i_{p,d}(T)$ of point

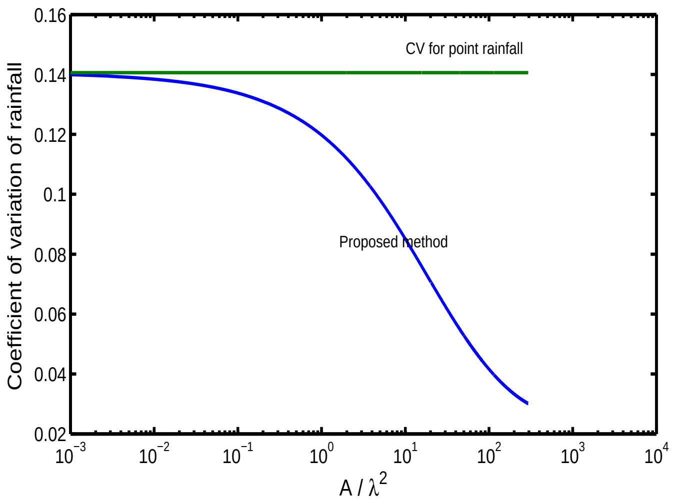

Figure 3.11: Coefficient of variation of areal maximum extreme rainfall intensities for 24-hr duration as a function of scaled catchment area A/λ^2 for the Flin Flon station.

precipitation can be found using (3.25) with $F = 1 - 1/T$ where T is the return period. Areal precipitation quantiles $i_{A,d}(T)$ can be derived using the expressions of α_{nA} and u_{nA} in (3.27a) and (3.27b). The ARF can then be expressed as:

$$ARF[\nu^2(A/\lambda^2), d, T] = \frac{\alpha_{np}(d)u_{np}(d)\nu^2 f_2(\nu^{-2}) - \frac{\nu^2}{f_1(\nu^{-2})}\log(\log(\frac{T}{T-1}))}{\alpha_{np}(d)u_{np}(d) - \log(\log(\frac{T}{T-1}))} \tag{3.32}$$

Equation (3.32) shows that the ARF depends on the catchment size, the return period, the duration, and the spatial correlation length. Figure 3.12 and 3.13 show that the ARF decreases with the increase of catchment area and return period. In Figure 3.12, ARFs were estimated for three return periods [$T = 2, 10, 100$] for the 24-hr duration.

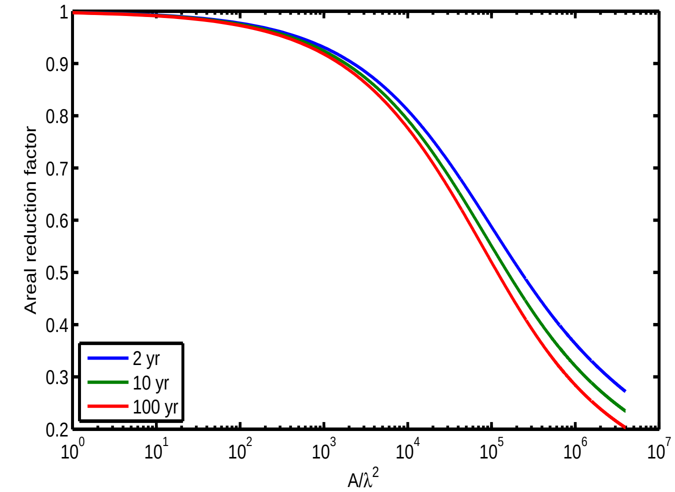

Figure 3.12: Areal reduction factor at the Flin Flon station for 24-hr precipitation as a function of scaled catchment area A/λ^2 and return period of T.

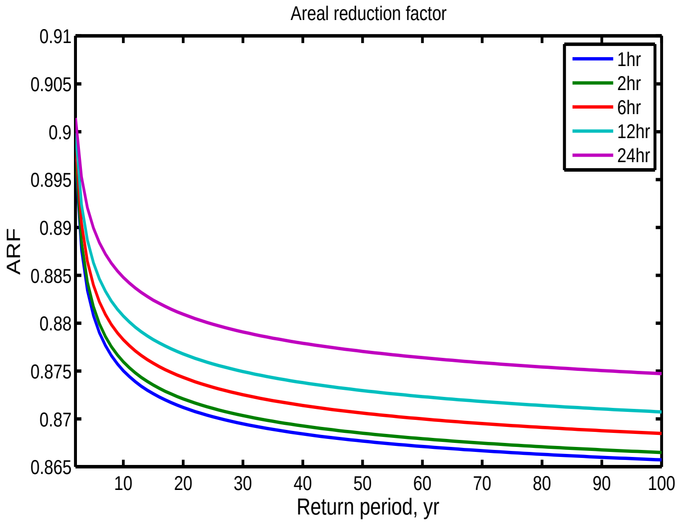

Figure 3.13: Areal reduction factor versus return period.

Chapter 4

IDF curves at the grid box scale

In this chapter, CRCM-simulated annual maximum rainfall depth series for 1-hr, 2-hr, 6-hr, 12-hr and 24-hr over Manitoba are analyzed and compared with the available observed data. The CRCM simulation were driven by the CGCM3 with the SRES-A2 scenario. Two periods were considered: 1961-2000 and 2041-2070. Areal reduction factors are used in combination with observations to produce areal IDF-curves that can be compared with IDF curves from CRCM simulations.

Gridded annual maxima precipitation from the CRCM are used to develop areal IDF curves in control and future climates using the Gumbel distribution. Figure 4.1 shows the expected changes in the future climate. One finding from the figure is that rainfall intensities increase significantly more for shorter durations because the rainfall depth is more localized at smaller durations.

The ratio of future and control rainfall intensities for a specific duration and a specific return period of simulated data is shown in Figure 4.2. The figure provides

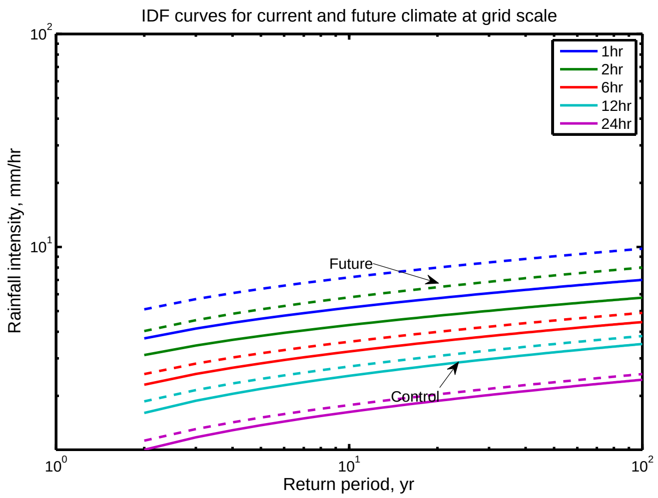

Figure 4.1: IDF curves for control and future climate at the Flin Flon station. Solid lines: control climate; dashed lines: future climate. Similar colors correspond to the same duration.

a quick view of the anticipated increase of rainfall intensities due to climate change. If the ratio is greater than 1, the rainfall intensity will increase and if the ratio is less than 1, the rainfall intensity will decrease in future.

Observation-based areal averaged IDF curves derived analytically can be compared with IDF curves at the grid box scale for the control climate. There is a significant difference between these IDF curves, particularly for shorter durations. Figure 4.3 shows IDF curves for 24-hr duration for which the difference between curves is minimum. This suggests that the CRCM cannot simulate maximum values very well, especially for shorter durations. The figures for other durations are given in Appendix A.1. Cumulative probability curves for the control and the future climate are presented in Figure 4.4 from which for a given rainfall intensity, the corresponding probability in the control and the future climate can be estimated.

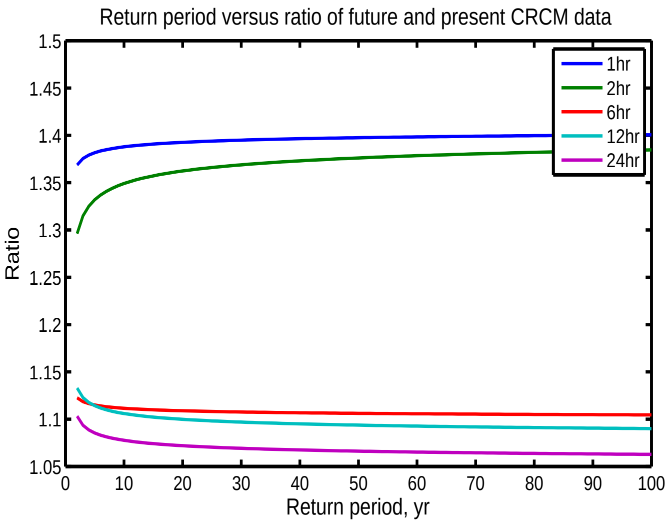

Figure 4.2: Ratio of future and control climate of simulated data at the Flin Flon station.

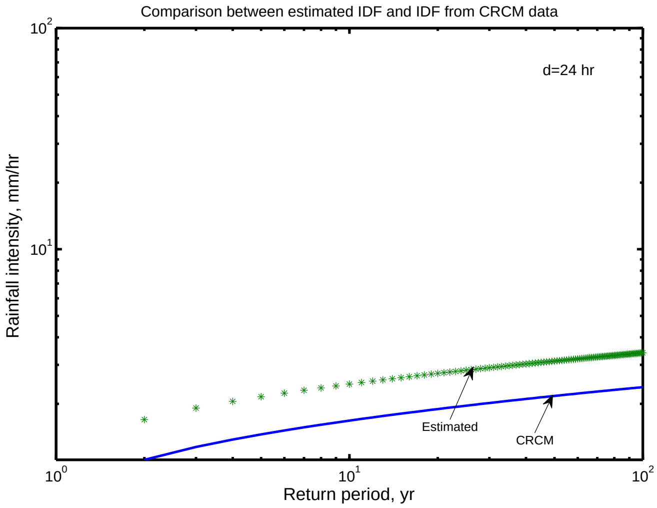

Figure 4.3: Comparison of IDF curves of areal and CRCM precipitation for 24-hr duration at the Flin Flon station.

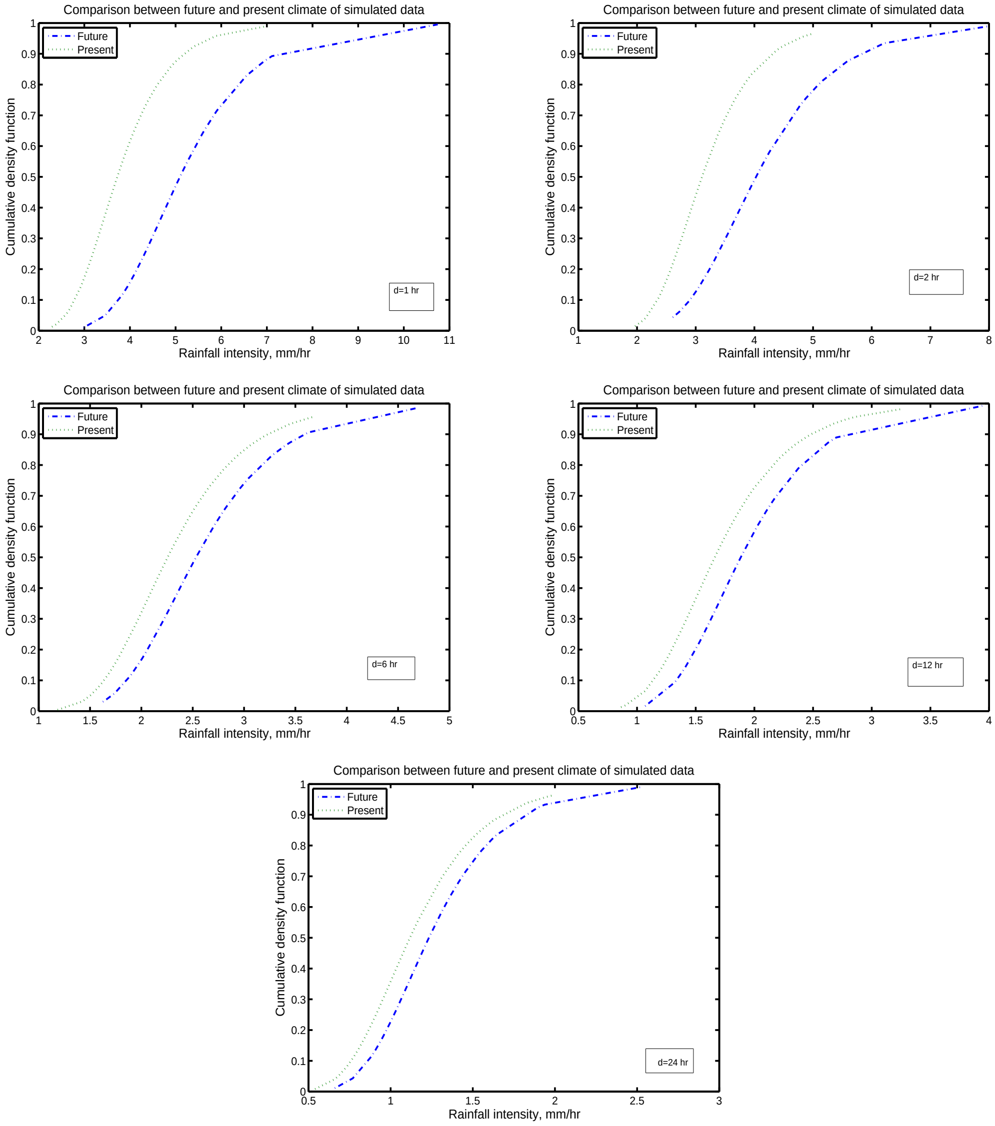

Figure 4.4: Cumulative probability curves for the control and the future climate for each duration at the grid box scale.

4.1 Estimation of maximum annual rainfalls at the station scale

IDF curves are usually developed for point locations. Therefore some hypotheses must be put forward in order to transpose the gridded climate model data to the station scale. In this study, two methods are used:

- Constant ARF approach
- Δ-method

These two methods are briefly described in the following sections.

4.1.1 Constant ARF approach

In the previous sections, ARFs were derived analytically from observed daily data. Generally, ARF tends to one for 24-hr duration and then decrease for shorter durations. ARF may alternatively be derived using a combination of observed data and CRCM simulated data. One can define ARFs as the ratio of rainfall quantiles for a specific duration and a specific return period from CRCM simulations and quantiles from observations for the same duration and return period. The relationship at the grid box and the station scale can be expressed by

$$ARF(d, T) = \frac{i_{A,d}(T)}{i_{p,d}(T)} \qquad (4.1)$$

ARFs defined in this way integrate model bias with the traditional correction needed to convert areal (gridded) data to point data. There are generally high discrepancies between analytically derived ARFs and ARFs derived from the CRCM. For the Flin Flon location, ARFs based on the CRCM are quite small, indicating biases in the CRCM. The results for Flin Flon are shown in Figure 4.5. These figures can be used to correct biases involved in the CRCM data. ARFs estimated analytically from observations were based on 24-hr duration rainfall intensities. ARFs for shorter durations are higher. If duration-dependent ARFs had been used, the results presented in Figure 4.5 would be different.

The approach was used to generate future IDF curves at the station scale. Increases in rainfall depths for a specific duration and a specific return period at the grid box scale were used to estimate the rainfall depths at the station scale for the future climate according to the following formula:

$$i_{pf,d}(T) = i_{p,d}(T)[1 + \delta^{g}_{control-future}(d,T)] \tag{4.2}$$

where

$$\delta^{g}_{control-future}(d,T) = \frac{i_{Af,d}(T) - i_{A,d}(T)}{i_{A,d}(T)} \tag{4.3}$$

By substituting (4.3) in (4.2), one obtains

$$i_{pf,d}(T) = i_{p,d}(T)\frac{i_{Af,d}(T)}{i_{A,d}(T)} \tag{4.4}$$

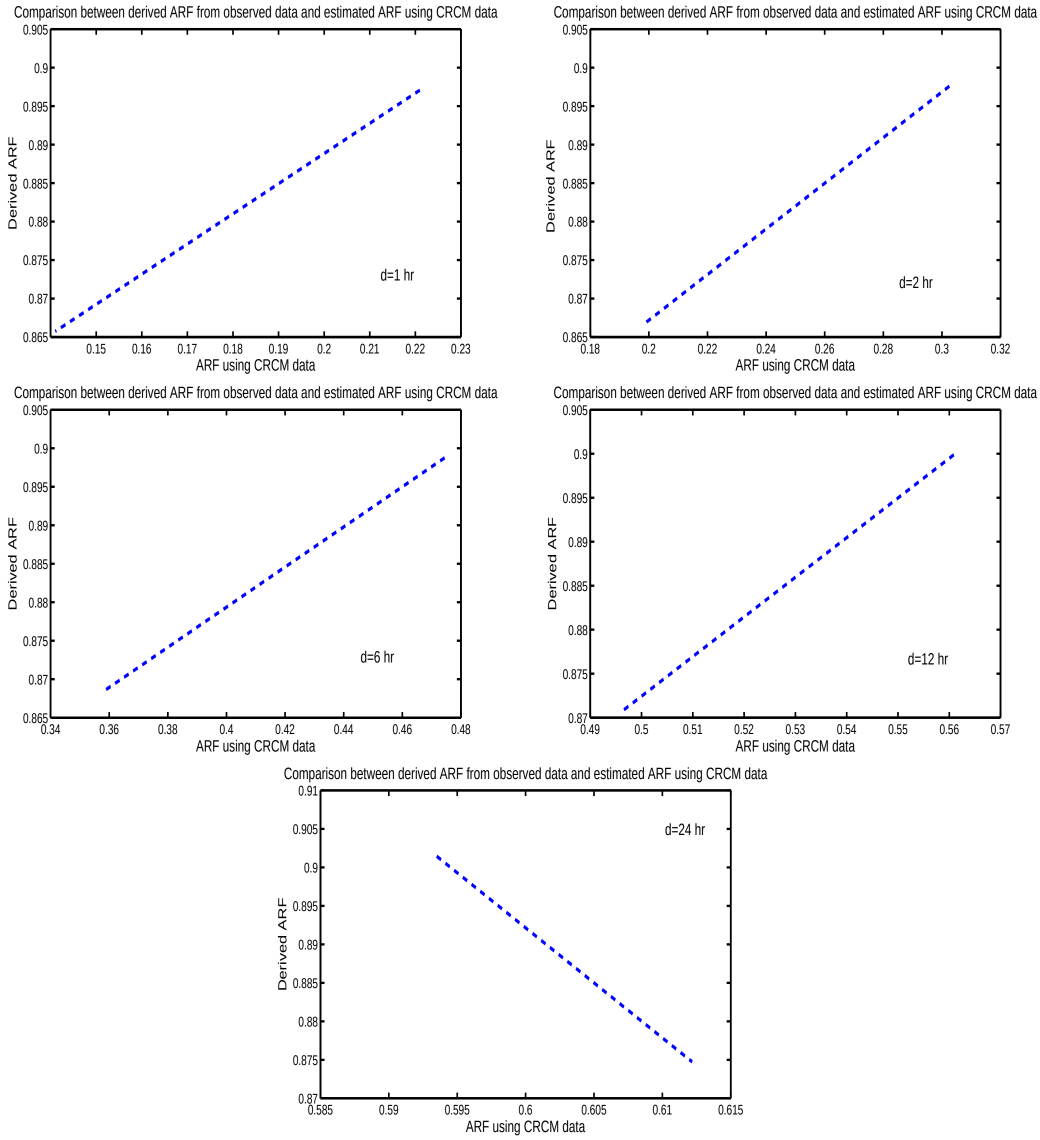

Figure 4.5: ARF's derived analytically from observations versus ARF's defined as the ratio of CRCM quantiles and observed quantiles. Data are from the Flin Flon station.

where

- $i_{p,d}(T)$=Rainfall quantiles at the station scale for present climate,
- $i_{pf,d}(T)$=Rainfall quantiles at the station scale for future climate,
- $i_{A,d}(T)$= Areal averaged rainfall quantiles for present climate,
- $i_{Af}(T)$=Areal averaged rainfall quantiles for future climate.

The assumption inherent in (4.4) is that ARFs do not change between current and future climate, i.e. that

$$ARF_f = ARF_p \tag{4.5}$$

Areal IDF curves were determined using the Gumbel distribution and the procedure described in Chapter 3, in particular Equations (3.27a) and (3.27b). Areal IDF curves and IDF curves at the station scale are shown in Figures 4.6 and 4.7. The figures suggest that rainfall quantiles will increase. The predicted changes are relatively larger for shorter durations.

Cumulative probability curves using the Gumbel distribution were developed for point, areal, and simulated data for the present climate at the Flin Flon station. The CRCM simulation underestimates extreme values for shorter durations. The 1-hr and 24-hr duration cumulative probability curves are shown in Figure 4.8. The difference between estimated areal and simulated rainfall depth is significant. For the 1-hr duration, there is a big difference between point and simulated data. For the 24-hr duration, the difference is still big but not as high as for the 1-hr duration. Bias

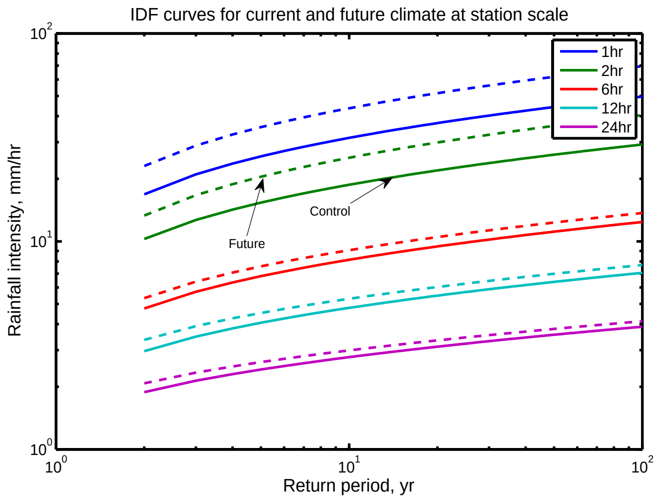

Figure 4.6: Comparison of IDF curves of the control and future climate at the station scale for the Flin Flon station. Solid lines: control climate and dashed lines: future climate. Similar colors correspond to the same duration.

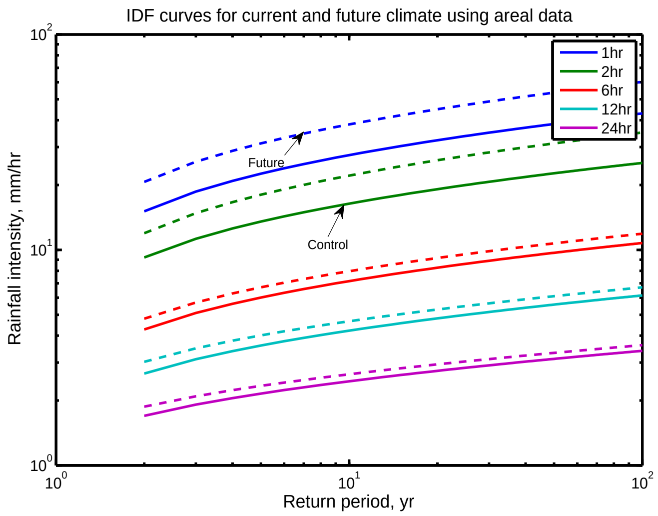

Figure 4.7: Comparison of IDF curves estimated from areal data for the control and future climate at the Flin Flon station. Solid lines: control climate and dashed lines: future climate. Similar colors correspond to the same duration

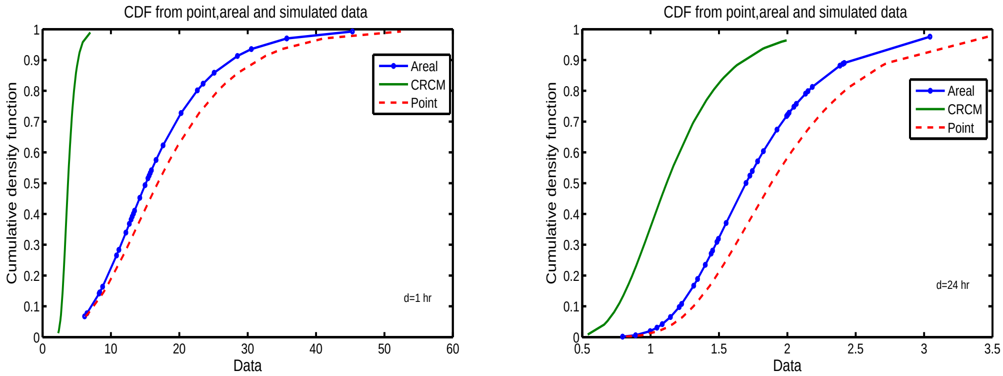

Figure 4.8: Cumulative probability curves for 1-hr and 24-hr duration for the present climate.

correction is not applied to adjust any distortion and for shorter durations, CRCM simulated data underestimate the true quantiles. The results for other durations can be found in Appendix A.2.

Cumulative probability curves were developed for other stations and showed discrepancies fairly similar to those for the Flin Flon station. For a few selected stations the results for the 24-hr duration are shown in Figures 4.9, 4.10, and 4.11.

4.1.2 Δ-approach for future prediction

In this method, a Δ-factor is determined as the ratio of the mean of the future simulation and the mean of the control simulation for each duration:

$$\Delta_d = \frac{mean(i_{Af,d})}{mean(i_{A,d})} \tag{4.6}$$

The inherent assumption is that the mean change of simulated data will be the same at the station scale and that the change only depends on durations, not on return

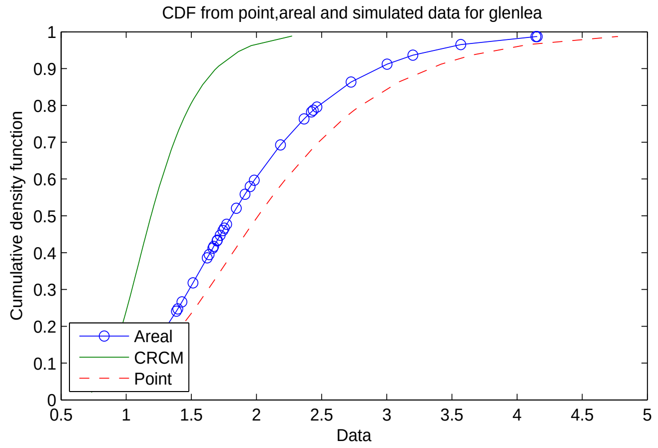

Figure 4.9: Cumulative probability curves at the Glenlea station for 24-hr duration.

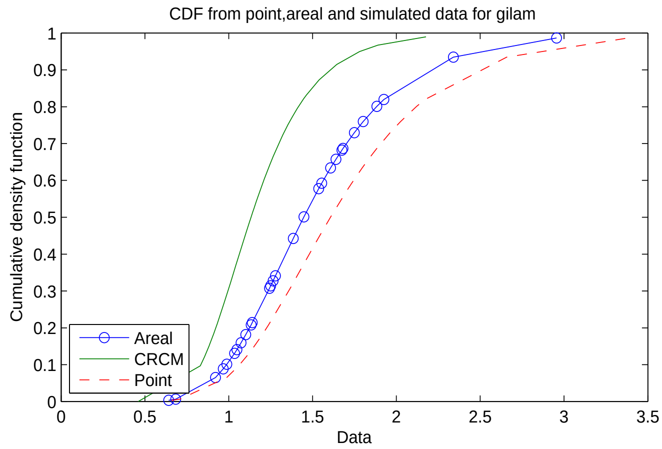

Figure 4.10: Cumulative probability curves at the Gillam station for 24-hr duration.

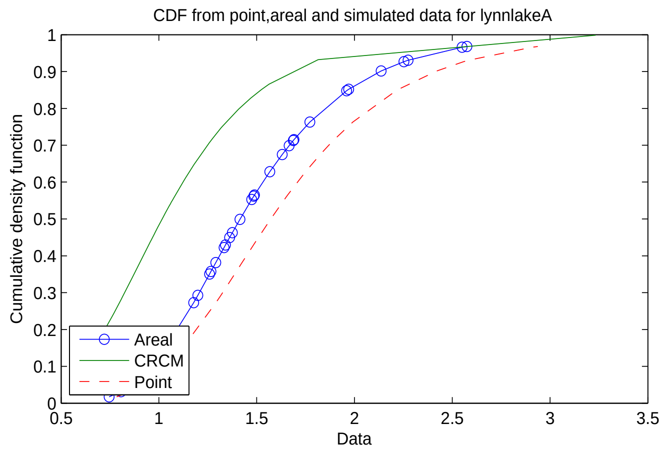

Figure 4.11: Cumulative probability curves at the Lynnlake station for 24-hr duration.

periods. The station data is multiplied by the Δ-factor to determine station data in the future climate. Therefore, according to this method the rainfall intensity at the station scale for the future climate is

$$i_{pf,d} = i_{p,d}\Delta_d \tag{4.7}$$

A similar procedure is done for areal data estimated from the observed data. Figures 4.12, 4.13 and 4.14 show that the rainfall intensity is projected to increase in future.

4.2 Comparison between constant ARF and Δ-method

Areal IDF curves estimated from point IDF curves and from climate model information are shown in Figure 4.15. The figure shows that the CRCM based rainfall quantiles are significantly smaller than the estimated areal rainfall intensities.

As there is a big difference between the estimated areal rainfall intensity and the CRCM rainfall intensity, it is necessary to correct biases in the CRCM. The two methods described above, the constant ARF approach and the Δ-method, were used to estimate future changes. For 100-year events, the relative changes are shown in Table 4.1. The relative changes are determined by

$$RD = \frac{i_{future,d}(T) - i_{control,d}(T)}{i_{control,d}(T)} \times 100 \tag{4.8}$$

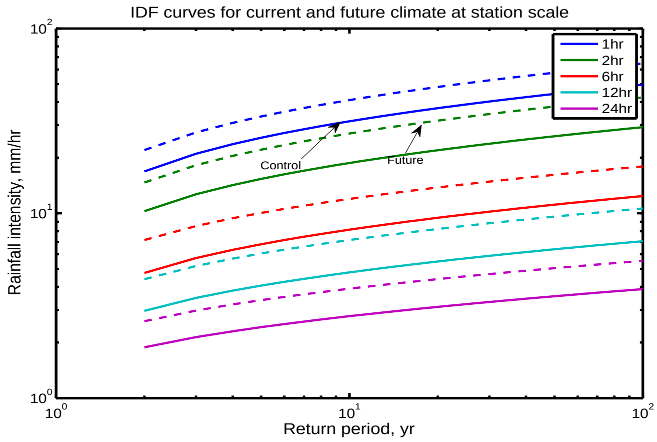

Figure 4.12: IDF curves at the Flin Flon station using Δ-method. Solid lines: control climate; dashed lines: future climate. Similar colors correspond to the same duration.

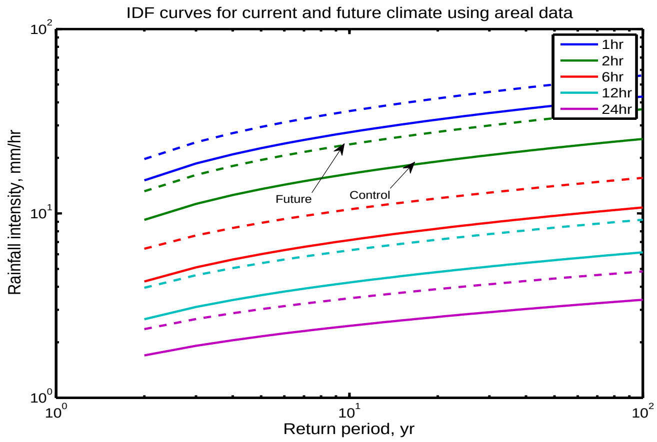

Figure 4.13: IDF curves for areally averaged rainfall intensity at the Flin Flon station using Δ-method. Solid lines: control climate; dashed lines: future climate. Similar colors correspond to the same duration.

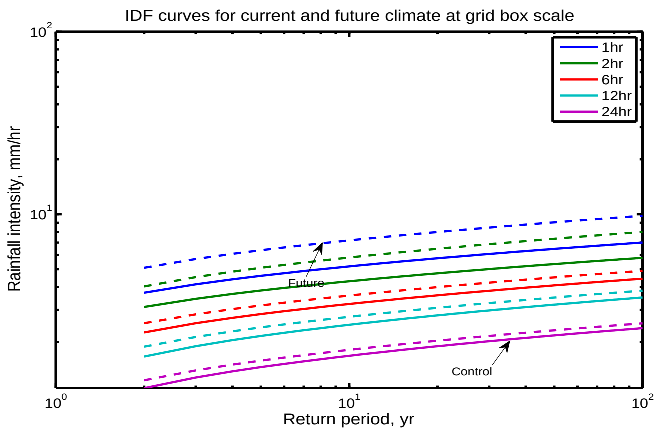

Figure 4.14: IDF curves at the grid box scale for the Flin Flon station. Solid lines: control climate; dashed lines: future climate. Similar colors correspond to the same duration.

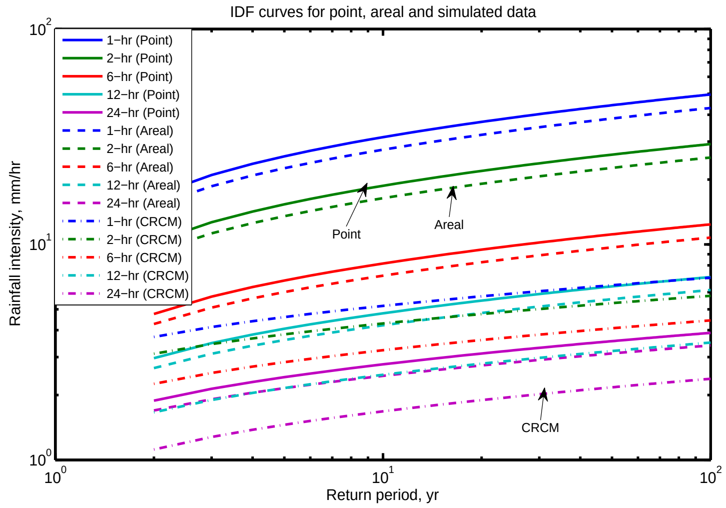

Figure 4.15: Comparison between observed, CRCM, and estimated areal rainfall intensity at the Flin Flon station.

Table 4.1: Relative changes (percentage) in the future climate from the constant ARF method and the Δ-method.

Method	1 hr	2 hr	6 hr	12 hr	24 hr
Constant ARF approach (CRCM and estimated areal)	28	27	9	8	6
Δ approach (Estimated areal)	23	31	30	33	29
Δ approach (CRCM)	28	27	9	8	6

It is noticeable that in the constant ARF approach, future changes decrease with the increase of duration. It is also found that future changes increase with the increase of return period. The constant ARF approach depends on both duration and return period. The relative changes for point, areal and CRCM are similar as the changes only depend on the ratio of rainfall quantiles for the future climate and rainfall quantiles for the control climate from simulations. The Δ-method depends only on duration. The percent change between the future and the control climate is the same at each point. There is no variation with return periods. The relative change only varies with durations.

Chapter 5

Scaling models for IDF curves

5.1 Regionalization

In this section, regional IDF curves are developed. Regionalization is useful to reduce the impact of local variability, providing more stable information about extreme precipitation statistics for a region. For the purpose of this study, stations were grouped according to their geographical location. Four groups were selected and shown in Table 5.1.

The cumulative probability distributions were plotted for the four regions (Figure 5.1). The curves are close to each other for each region. The figures were plotted using the generalized extreme value distribution (GEV). The Churchill station is located at the northern edge of the province of Manitoba and gives results that are different from other stations. For this reason, this station was grouped alone where other stations were grouped according to their proximity. Within each region,

Table 5.1: Grouping according to geographical location.

Region 1	Region 2	Region 3	Region 4
Churchill	Lynn lake	Flin Flon	Dauphin
	Thompson	Norway house forestry	Bissett
	Gilam	Island lake	Brandon
		The Pas	Brandon CDA
			Neepawawater
			Portage Southport
			Glenlea
			Indian Bay
			Pilot Mound
			Morden
			Deerwood

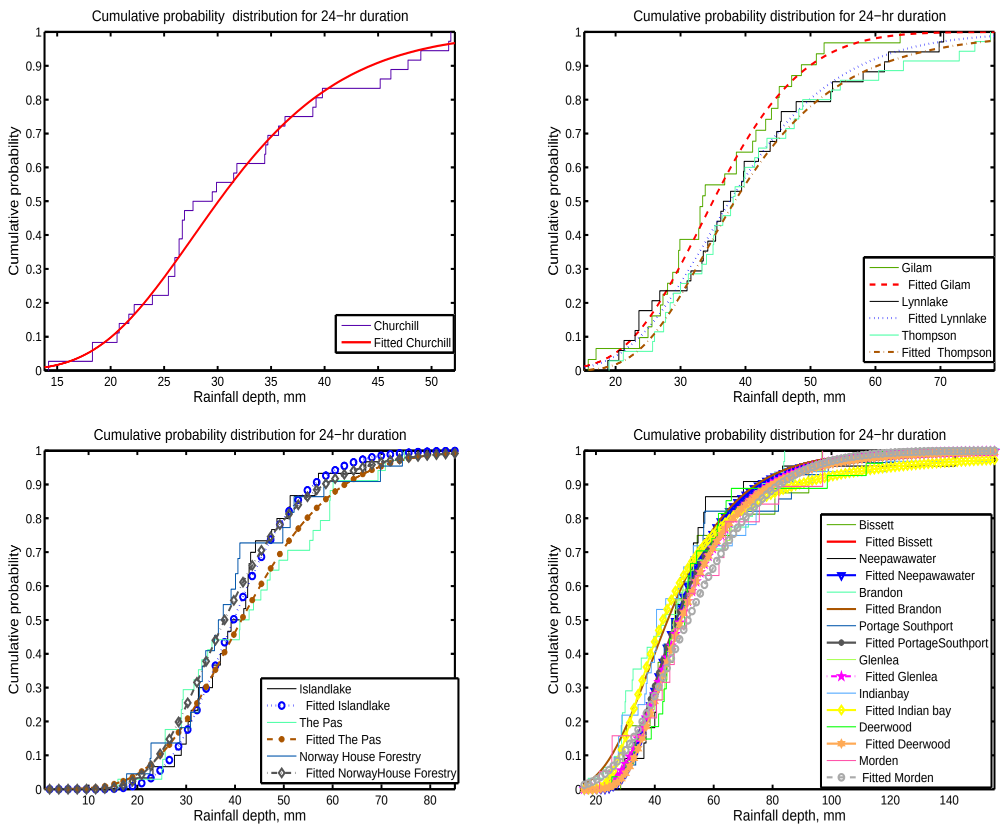

Figure 5.1: Cumulative probability distribution for each region for 24-hr duration annual extreme rainfall.

stations give fairly similar results. Some stations were later discarded as they did not follow the simple scaling law. From Region 3, Flin Flon was discarded and from Region 4, Dauphin, Pilot Mound, and Brandon CDA were discarded.

5.2 Generalized extreme value distribution

Hydrologic variables such as maximum rainfall and floods are often described by extreme value distributions. The generalized extreme value (GEV) distribution was used to construct IDF curves in this study. The GEV cumulative distribution function of x can be written in the form (given by *Aronica and Freni* (2005))

$$F(x) = \exp(1 - \kappa \frac{x - \alpha}{\epsilon})^{\frac{1}{\kappa}} \tag{5.1}$$

where ϵ is the location parameter, α is the scale parameter, and κ is the shape parameter. The range of the variable x depends on the sign of κ. When κ is negative, the GEV distribution is a Type II extreme value distribution (EV2). In this case $C_s > 1.14$ and the variable x is restricted to the interval $\epsilon + \frac{\alpha}{\kappa} < x < \infty$. When κ is positive, the GEV distribution is a Type III (EV3) extreme value distribution with $C_s < 1.14$, and is restrcited to the interval $\infty < x < \epsilon + \frac{\alpha}{\kappa}$. When $\kappa = 0$, the GEV distribution becomes a Type I extreme value distribution (EV1) which is the same as the Gumbel distribution used previously in the thesis.

Parameters can be estimated by the method of moments, probability weighted moments (PWM), and maximum likelihood (ML). Here, the parameters were estimated by the method of moments. The moment equations can be expressed as

$$C_s = \frac{\kappa[-\Gamma(1+3\kappa) + 3\Gamma(1+\kappa)\Gamma(1+2\kappa) - 2\Gamma(1+\kappa)^3]}{|\kappa|(\Gamma(1+2\kappa) - \Gamma(1+\kappa)^2)^{1.5}}, \quad \kappa > -\frac{1}{3} \tag{5.2a}$$

$$\alpha = \sqrt{\frac{\kappa^2 S^2}{\Gamma(1+2\kappa) - \Gamma(1+\kappa)^2}} \tag{5.2b}$$

$$\epsilon = E - \frac{\alpha}{\kappa}(1 - \Gamma(1+\kappa)) \tag{5.2c}$$

where Γ denotes the gamma function, and E, S, and C_s are the sample mean, standard deviation, and coefficient of skewness respectively. In practice, the shape parameter κ can be determined by tabulating the C_s-κ relationship and using table interpolation to find the value of κ that corresponds to an observed value of C_s. The relationship between C_s and κ is shown in Figure 5.2. The distribution function of x can be written in inverse form as

$$x_T = \epsilon + \frac{\alpha}{\kappa}\left[1 - \exp\left\{-\kappa(-\log(\log(\frac{T}{T-1})))\right\}\right] \tag{5.3}$$

5.3 Mean values bias correction

In Chapter 3, it was shown that the CRCM cannot simulate extreme precipitation very well. Some types of bias corrections are therefore required before using model output for decision making. In this study, two types of bias corrections were used:

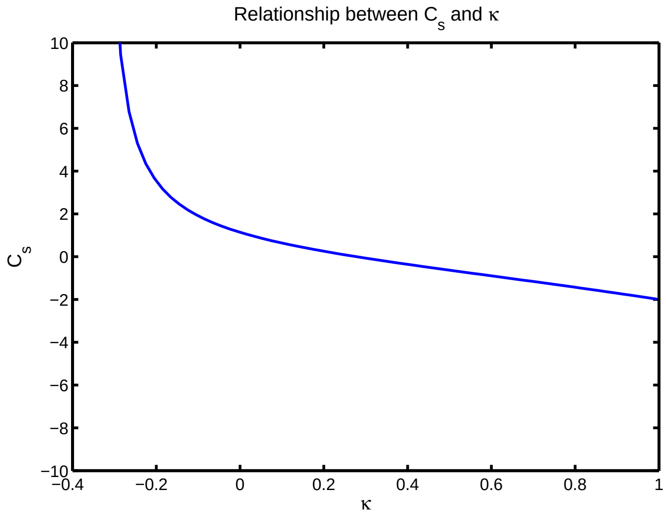

Figure 5.2: Relationship between the skewness coefficient and κ for the GEV distribution.

- Mean values bias correction
- QQ bias correction

CRCM simulation runs were used to construct future IDF curves using the GEV distribution. For each duration, δ was determined as the ratio of the mean of observations (x_{obs}) and the mean of control simulation run (x_{sim}).

$$\delta = \frac{\overline{x}_{obs}}{\overline{x}_{sim}} \tag{5.4}$$

With the mean value bias correction method, future simulation values were multiplied by δ values to correct model biases. In a similar way, the control run was also corrected and used to construct IDF curves.

5.4 QQ bias correction

The CRCM extreme annual precipitation was also corrected using the method of QQ mapping in which the CDF of CRCM rainfall amounts from the control run is mapped into the observed rainfall depth distribution. Both the observed rainfall and the CRCM rainfall are well fitted by the GEV distribution. Let F_{obs} be the cumulative distribution function of observed annual extreme rainfalls and F_{sim} be the cumulative distribution function of the corresponding simulated precipitation from the control simulation. Corrected CRCM precipitation can be calculated by

$$x' = F_{obs}^{-1}(F_{sim}(x)) \tag{5.5}$$

5.5 Scaling method

Let $P(t)$ be the instantaneous rainfall rate at time t at a point in space (rain gauge station). The rainfall depth over a duration d is then

$$P_d(t) = \int_{t-d/2}^{t+d/2} P(\tau)d\tau \tag{5.6}$$

According to *Burlando and Rosso* (1996), the annual maximum value H_d for a duration d is defined by the property of scale invariance

$$H_{\lambda d} \overset{dist}{=} \lambda^{\beta} H_d \tag{5.7}$$

where λ is a scale factor and β is a scale exponent. This property is called strict sense simple scaling (*Gupta and Waymire*, 1990). Quantiles and raw moments of any order are scale invariant, i.e.

$$h_{\lambda d,T} = \lambda^{\beta r} h_{d,T} \tag{5.8}$$

$$E[H_{\lambda d}^{r}] = \lambda^{\beta r} E[H_{d}^{r}] \tag{5.9}$$

where r is the order of moments and $\beta r = n_r$ is the scaling exponent of the mean. The strict sense simple scaling implies that $H(d)$ and $(\lambda^{-\beta} H(\lambda d))$ have the same probability distribution whereas in wide sense simple scaling, they are only required to have the same moments. In practice, it is much easier to test the variability of scaling laws on the basis of moments and this will be the approach used here. While strictly one cannot infer that the scaling of moments imply strict sense simple scaling, this will be the pragmatic assumption in what follows.

The derivation of depth-duration-frequency curves depend on the estimation of β. The scaling method is useful when data for some time intervals of interest do not exist but longer duration data are available.

5.5.1 Simple scaling GEV model

Maximum annual rainfall intensities for all available durations are modelled by the GEV distribution which is well fitted to observations. Quantiles $H_{d,T}$ can be found by

$$h_{d,T} = E[H_{24}^1] x_T \lambda^\beta \tag{5.10}$$

where x_T is the Tth quantile of annual maximum storm depth normalized by its mean for any duration in the range of existence of a scaling behavior and $E[H_{24}^1]$ is the mean annual maximum rainfall depth of the reference duration, assumed here to be 24-hr and λ is the ratio of duration and the reference duration. For example, for a 12-hr storm, λ would be 0.5. For the GEV distribution, x_T can be computed by (5.3). An implication of the simple scaling hypothesis is that the scale and the shape parameters are independent of the duration (*Burlando and Rosso*, 1996).

5.5.2 Log-normal multiscaling model

Sometimes temporal rainfall and extreme events in particular are far from the simple scaling behavior and precipitation fields may show so-called multiscaling behavior. According to the multiscaling definition, $n_r \neq \beta r$ which means the scaling exponent, n_r is not proportional to the order r of the moment. One can assume that

$$E[H_{\lambda d}^r] = \lambda^{\beta \phi_r r} E[H_d^r] \tag{5.11}$$

where ϕ_r is a dissipation function describing the departure of the growth of curve from the linear behavior with respect to the order r of the raw moment ($\phi_r = 1$). In multiscaling, the coefficient of variation, the skewness and the kurtosis increase with duration while these are constant in simple scaling. In this study, a log-normal multiscaling hypothesis was used to derive a parsimonious model of IDF curves.

Let d_* denote the reference duration. Then $\lambda = d/d_*$ and (5.11) becomes

$$E[H_d] = (\frac{E[H_{d_*}]}{d_*^{\beta}})d^{\beta} \tag{5.12}$$

Equation (5.12) can be written as

$$E[H_d] = a_1 d^{\beta} \tag{5.13}$$

where a_1 is the rescaled mean annual maximum rainfall for the reference duration. For the second order moment, (5.11) becomes

$$E[H_d^2] = (\frac{E[H_{d*}^2]}{d^{2\phi_2\beta}})d^{2\phi_2\beta} \tag{5.14}$$

Equation (5.14) can be written in the form of

$$E[H_d^2] = a_2 d^{2\phi_2\beta} \tag{5.15}$$

where a_2 is the rescaled second order raw moment of annual maximum rainfall for the reference duration and $H[d_*]$ is the maximum rainfall depth for the reference duration d_*. The two-parameter log normal distribution is widely used to describe extreme rainfalls. Its the probability density function can be written as

$$f_d(h) = \frac{1}{h\sqrt{2\pi}\sigma} \exp\left[-\frac{1}{2}(\frac{\log h - \mu}{\sigma})^2\right], \quad h > 0 \tag{5.16}$$

The parameters μ and σ are related to the mean and the standard deviation through the following equations

$$\mu = \log E[H_d] - \frac{1}{2}\log(1 + \frac{V[H_d]}{E^2[H_d]}) \tag{5.17a}$$

$$\sigma = \sqrt{\log\left(1 + \frac{V[H_d]}{E^2[H_d]}\right)} \tag{5.17b}$$

The T-year quantile can be written as

$$\log h_{d,T} = \mu + K_T\sigma \tag{5.18}$$

where K_T is the frequency factor of the standard normal distribution.

The log-normal multiscaling model for IDF curves can be derived by substituting (5.12) and (5.14) into (5.17a) and (5.17b). The resulting equations can be written as

$$\mu = \log\left(a_1 d^\beta\right) - \frac{1}{2}\log\left(\frac{a_2}{a_1^2} d^{2\beta(\phi_2 - 1)}\right) \tag{5.19a}$$

$$\sigma = \sqrt{\log\left[\frac{a_2}{a_1^2} d^{2\beta(\phi_2-1)}\right]} \tag{5.19b}$$

Substituting these expressions for μ and σ into (5.18) yeilds:

$$h_{d,T} = \frac{a_1^2}{a_2} \exp\left[K_T \sqrt{\log\left(\frac{a_2}{a_1^2} d^{2\beta(\phi_2-1)}\right)}\right] d^{(2-\phi_2)\beta} \tag{5.20}$$

Equation 5.20 has four parameters: the exponent β of the scaling relationship between the mean annual maximum rainfall and the temporal duration, the deviation ϕ_2 of the exponent of the second order raw moment from the simple scaling, a_1, and a_2. The parameters β and a_1 can be estimated by regression of the log-transformed sample means of rainfall depth against the corresponding log-transformed durations. Similarly, the values of n_2 and a_2 can be determined by regression of the log-transformed sampling second order raw moments against the corresponding log-transformed durations and $\phi_2 = \frac{n_2}{2\beta}$.

5.6 Development of regional IDF curves

Regional IDF curves were developed using the GEV distribution. When examining the observed and simulated data (Figures 5.3 and 5.4), it was found that some points appear inconsistent with the rest of the data. These data points are considered outliers. The box plots shown in Figure 5.3 and 5.4 are for the raingauge station at The Pas.

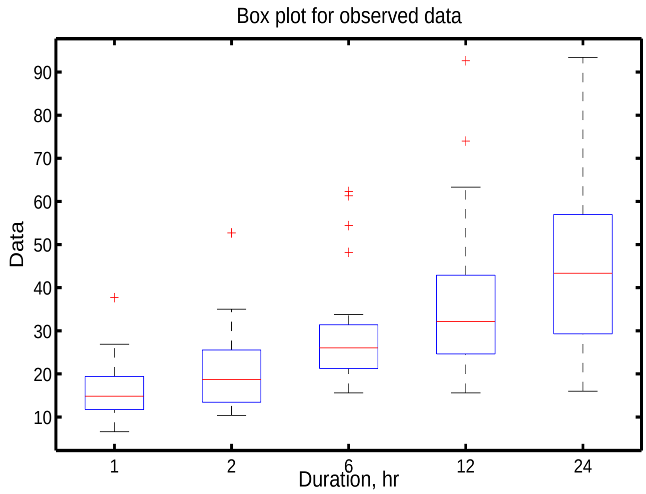

Figure 5.3: Box plot of precipitation depth for observations at The Pas station.

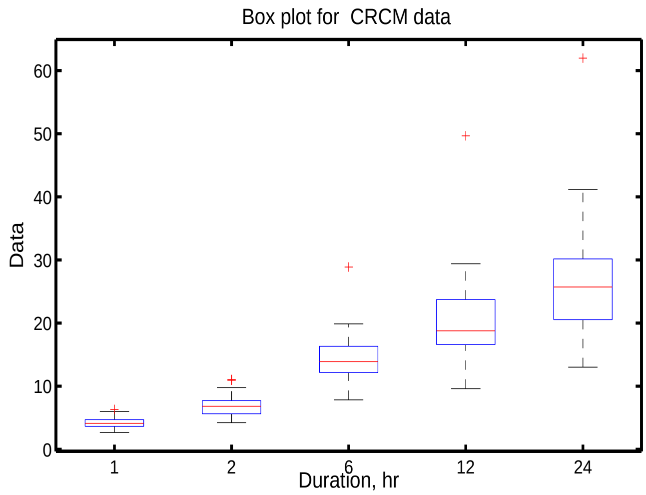

Figure 5.4: Box plot of precipitation depth for simulations at The Pas station.

To determine regional precipitation distributions, E, S, and C_s from individual sites in a region were averaged.

$$\widehat{C}_s = \frac{\sum_{i=1}^{m} C_{si} n_i}{\sum_{i=1}^{n} n_i} \tag{5.21a}$$

$$\widehat{E} = \frac{\sum_{i=1}^{m} E_i n_i}{\sum_{i=1}^{n} n_i} \tag{5.21b}$$

$$\widehat{S} = \frac{\sum_{i=1}^{m} S_i n_i}{\sum_{i=1}^{n} n_i} \tag{5.21c}$$

where m is the number of stations in a group and n_i is the number of data for station i. The regionalized values of E, S, and C_s were then used to determine the parameters of the regional GEV distribution using (5.2a) to (5.2c). The above calculation was done both for station data and for model data.

5.7 Development of regional IDF scaling model

To determine a regional simple scaling model, average regional values were estimated as

$$\widehat{E}[H_{24}^1] = \frac{\sum_{i=1}^{m} E_i[H_{24}^1] n_i}{\sum_{i=1}^{n} n_i} \tag{5.22a}$$

$$\widehat{\beta}_r = \frac{\sum_{i=1}^{m} \beta_{i,r} n_i}{\sum_{i=1}^{n} n_i} \tag{5.22b}$$

where m is the number of stations in a group and n_i is the sample size for station i. These regional values were used in (5.10) to determine precipitation quantiles.

Chapter 6

Results and Evaluation

In this chapter, the results from the methodologies described in Chapter 5 are presented and evaluated. Two methods are used for the prediction:

1. Bias correction for each duration (either δ-factor correction or QQ mapping)

2. Bias correction for the reference duration and use of the scaling laws estimated from observed data to obtain results for all other durations

6.1 Mean value bias correction

CRCM simulation runs were corrected by the mean value correction method. For each duration, δ was determined as the ratio of the mean of observations and the mean of the control simulation run (Equation 5.4). Figure 6.1 shows that δ is a decreasing function of duration. The nature of this relationship suggests that biases are particularly high for shorter durations which makes it difficult to compare observed

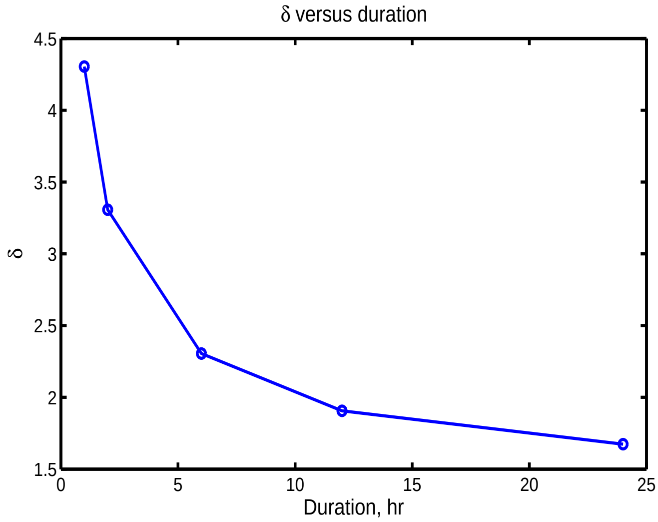

Figure 6.1: δ versus duration at the Brandon station. δ was determined as the ratio of the mean of observations and the mean of the control run for annual maximum rainfall.

Table 6.1: Scaling exponents from observed, control simulated, and future simulated data

Station	β from observations	β from control simulations	β from future simulations
Brandon	0.24	0.54	0.53
Glenlea	0.18	0.51	0.51
Lynn Lake	0.29	0.63	0.63
Churchill	0.32	0.59	0.59

and simulated precipitation quantiles. The shape of Figure 6.1 is not unexpected since the difference between point and areal precipitation quantiles will be higher for shorter durations. However, it is clear that model biases dominate, especially for shorter duration precipitation. Figure 6.1 suggests that scaling laws for observed and simulated precipitation will be different. More specifically, though both observations and control simulations follow simple scaling, the scaling exponents are different (Table 6.1). The difference can be established theoretically. From the simple scaling assumption in (5.7) applied to observations, one has

$$H_{\lambda d}^{obs} \overset{dist}{=} \lambda^{\beta_{obs}} H_d^{obs} \tag{6.1}$$

where H_d is the annual maximum value for a duration d, β_{obs} is the scaling exponent, and λ is the scale factor. The following relationship between mean values applies

$$\overline{H_{\lambda d}^{obs}} = \lambda^{\beta_{obs}} \overline{H_d^{obs}} \tag{6.2}$$

From the definition of δ, we have

$$\overline{H}_d^{obs} = \delta_d \overline{H}_d^{control} \tag{6.3}$$

and

$$\overline{H}_{\lambda d}^{obs} = \delta_{\lambda d} \overline{H}_{\lambda d}^{control} \tag{6.4}$$

Substitution of (6.3) and (6.4) into (6.2) yeilds:

$$\delta_{\lambda d} \overline{H}_{\lambda d}^{control} = \lambda^{\beta_{obs}} \delta_d \overline{H}_d^{control} \tag{6.5}$$

or

$$\overline{H}_{\lambda d}^{control} = \lambda^{\beta_{obs}} \frac{\delta_d}{\delta_{\lambda d}} \overline{H}_d^{control} \tag{6.6}$$

If the control simulation follows a simple scaling law, a relationship similar to (6.2) must apply:

$$\overline{H}_{\lambda d}^{control} = \lambda^{\beta_{control}} \overline{H}_{d}^{control} \tag{6.7}$$

From (6.6) and (6.7) one can deduce that

$$\lambda^{\beta_{control}} = \lambda^{\beta_{obs}} \frac{\delta_d}{\delta_{\lambda d}} \tag{6.8}$$

From (6.8), we must have

$$\frac{\delta_d}{\delta_{\lambda d}} = \lambda^{c} \tag{6.9}$$

and the scaling exponent for the control simulation run will be

$$\beta_{control} = \beta_{obs} + c \tag{6.10}$$

A value of c different from zero implies that there are biases in the CRCM simulation at least for some durations. Because of biases, the control simulation run has a scaling exponent that is around two times higher than for observed data. Figure 6.2 shows that a scaling model has some biases and that biases are larger for shorter durations. These δ-values determined from the mean value correction method were used to correct CRCM simulated data which do not represent extreme values very well. In this work, the Brandon raingauge station is used as an example.

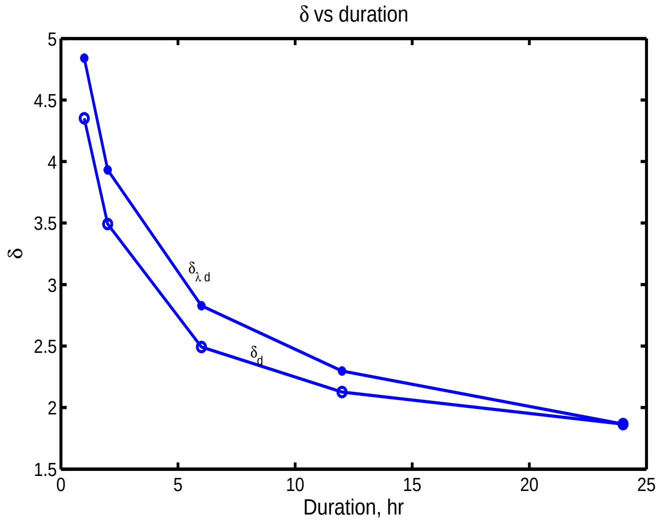

Figure 6.2: δ versus duration at the Brandon station. $\delta_{\lambda d}$ is determined from (6.9).

6.2 Δ- method

For each duration, Δ is defined as the mean of the future run (x_{fsim}) divided by the mean of the control run.

$$\Delta = \frac{\overline{x}_{fsim}}{\overline{x}_{sim}} \tag{6.11}$$

Observations are multiplied by Δ, resulting in bias corrected IDF curves for the future climate. The purpose of the Δ-values is to estimate IDF curves for the future climate at the station scale. Figure 6.3 shows Δ as a function of duration. It appears that there is no systematic relationship between Δ and duration.

6.3 Scaling method

The GEV distribution was used to construct IDF curves. The result is shown in Figure 6.4 where the lines are the direct output from the future simulation, stars are

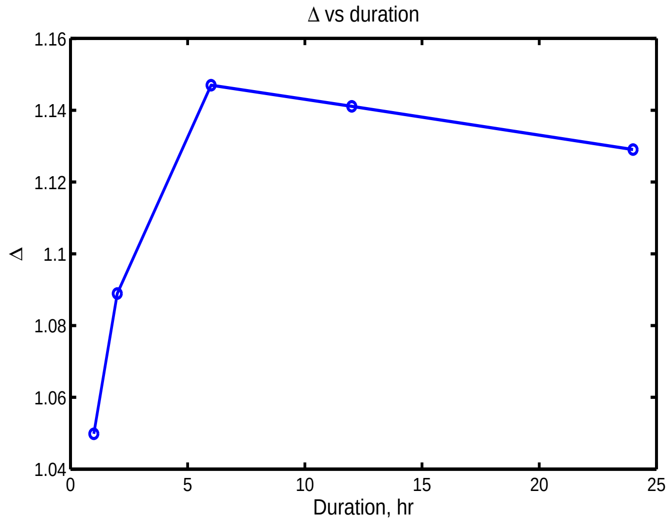

Figure 6.3: Δ versus duration at the Brandon station. Δ is determined as the ratio of the mean of the future run and the mean of the control run.

from bias-corrected future simulation, and circles are from the Δ-method. Projections by the two methods are fairly comparable with the bias-corrected simulation a bit lower than the Δ-method, especially for shorter durations.

The bias-corrected 24-hr precipitation was used in conjunction with scaling laws to produce corrected future precipitation at shorter durations. The assumptions are

- As durations become shorter, the model data become increasingly inaccurate and unlikely to be useful, even after bias correction

- The scaling properties are intrinsic to the climate system and will apply in the future as they do now.

For the corrected future simulation, IDF curves were developed using the simple scaling GEV distribution and are shown in Figure 6.5. It shows good agreement with the intensities found from the GEV distribution. For observations in the future

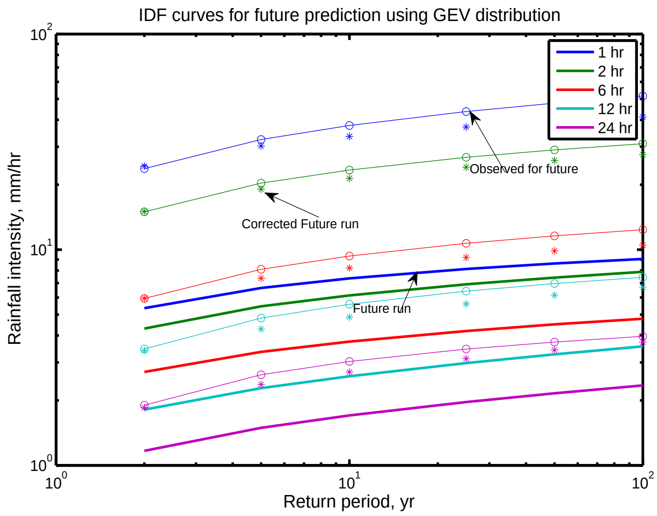

Figure 6.4: IDF curves for future prediction using the GEV distribution at the Brandon station. Corrected future run is determined by multiplying the future run by δ. Observed future data are determined by multiplying observed data by Δ. Solid lines: future simulations; circles: observed data for future climate using Δ-method; stars: corrected future simulations.

climate, IDF curves were also developed using the GEV distribution and the simple scaling GEV model and are shown in Figure 6.6. The simple scaling GEV model shows good agreement with the GEV distribution and hence, scaling laws can be used to develop IDF curves. The scaling-based curves were developed using the 24-hr duration as reference duration. This duration was preferred as 24-hr duration precipitation data are generally available. The advantage of this method is that extreme precipitation can be reproduced for each return period and each duration using only one scaling exponent.

For observations for the future climate and the corrected future simulation, IDF curves were developed using scaling laws. Figure 6.7 compares curves from these two approaches. Observations for the future climate are a little bit lower than the corrected future simulation because mean values cannot completely remove bias which can be seen by examining the quantile-quantile plot (Figure 6.8). The 24-hr duration quantile-quantile plot is shown in this figure which is based on the corrected simulation run and observations. For other durations, quantile-quantile plots are shown in Appendix A.3. The quantile-quantile plots show that for higher durations, the points fall roughly on the 45° line. These quantile plots were developed using Matlab's function qqplot.

IDF curves were developed for observations and control simulations using scaling laws. For observations and corrected control simulations, raw moments were plotted against durations and used to demonstrate that simple scaling applies. The detailed results are shown in Appendix A.4-A.7. Here, control simulated data were also determined by multiplying the control simulation run by the ratio of the mean of observations and the mean of the control run.

The observation-based IDF curves were developed using the simple scaling GEV model described in Section 5.5.1. The scaling model and the conventional GEV distribution agree well as shown in Figure 6.9 and so does the corrected control simulation run (Figure 6.10). A reference duration of 24-hr is considered because daily precipitation is generally available, so the scaling model can be used to reproduce precipitation quantiles for other durations. IDF curves for observed and corrected simulated extreme precipitation are compared in Figure 6.11. Observed curves are a bit higher than the control simulation after correction because the mean correction cannot completely remove biases.

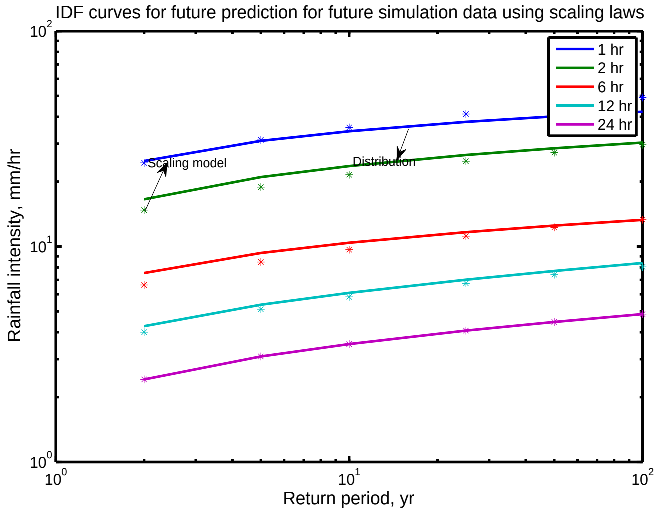

Figure 6.5: IDF curves for future prediction using future simulation along with scaling laws. Solid lines: GEV distribution; stars: simple scaling GEV model. The same color is used for each duration.

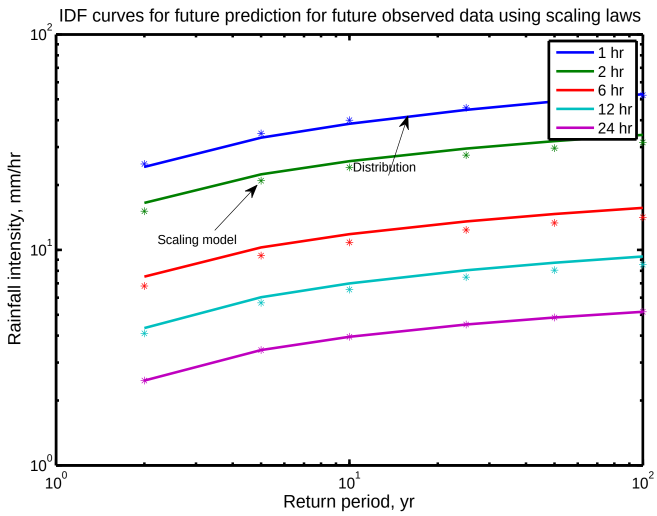

Figure 6.6: IDF curves for future prediction for Δ-method quantiles along with scaling laws. Solid lines: GEV distribution; stars: simple scaling GEV model. The same color is used for each duration.

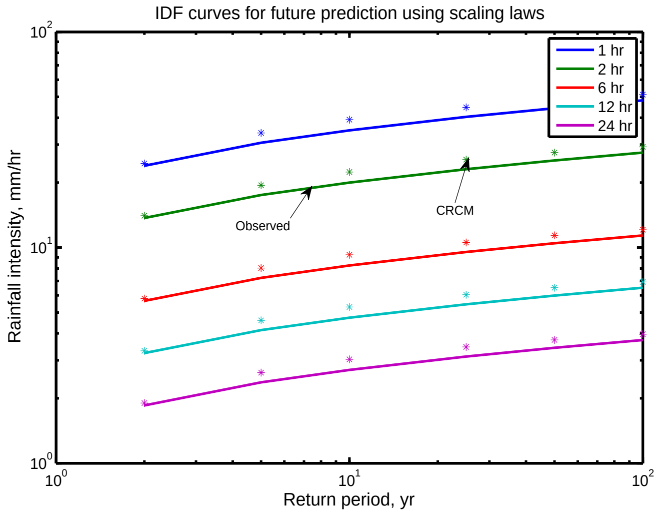

Figure 6.7: IDF curves from corrected CRCM data and future observed data for future prediction using scaling laws. Solid lines: observations; stars: CRCM simulations. The same color is used for each duration.

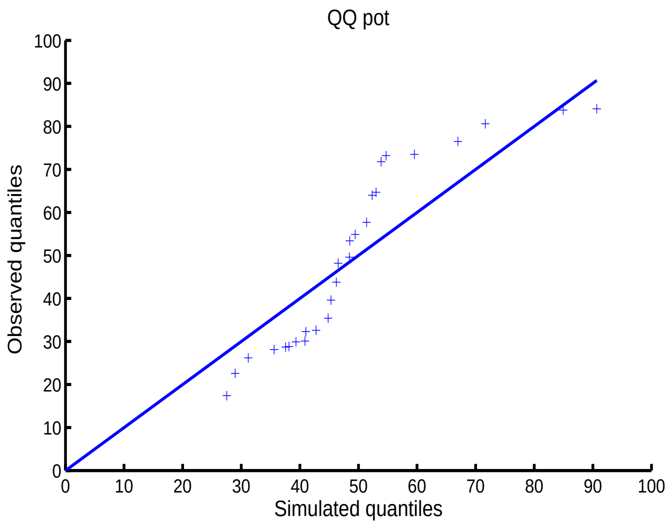

Figure 6.8: Quantile-Quantile plot for 24-hr duration after correcting the control run by the δ-method.

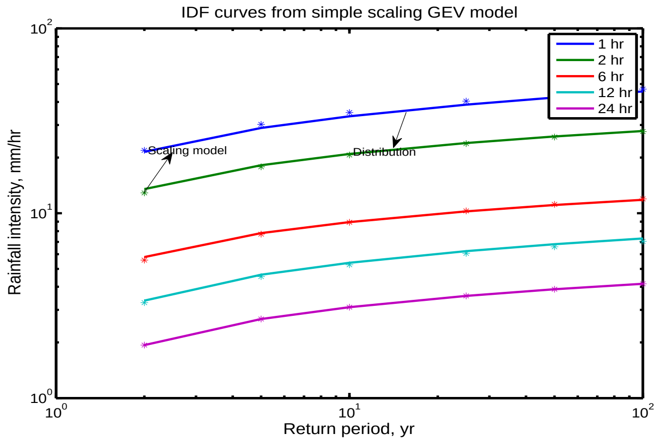

Figure 6.9: IDF curves for observations. Solid lines: GEV distribution; stars: simple scaling GEV model. The same color is used for each duration.

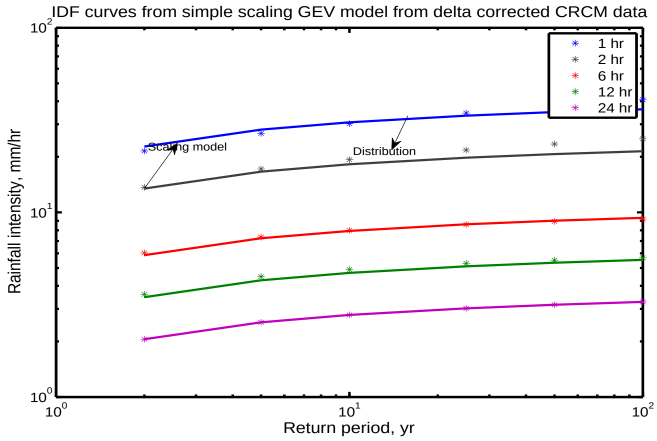

Figure 6.10: IDF curves for the corrected control simulation run. Solid lines: GEV distribution; stars: simple scaling GEV model. The same color is used for each duration.

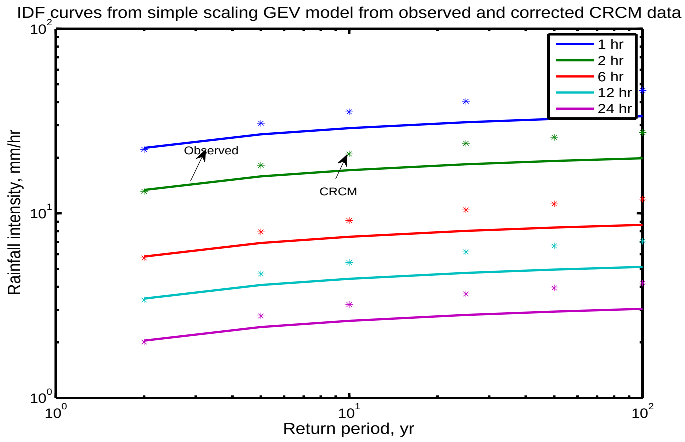

Figure 6.11: Comparison between observations and control simulation run using the GEV scaling model. Solid lines: observations; stars: CRCM simulations. The same color is used for each duration.

The difference in precipitation quantiles between the corrected control simulation and the observed rainfall is as much as 30 percent for certain durations whereas in the case of the future climate the difference is negligible. The difference depends on the choice of ensemble member. There is a noticeable difference between the control simulation from ensemble member 1 and ensemble member 5, resulting in different change factors δ (Figure 6.12). The control simulation from ensemble 5 shows better agreement with observations than the control simulation from ensemble 1. When the ensemble member 5 (experiment aew) is used, the difference in precipitation quantiles between corrected control simulations and observations reduces to 25 percent. The results are shown in Figure 6.13 and 6.14. In this study, δ values from ensemble member (5) have been used for bias correction for the future climate. Simulated data from ensemble 5 and the Δ-method quantiles show good agreement with each other. Ensemble forecasting is accomplished by using slightly different initial conditions.

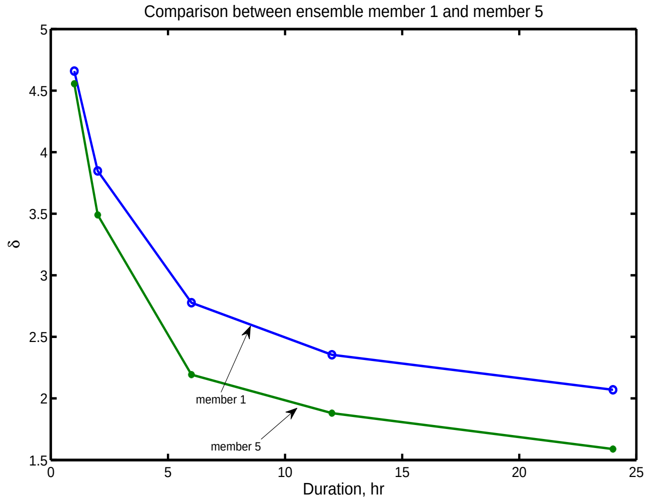

Figure 6.12: Comparison between ensemble member 1 and member 5.

Table 6.2: t-test results; p-value, statistics.

t-test	
p-value	0.3551
tstat	0.9302
df	78
sd	9.9665

The results obtained in this study show that IDF curves for annual extreme precipitations are sensitive to the use of ensemble members. A t-test has been performed to test the null hypothesis that data from ensemble member 1 and from ensemble member 5 are independent samples from normal distributions with equal mean and equal but unknown variances. The test does not reject the null hypothesis at the 5 percent significance level. The p-value and statistics are given in Table 6.2.

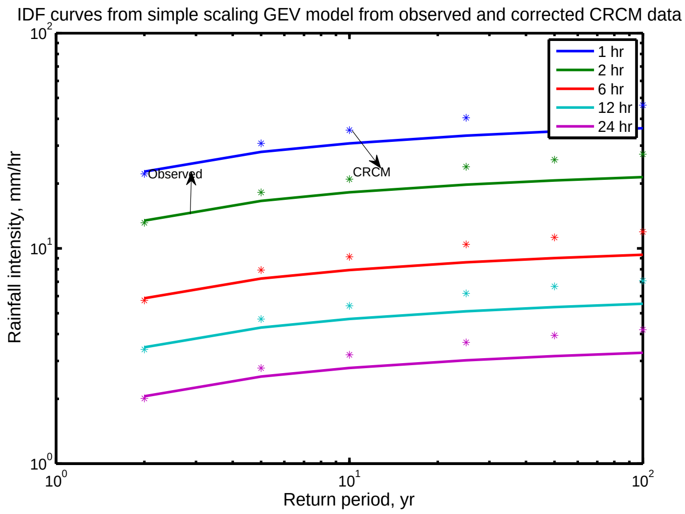

Figure 6.13: Comparison between observations and control simulation run (ensemble member 5) using GEV scaling model. Solid lines: observations; stars: CRCM simulations. The same color is used for each duration.

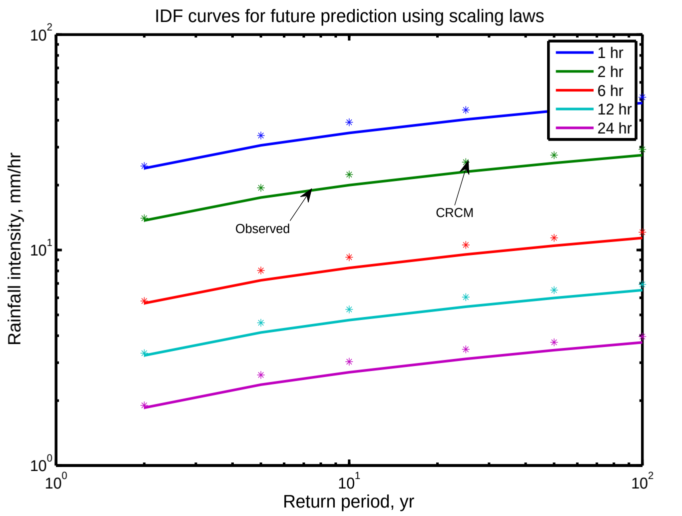

Figure 6.14: IDF curves for future prediction (using ensemble 5) using scaling laws. Solid lines: observations; stars: CRCM simulations. The same color is used for each duration.

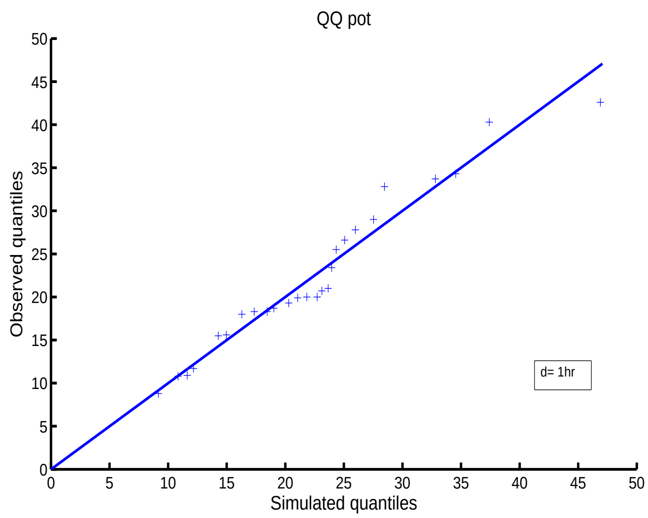

Figure 6.15: Quantile-Quantile plot for 1-hr duration for the control climate after applying QQ mapping.

6.4 Quantile-Quantile mapping

The control simulation run and the future simulation run were corrected by QQ mapping as described in Section 5.5. Figure 6.15 shows plots for 1-hr duration and plots for other durations are shown in Appendix A.8. Quantiles from observations and quantiles from corrected control data fall on 45° line.

The QQ mapping is defined by first multiplying observations by Δ and then mapping quantiles of future simulations into the Δ-method quantiles. Quantiles points fall on 45° line. Results for other durations are shown in Appendix A.9. Future IDF curves based on QQ-mapping are shown in Figure 6.16. From the figure, one sees that QQ mapping gives a slightly different result than the mean value method. The corrected future simulations are a bit higher than observations for the future climate. When the control simulation run from ensemble member 5 was used,

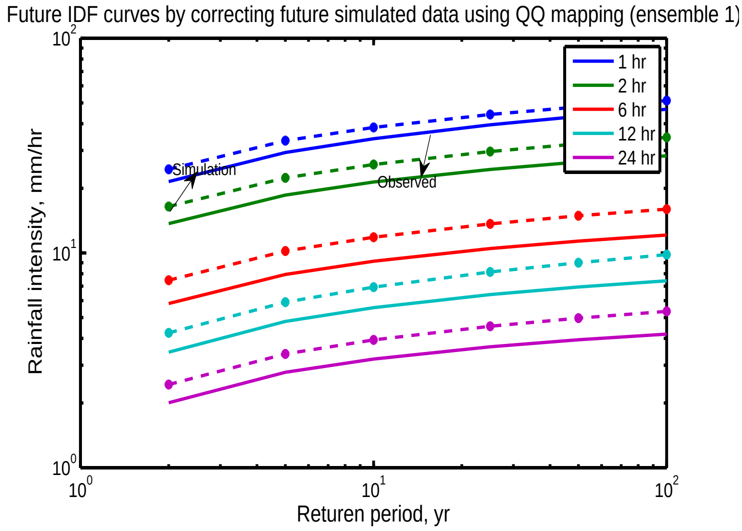

Figure 6.16: Future IDF curves by applying QQ mapping to the future simulation run. Solid lines: observations; stars: CRCM simulations. The same color is used for each duration.

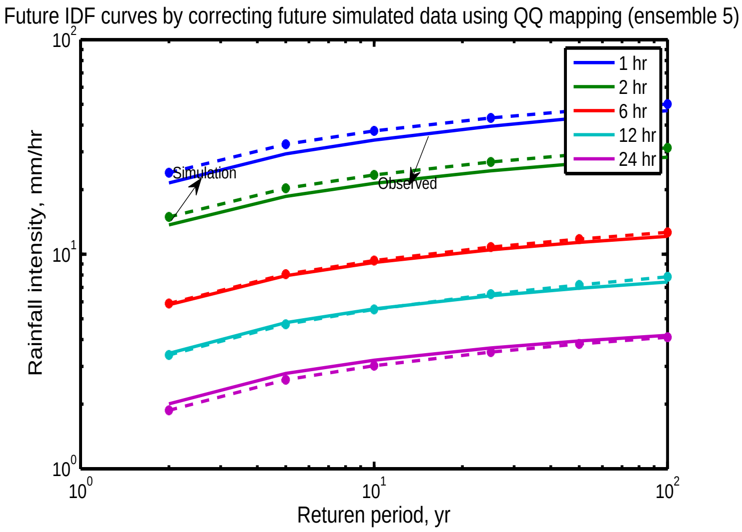

Figure 6.17: Future IDF curves by correcting future simulation run (ensemble member 5) by QQ mapping. Solid lines: observations; stars: CRCM simulations. The same color is used for each duration.

this method gave good agreement with observed data for the future climate. The results are shown in Figure 6.17. For longer durations, the corrected simulation run is in good agreement with observed rainfall while there are discrepancies for shorter durations.

The δ-factor correction gives more reliable results than QQ-mapping because one expects higher discrepancies with shorter durations and for both ensembles, with the mean value method, the discrepancies are higher at shorter durations. However, QQ mapping gives different results for different ensemble members. As the ensemble 5 shows good agreement with observations, the ensemble 5 will be used in the rest of the work to develop regional IDF curves.

6.5 Summary

Three methods were presented to remove biases from the CRCM and make it more suitable for use in predicting extreme precipitation. δ values are a decreasing function of duration. On the other hand, Δ is independent of duration. Two methods were compared to develop future IDF curves: 1) bias correction for each duration (either Δ factor correction or QQ mapping) and 2) bias correction for the reference duration and use of scaling laws estimated from observed data to obtain results for all other durations. The argument in favor of (2) is 1) as durations become shorter, the model data become increasingly inaccurate and unlikely to be useful- even after bias correction and 2) the scaling properties of precipitation is intrinsic to the climate system. For future prediction using the QQ-mapping method different results were observed for ensemble member 5 and ensemble member 1. From ensemble 1, for shorter durations the precipitation quantiles from the corrected simulation data and observed data are close to each other but for longer durations quantiles do not agree which was not expected. In the case of ensemble member 5, the discrepancies between observed and simulated precipitation quantiles are not high and for longer durations the quantiles for observed and simulated data show good agreement. However, by applying a mean value correction to the 24-hr duration extreme precipitation in the simulation run and using the GEV simple scaling laws, it was found that precipitation intensities are close to each other for each durations for both ensemble members. For shorter durations, intensities from observed data are a little bit off from corrected simulated data but this behavior was expected.

The major advantage of using the scaling model over the traditional quantile estimation technique is the parsimonious parameterization. In the traditional technique, 15 parameters have to be estimated but in the scaling model only nine parameters need to be estimated. Therefore, the scaling model reduces the amount of parameters required to compute the quantiles. The results of the study are of significant practical importance. The scaling model shows satisfactory performance in reproducing the observed data. Therefore, mean value correction and use of scaling laws will be used to develop regional IDF curves in the following sections.

6.6 Comparison of IDF curves from observations and CRCM data

In the regionalization analysis in Chapter 5, four regions were identified based on geographical location. Annual maximum precipitations of 1-hr, 2-hr, 6-hr, 12-hr, and 24-hr durations were used to develop IDF curves. CRCM data were corrected by the mean value method. The methodology was described in Chapter 5 and the results for a single station was presented in the previous section. The results are here extended to the regional groups.

6.6.1 Region 1

In Region 1, there is only one station, Churchill, located on the northern edge of the Province of Manitoba. This station is different from the other stations. It does not follow the simple scaling law. A multiscaling model was therefore developed for this station. Data were well fitted by the LN distribution. As seen in Figure 6.18, the CDFs of the fitted LN and GEV distribution are very similar and in good agreement with the data. It is easier to develop a log normal multiscaling model as the LN distribution has only two parameters compared to the GEV distribution which has three parameters.

For observations, IDF curves were developed using the LN multiscaling model described in Section 5.5.2. The scaling model and the conventional LN distribution

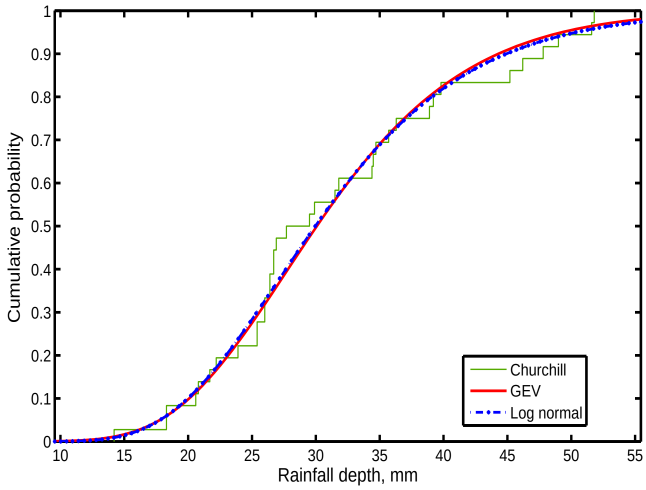

Figure 6.18: Cumulative probability distribution at the Churchill station.

are in good agreement with each other as seen in Figure 6.19. IDF curves for bias-corrected simulated extreme precipitations were developed and Figure 6.20 shows that the LN multiscaling model and conventional LN distribution are in good agreement. The future simulation was corrected by the δ factor and IDF curves from the multiscaling LN model and the conventional LN distribution are shown in Figure 6.21. The scaling model of the Δ-method for the future climate involves multiplying observed data by the Δ-factor. The results for this method are shown in Figure 6.22.

Both the Δ-method quantiles and the bias corrected future CRCM simulation show that with the increase of return periods, the relative changes increase and higher changes are observed for shorter durations and higher return periods. Figure 6.23 shows that there is an increasing trend of extreme precipitation in the future, with up to 23 percent increase for certain durations.

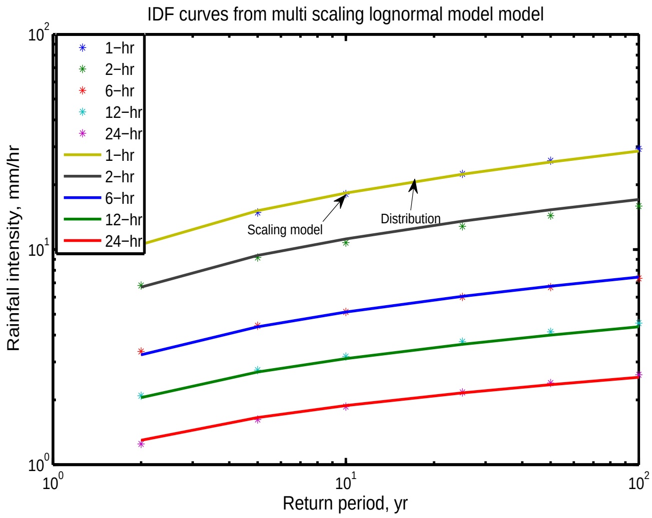

Figure 6.19: IDF curves for the control climate for observed data at the Churchill station. Solid lines: GEV distribution; stars: LN multiscaling model.

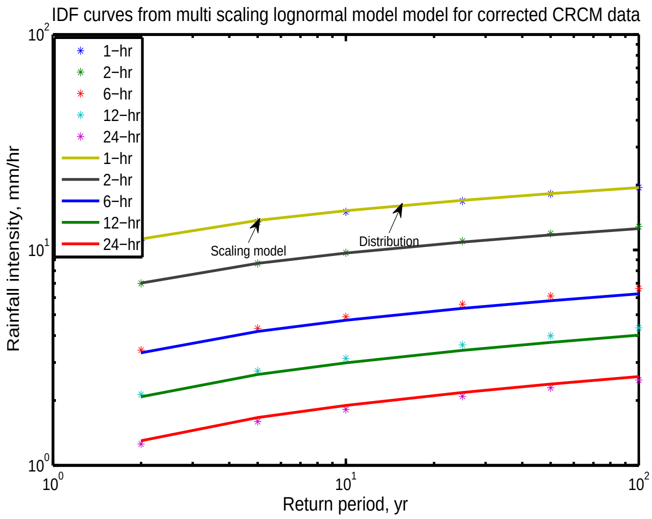

Figure 6.20: IDF curves for the control climate for the CRCM simulation at the Churchill station. Solid lines: GEV distribution; stars: LN multiscaling model.

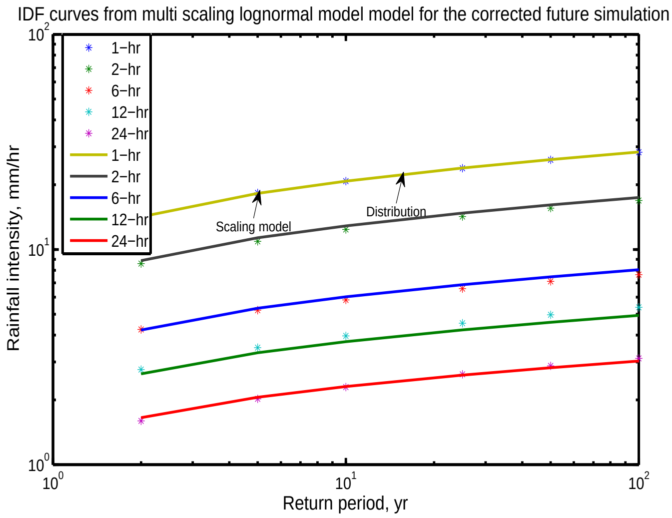

Figure 6.21: IDF curves for the future climate for the CRCM simulation at the Churchill station. Solid lines: GEV distribution; stars: LN multiscaling model.

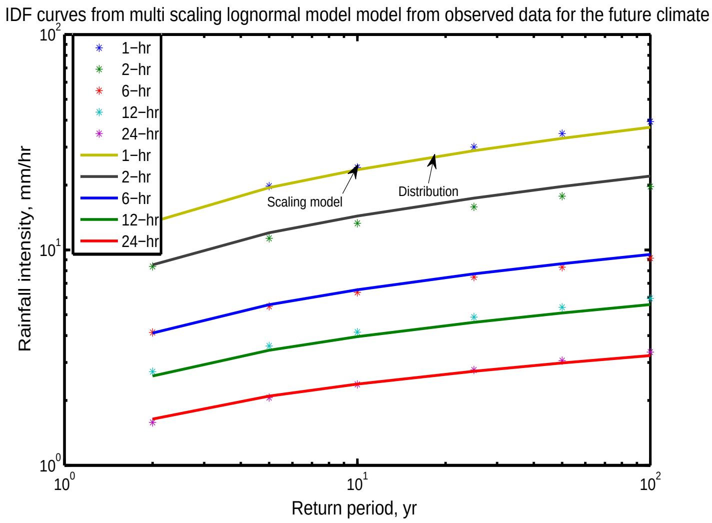

Figure 6.22: IDF curves for the future climate for observations at the Churchill station. Solid lines: GEV distribution; stars: LN multiscaling model.

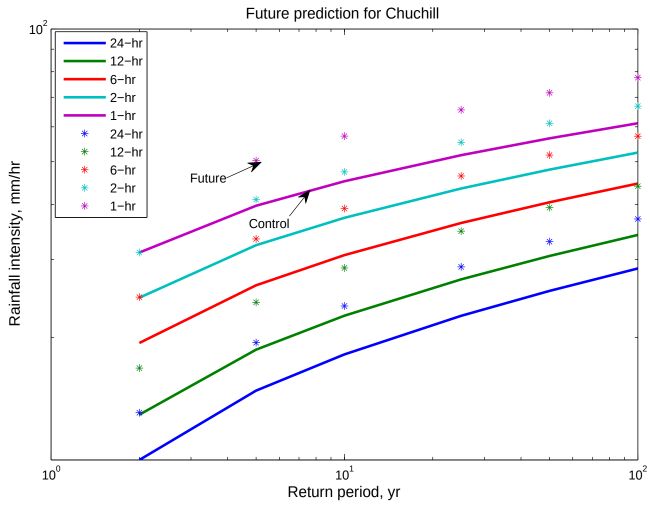

Figure 6.23: Comparison of IDF curves for future climate and control climate at the Churchill station. Solid lines: control climate; stars: future climate. The same color is used for each duration.

6.6.2 Region 2

In Region 2, there are three stations - Lynnlake, Thompson, and Gillam and these stations follow the simple scaling law. The GEV simple scaling model was developed for this region. For observations, the GEV distribution and the simple scaling model are in good agreement with each other (Figure 6.24) but in case of the CRCM simulation, there are discrepancies between the GEV distribution and the simple scaling model. These discrepancies are higher for shorter durations. For example, for the 1-hr duration there is about 19 percent difference between the GEV distribution and the simple scaling GEV model for larger return periods as seen in Figure 6.25. The model and the distribution are in good agreement with each other in case of shorter return periods.

A comparison of the observed and bias-corrected CRCM simulations for the con-

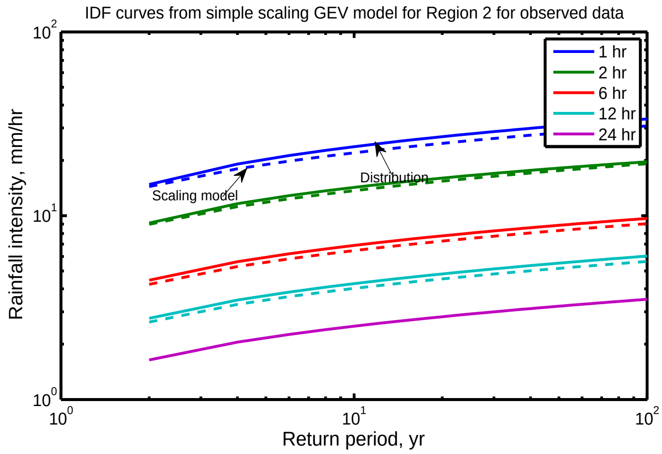

Figure 6.24: IDF curves from observed data for the control climate for Region 2. Solid lines: GEV distribution; dashed lines: simple scaling GEV model. The same color is used for each duration.

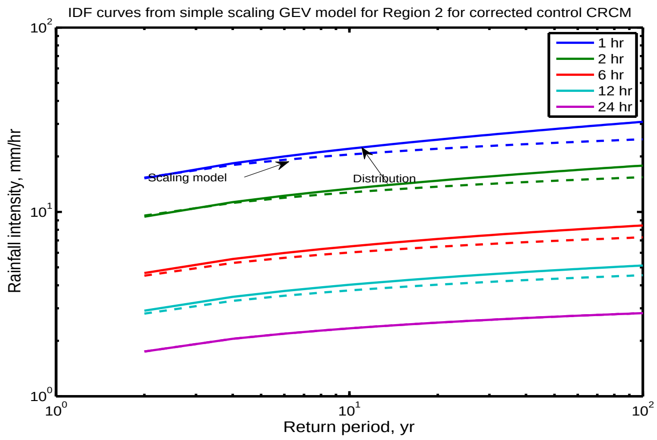

Figure 6.25: IDF curves from corrected CRCM data for the control climate for Region 2. Solid lines: GEV distribution; dashed lines: simple scaling GEV model. The same color is used for each duration.

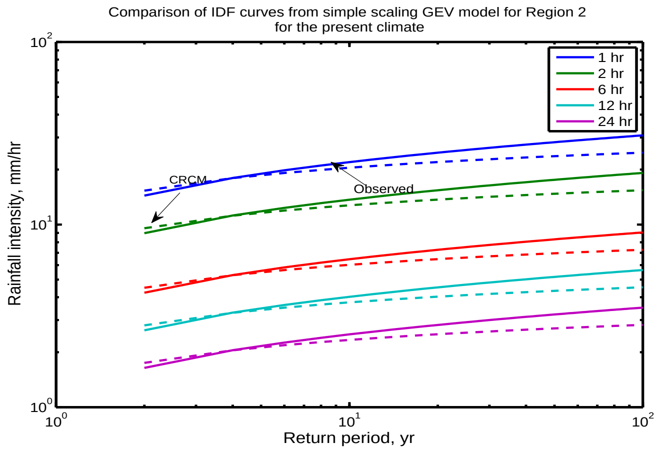

Figure 6.26: Comparison of IDF curves for control climate for Region 2. Solid lines: observations; dashed lines: CRCM simulations. The same color is used for each duration.

trol climate using the GEV simple scaling model show discrepancies that increase with the increase of return period (Figure 6.26). However, for the future climate, the Δ-method quantiles and the bias-corrected CRCM quantiles are very close (Figure 6.27) and the simple scaling model and the distribution are in good agreement with both types of data. The detailed results are shown in Appendix B.1 and B.2.

In Region 2, extreme precipitation is projected to increase in the future climate. The relative changes were estimated for bias-corrected CRCM rainfall intensities and are shown in Figure 6.28. The relative changes were estimated as

$$RD = \frac{I_{future} - I_{control}}{I_{control}} \times 100 \tag{6.12}$$

The figure shows that relative changes depend on duration and return period. The changes are maximum for shorter durations. The change is maximum 32 percent for the 24-hr duration and a 100-year return period.

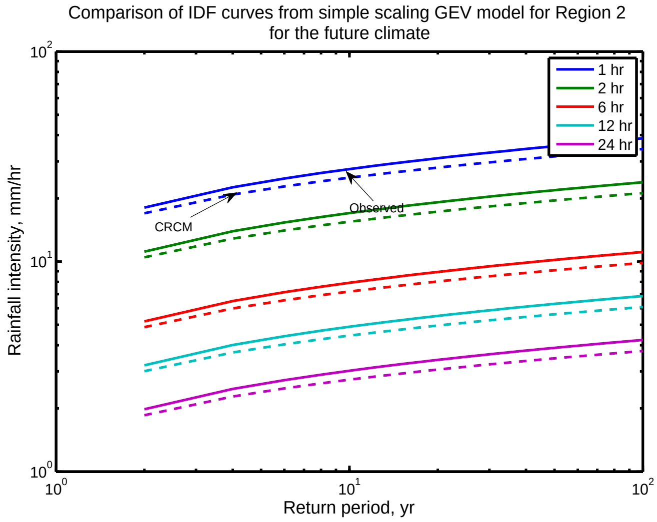

Figure 6.27: Comparison of IDF curves from observed and corrected CRCM data for the future climate for Region 2. Solid lines: observations; dashed lines: CRCM simulations. The same color is used for each duration.

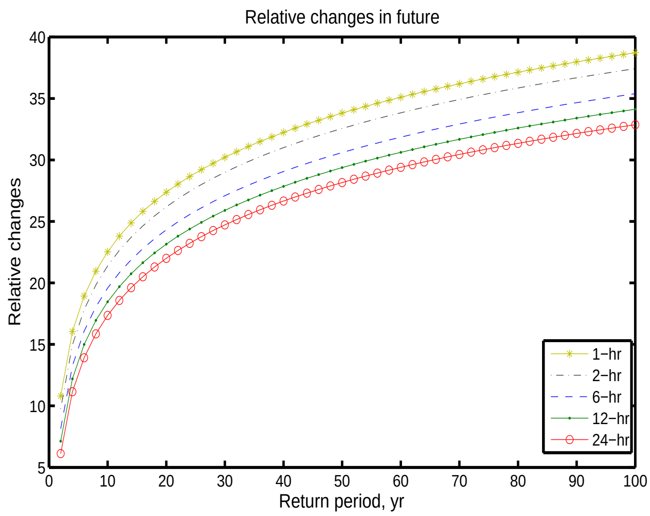

Figure 6.28: Relative changes between control and future climate for Region 2.

6.6.3 Region 3

In Region 3, three stations were selected - The pas, Norway House, and Island Lake. The stations in Flin Flon, Grand Rapids and Berens River were discarded as they do not follow simple scaling laws. In addition, the last two stations do not have much data. The simple scaling GEV model was applied in this region and shows good agreement with the GEV distribution fitted to observations and bias corrected simulations. The detailed results are found in Appendix B.3 and B.4.

The comparison between the observed and the bias corrected CRCM data was made for the present climate using the simple scaling GEV model, see Figure 6.29. For the present climate, the two types of data give similar results for this region whereas in Region 2, there were some discrepancies between observed and bias corrected simulated rainfall quantiles. In Region 2, the Gillam station has a limited number of annual extreme rainfall records and gave results slightly different from the other two stations in terms of CDF-plots.

For the future climate, the CRCM future simulation was corrected by the δ-factor and the simple scaling GEV model was applied, with results shown in Figure 6.30. When comparing the control and future climate, there is a clear indication of an increasing trend of extreme precipitation for this region, see Figure 6.31.

From Figure 6.32, it can be seen that changes are maximum for short durations and generally increase with increasing return periods. For the 1-hr duration, the relative change is around 48 percent, and for the 24-hr duration, 100-year return

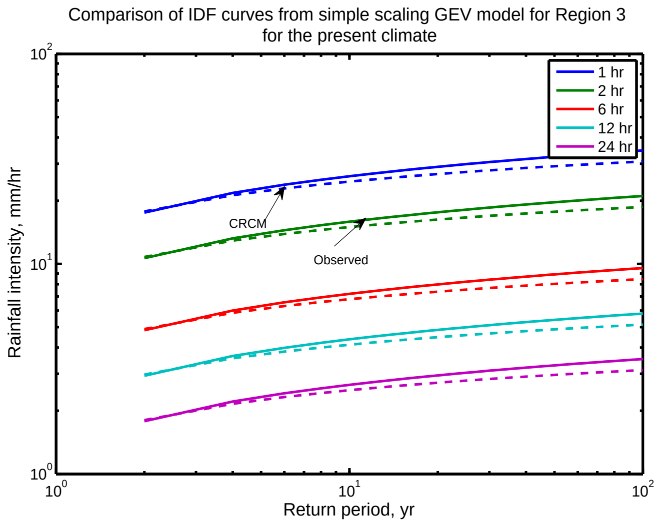

Figure 6.29: Comparison of simple scaling GEV model from observed data and corrected CRCM data for the control climate for Region 3. Solid lines: observations; dashed lines: CRCM simulations. The same color is used for each duration.

period the change is around 34 percent for Region 3. These changes are greater than those for Region 2.

6.6.4 Region 4

In Region 4, there are eight stations. Of these, three stations, Dauphin, Bissett, and Gimli, were discarded as they do not follow simple scaling laws. For Region 4, the simple scaling GEV model shows a good agreement with the GEV distribution (Appendix B.5-B.6). For the future climate, the comparison between the Δ-method quantiles and the bias corrected CRCM quantiles also shows that they give similar results although there are some small discrepancies at shorter durations. The detailed results are shown in Appendix B.7-B.9.

Figure 6.33 shows that there is an increasing trend of extreme precipitation, but

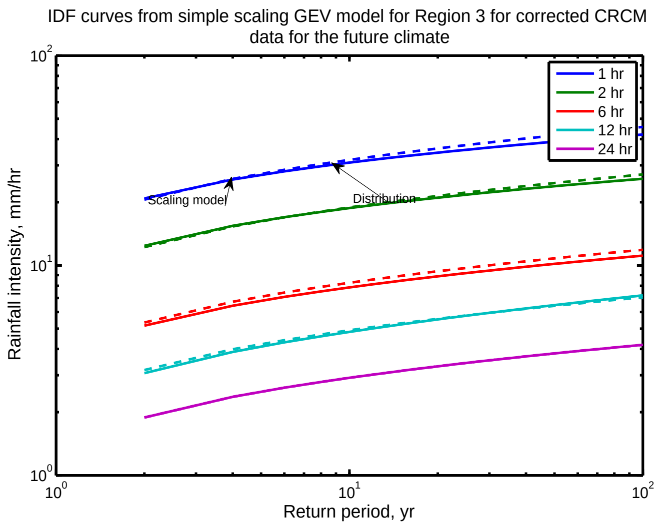

Figure 6.30: IDF curves from simple scaling GEV model for corrected CRCM data for the future climate for Region 3. Solid lines: GEV distribution; dashed lines: simple scaling GEV model. The same color is used for each duration.

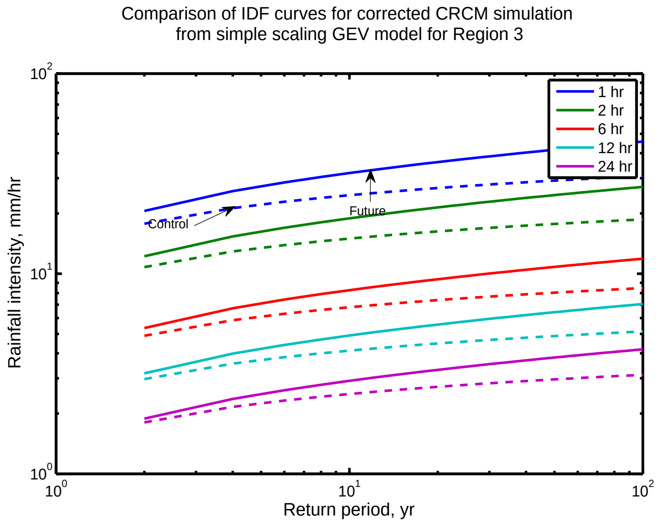

Figure 6.31: IDF curves for the corrected CRCM data for Region 3. Solid lines: future climate; dashed lines: control climate. The same color is used for each duration.

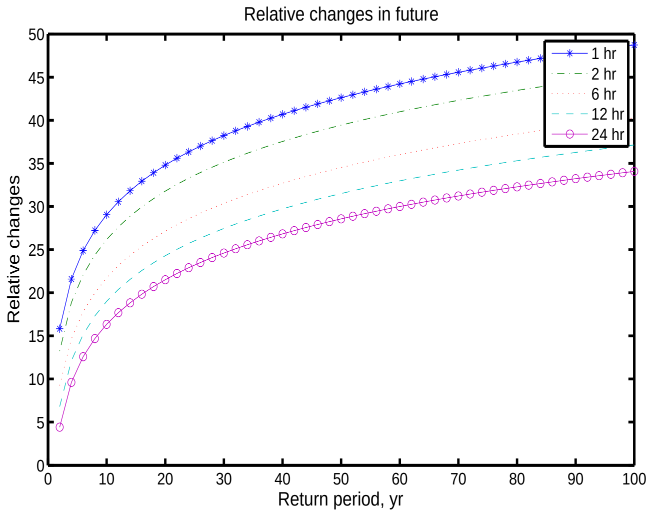

Figure 6.32: Relative changes between control and future climate for Region 3.

the increase is not as high as for Region 2 and Region 3. In this region, the increase is highest for the 24-hr duration. It is around 19 percent whereas in case of Region 2 and Region 3 the change is maximum for the 1-hr duration. The result is shown in Figure 6.34.

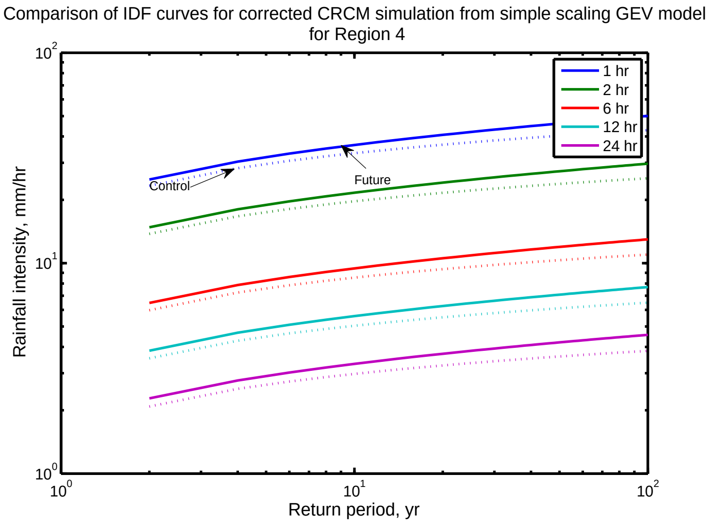

Figure 6.33: IDF curves for the bias corrected CRCM data for Region 4. Solid lines: future climate; dashed lines: control climate. The same color is used for each duration.

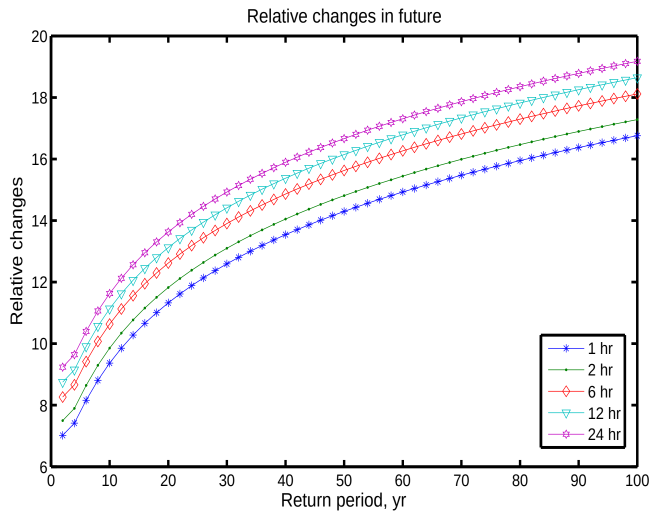

Figure 6.34: Relative changes between control and future climate for Region 4.

Chapter 7

Uncertainty analysis

Climate change projections are subject to considerable uncertainties due to factors such as emission scenarios and model choice. Uncertainty analysis is useful in the design of infrastructure and decision making. The North American Regional Climate Change Assessment Program (NARCCAP) is a collection of high-resolution climate change scenarios, useful for investigating uncertainties. In this study, five different simulations were used, described in Section 2.3. For each set of model data, IDF curves using the simple scaling GEV model were developed. Durations of 3-hr, 6-hr, 12-hr, 18-hr, and 24-hr were used. It is easier to extract those durations as NARCCAP simulations are provided at a 3-hr time resolution. Before developing the simple scaling GEV model, the climate model data were fitted by the GEV distribution. Figure 7.1 shows that model data are well fitted with the GEV distribution. There are some data points which are inconsistent with the rest of the data (Figure 7.2).

At first, for Region 2, Depth-Duration-Frequency curves were developed for the

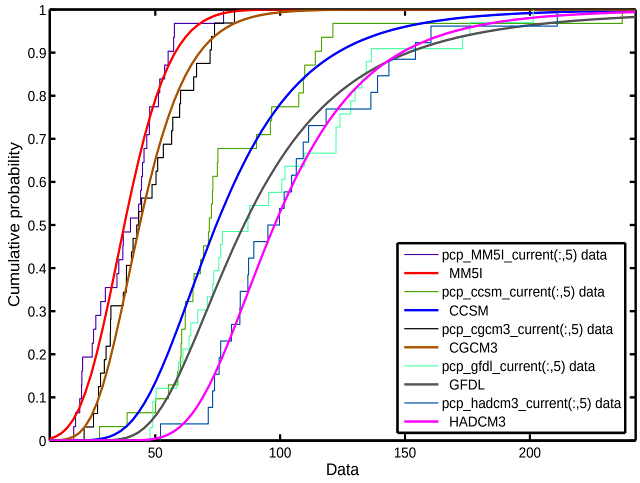

Figure 7.1: Cumulative probability plots for five regional climate models from NARCCAP simulations at the Thompson station for the 24-hr duration.

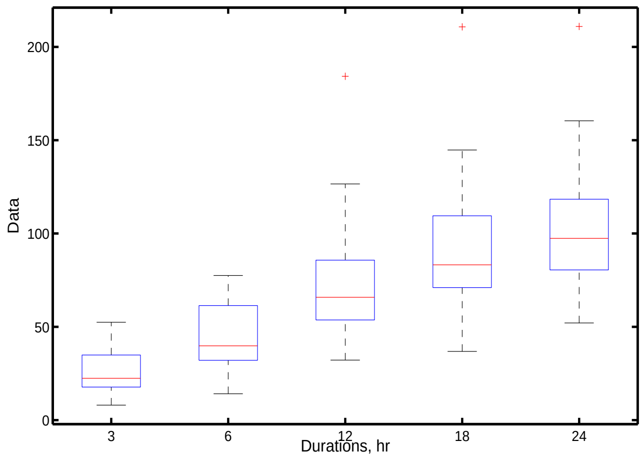

Figure 7.2: Boxplot of precipitation depth for NARCCAP simulations at the Thompson station.

control climate and the future climate using the simple scaling GEV distribution and the conventional GEV distribution. The results for CRCM-CGCM3 are shown in Figures 7.3 and 7.4 and the results for other models are shown in Appendix B.10-B.17. Figures 7.3 and 7.4 show that rainfall quantiles from the simple scaling GEV model and the conventional GEV model using the CRCM-CGCM3 simulation data are in good agreement although in the future climate, for the 6-hr duration, there are discrepancies that increase with the increase of return periods. IDF curves from the simple scaling GEV model using the CRCM-CCSM simulation also fit well with the GEV distribution for the future climate but for the control climate, there are discrepancies for certain durations, especially for shorter durations. For the MM5I-CCSM simulation, the simple scaling GEV model fits well with the GEV distribution for the future climate but for the control climate, the model is departing from the GEV distribution though it is not much higher. Rainfall quantiles from the HRM3-GFDL and the HRM3-HADCM3 do not show good agreement with the model and the GEV distribution, particularly for shorter durations. For the control climate of the HRM3-HADCM3 model, the differences between the scaling model and the conventional distribution is maximum 14 percent and the difference is highest for shorter durations and longer return periods but for the future climate for 6-hr duration the difference is around 30 percent which is very high. In the case of the HRM3-GFDL, there is a maximum difference of 19 percent for the control climate but for the future climate for 12-hr duration the difference is 23 percent. In a summary,

Table 7.1: ARF from NARCCAP simulations for Region 2.

No	Model	6 hr	12 hr	24 hr
1	CRCM-CGCM3	0.63	0.84	1.07
2	CRCM-CCSM	0.99	1.26	1.77
3	MM5I-CCSM	0.80	0.79	0.99
4	HRM3-GFDL	1.31	1.89	2.31
5	HRM3-HADCM3	1.87	2.57	2.96

the difference between the scaling model and the GEV distribution gets higher for shorter durations and longer return periods and this is true for all models.

Areal reduction factors for 6-hr, 12-hr, and 24-hr durations were estimated and for the CRCM-CGCM3 simulations, ARFs are shown in Figure 7.5. Areal reduction factors for 6-hr, 12-hr, and 24-hr durations for the 100-year event are shown in Table 7.1. The table shows that those model data which show good agreement with the simple scaling GEV model and the GEV distribution give lower areal reduction factors whereas the HRM3-GFDL and the HRM3-HADCM3 give higher areal reductions factors. There are some published curves which show that for the 24-hr duration the ARF will be around 1, for 12-hr duration around 0.8 and for 6-hr duration around 0.65. The CRCM-CGCM3 gives very close result with the established curves except for 24-hr duration as for that duration the ARF is slightly higher than 1. Every model has bias and in this study no correction factor was applied when developing the simple scaling GEV model. It should also be noted that in the observed data no adjustment is made due to winds, wetting losses, evaporation, etc.

Important differences in the projected climate are observed between models due to different spatial and temporal discretization of simulation domains, parameteri-

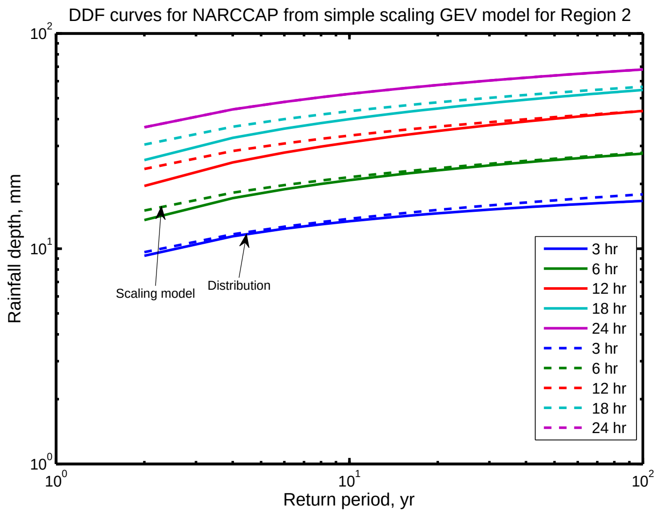

Figure 7.3: DDF curves from the simple scaling GEV model and the GEV distribution for the CRCM-CGCM3 for the control climate for Region 2. Solid lines: GEV distribution; dashed lines: simple scaling GEV model.

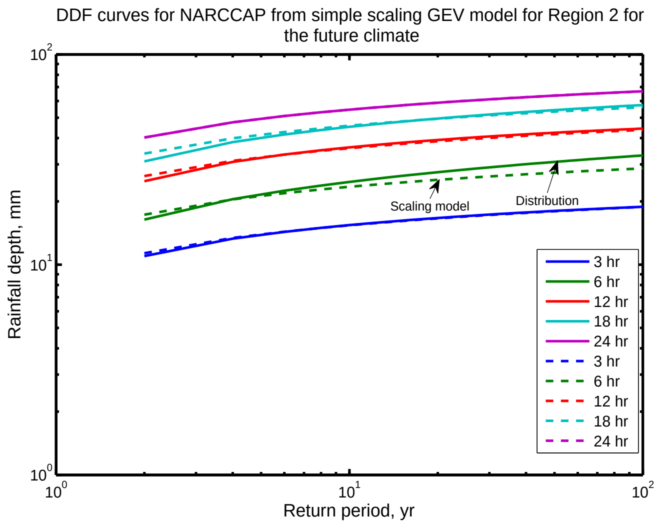

Figure 7.4: DDF curves from simple scaling GEV model and the GEV distribution for the CRCM-CGCM3 for the future climate for Region 2. Solid lines: GEV distribution; dashed lines: simple scaling GEV model.

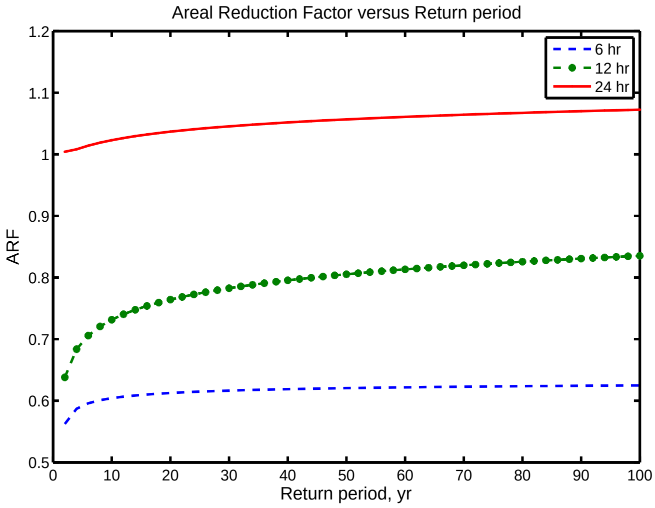

Figure 7.5: ARFs versus return period for Region 2 using CRCM-CGCM3 simulations. ARFs are estimated by the ratio of the precipitation intensity for a specific duration and a specific return period at the grid box scale and at the station scale. These ARFs are determined using the CRCM-CGCM3 simulations for durations of 6-hr, 12-hr, and 24-hr for Region 2.

Table 7.2: Relative changes in percent in future from NARCCAP simulations for Region 2.

No	Model	6 hr	12 hr	24 hr
1	CRCM-CGCM3	2	0.5	-2
2	CRCM-CCSM	23	20	16
3	MM5I-CCSM	15	14	13
4	HRM3-GFDL	11	12	13
5	HRM3-HADCM3	-6	-0.5	5

zations and boundary conditions. In Table 7.2, the relative changes for 6-hr, 12-hr, and 24-hr durations for the 100-year event are shown. Different models give different changes in the future and there is no consistency. It is worth noting that the Canadian Regional Climate model predicts higher increases of extreme precipitation in the future compared to NARCCAP simulations.

For Region 3, the simple scaling GEV model was developed and for the HRM3-GFDL and the HRM3-HADCM3, the difference of rainfall quantiles between the GEV distribution and the simple scaling GEV model is above 20 percent which is

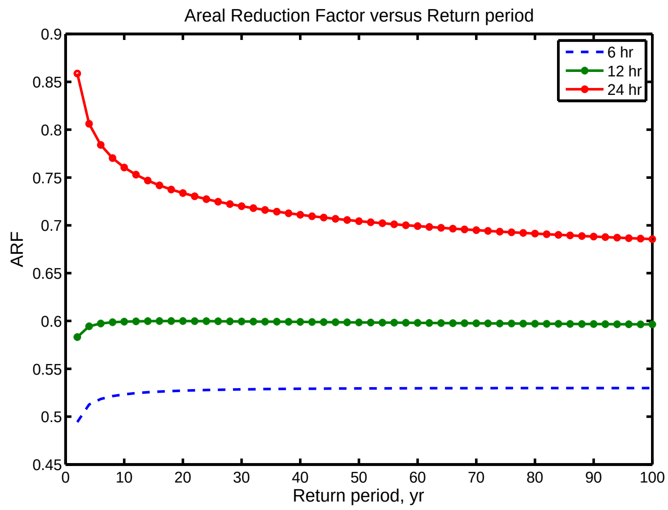

Figure 7.6: ARFs versus return period for Region 3 using CRCM-CGCM3 simulations. ARFs are estimated by the ratio of the precipitation intensity for a specific duration and a specific return period at the grid box scale and at the station scale scale. These ARF s are determined using the CRCM-CGCM3 simulations for durations of 6-hr, 12-hr, and 24-hr for Region 3.

Table 7.3: ARF from NARCCAP different simulations for Region 3.

No	Model	6 hr	12 hr	24 hr
1	CRCM-CGCM3	0.53	0.60	0.70
2	CRCM-CCSM	0.82	1.03	1.24
3	MM5I-CCSM	0.60	0.65	0.74
4	HRM3-GFDL	1.31	1.89	2.31
5	HRM3-HADCM3	1.35	1.94	2.30

also found in Region 2. However, the other three models agree with each other. The maximum difference between the distribution and the simple scaling GEV model is 17 percent. By analyzing areal reduction factors for 6-hr, 12-hr, and 24-hr durations, it is found that for Region 3, similar results as in Region 2 are obtained. ARFs are shown in Figure 7.6 for the CRCM-CGCM3 simulation. In Region 3, ARFs are smaller than for Region 2. In Table 7.3, 100-year events are shown for the five NARCCAP simulations. CRCM-CCSM, HRM3-GFDL, and HRM3-HADCM3 give areal reduction factors greater than 1 due in part to model bias.

Table 7.4: Relative changes (percent) in future from NARCCAP simulations for Region 3.

No	Model	6 hr	12 hr	24 hr
1	CRCM-CGCM3	28	31	34
2	CRCM-CCSM	-3	-4	-4
3	MM5I-CCSM	25	24	22
4	HRM3-GFDL	19	23	27
5	HRM3-HADCM3	13	9	5

In Table 7.4, the relative changes for 6-hr, 12-hr and 24-hr durations for the 100-year event are shown. Different models give different changes in the future and there is no consistency. In this region, the CRCM-CGCM3 predict higher extreme precipitation than in Region 2. The CRCM-CCSM predicts decrease of extreme precipitation where in Region 2, this model predicts increase in precipitation. The Canadian Regional Climate model predicts higher increase of extreme precipitation in the future than NARCCAP simulations.

In Region 4, there are eight stations and for this region, the simple scaling GEV model was also developed and like Region 2 and Region 3, CRCM-CGCM3, CRCM-CCSM and MM5I-CCSM give good agreement with the simple scaling GEV model and the GEV distribution. The results for the CRCM-CGCM3 are shown in Figure 7.7 and 7.8. As this region has more stations, better fit was found than in Region 2 and 3. In the case of the CRCM-CCSM for 6-hr duration there is a difference of 22 percent for the future climate but for other durations the model and the distribution are in good agreement.

Comparing observations and CRCM-CGCM3 simulations, one finds that ARFs are less than 1 except for 24-hr duration. This result is very close to Region 2 but

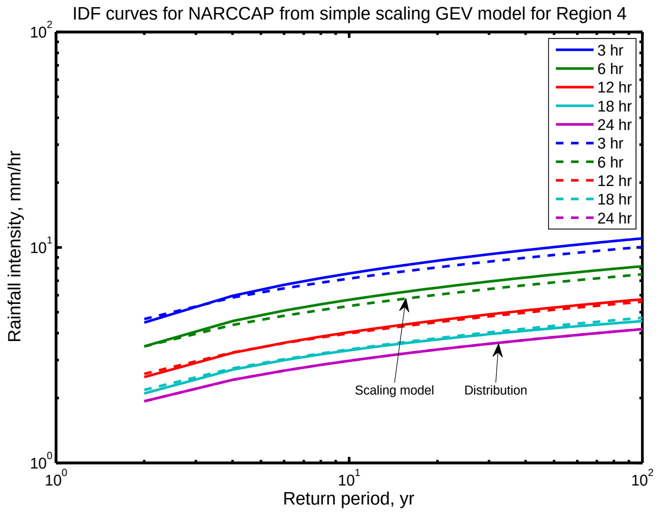

Figure 7.7: IDF curves from the simple scaling GEV model and the GEV distribution for the CRCM-CGCM3 simulation for the control climate for Region 4. Solid lines: GEV distribution; dashed lines: simple scaling GEV model.

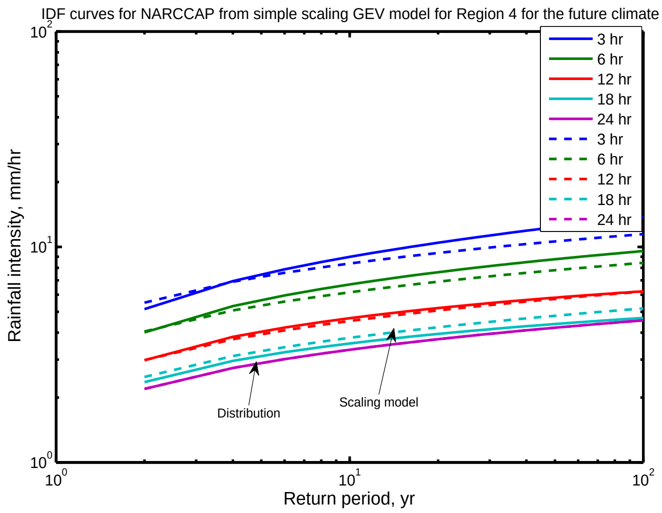

Figure 7.8: IDF curves from the simple scaling GEV model and the GEV distribution for the CRCM-CGCM3 simulation for the future climate for Region 4. Solid lines: GEV distribution; dashed lines: simple scaling GEV model.

Table 7.5: ARF from NARCCAP simulations for Region 4.

No	Model	6 hr	12 hr	24 hr
1	CRCM-CGCM3	0.72	0.81	1.08
2	CRCM-CCSM	0.91	1.1	1.52
3	MM5I-CCSM	1.05	1.1	1.30
4	HRM3-GFDL	1.73	2.14	2.61
5	HRM3-HADCM3	2.00	2.45	2.89

Table 7.6: Relative changes (percent) in future from NARCCAP simulations for Region 4.

No	Model	6 hr	12 hr	24 hr
1	CRCM-CGCM3	13	11	9
2	CRCM-CCSM	-9	-7	-6
3	MM5I-CCSM	2	5	8
4	HRM3-GFDL	9	7	5
5	HRM3-HADCM3	15	16	18

Region 3 gives slightly different results from the other two regions. In Table 7.5 ARFs for 6-hr, 12-hr, and 24-hr durations for 100-year events are shown and in the three regions, the HRM3-GFDL and the HRM3-HADCM3 give ARFs that are higher than 1.

Relative difference between grid points were estimated and the result for the CRCM-CGCM3 is shown in Figure 7.9. The CRCM-CGCM3 simulation predicts that extreme precipitation quantiles will decrease with the increase of return period whereas the Canadian Regional Climate Model predicts that extreme precipitation will increase with the increase of return period. Table 7.6 shows the relative changes for 100-year events for 6-hr, 12-hr, and 24-hr durations.

The CRCM-CCSM in both Region 3 and Region 4 predicts decrease of extreme precipitation whereas in Region 2 it predicts increase of extreme precipitation. Uncertainties in future projections can be assessed by combining the simulation results. By combining the results, it is possible to get a general regional overview of the study

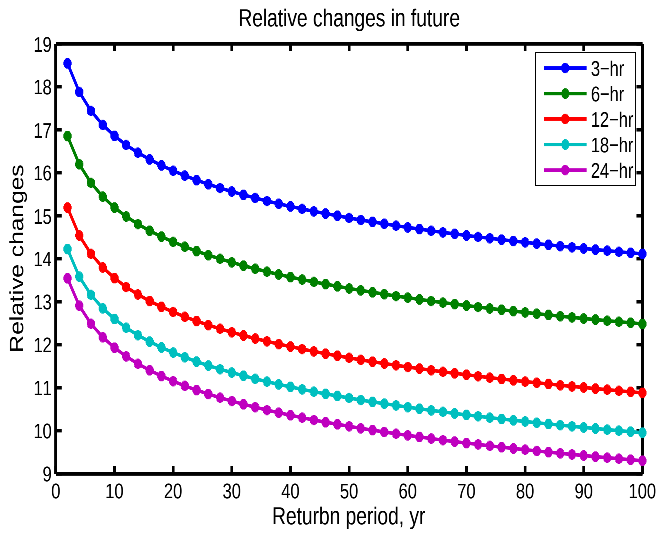

Figure 7.9: Relative changes for the model NARCCAP CRCM-CGCM3 at Region 4.

area. By considering each model separately, it is very difficult to have confidence in projected changes. However, in this study, it is obvious that there is an increasing trend in extreme precipitation but it varies from region to region. The variations between models investigated here are due to both the choice of regional climate model and global climate model used to produce the boundary conditions.

Chapter 8

Summary and Conclusion

The present study has focused on the impact of climate change on IDF curves. One of the difficulties involved in this type of study is the comparison of point data and gridded data. Areal reduction factors derived analytically were used to resolve the problem. ARFs decrease with the increase of the catchment area and the return period and the coefficient of variation of areal averages rainfall decreases with the increase of catchment area. According to the proposed methodology, the catchment IDF depends on the spatial correlation length which characterizes the storm type.

Areal reduction factors were used to compare IDF curves based on observations and CRCM data. ARFs account for part of the difference between observations and model data, but there are still considerable model biases. ARFs derived from observed data for the 24-hr duration are reasonable and consistent with the literature. As ARFs for other durations were based on the 24-hr duration which may have introduced some biases since it is known that ARFs are smaller for shorter durations.

Estimation of smaller ARFs as ratio of model data to station data compared to the published ARF values indicate that there are biases in the CRCM data. CRCM simulations cannot simulate the extreme values very well, particularly for shorter durations.

According to the results of this study, the CRCM data require correction before being used in a simple scaling model with the GEV distribution. Two methods were used to correct simulations: 1) mean-value correction and 2) QQ mapping. When applying the QQ method, the future IDF curves from the corrected simulation data and observed data for shorter duration are close to each other but for longer duration rainfall quantiles agree less well. The mean-value correction method was applied to the 24-hr duration extreme precipitation from the simulation run and then simple scaling laws with the GEV distribution was applied to develop IDF curves. Rainfall quantiles from corrected simulations and observations are close to each other, though for shorter durations, intensities are departing from each other as one would expect.

Manitoba was divided into four geographical regions to get a regional view. The simple scaling GEV model was applied to each region. The Canadian Regional Climate Model has been used for two periods: 1961-2000 for the control climate and 2041-2100 for the future climate, and the A2 emission scenario was selected for this study. The CRCM predicts that there will be an increasing trend of extreme precipitation with the increase of return period. To investigate uncertainties, five different simulations from NARCCAP: CRCM-CGCM3, CRCM-CCSM, MM5I-

CCSM, HRM3-GFDL and HRM3- HADCM3 were considered. CRCM-CGCM3, CRCM-CCSM and MM5I-CCSM give good agreement between the simple scaling GEV model and the GEV distribution but the other two models do not show good agreement. In each region, the HRM3-GFDL and the HRM3-HADCM3 give areal reduction factors greater than 1. Only the CRCM-CGCM3 gives areal reduction factors close to the published ARF curves though there are still some biases involved. ARFs greater than 1 indicate model biases. Each model predicts change in extreme precipitations at different rates varying from region to region. It is very difficult to reach a general conclusion about the amount of increase.

Finally, the outcomes of this study can be summarized as follows:

- Derivation of areal reduction factors allows for comparison between observed point data and modeled grid data. Comparison of areal IDF curves estimated from point data and CRCM data provides evidence that CRCM data cannot simulate extreme precipitation very well. The CRCM simulations need corrections.

- The relationship between the ratio of observed and simulated data and duration in Figure 6.1 implies that there are biases in the CRCM, at least for some durations. Two correction methods were employed in this study. The mean value correction method is better than QQ mapping. The QQ mapping is sensitive to the choice of ensemble member and this method gave quite different results for the two ensemble members used in the study.

- The simple scaling GEV model gives satisfactory performance for all simulations and using this model, it is possible to determine rainfall intensity quantiles for any duration and return period.

- The constant ARF approach is recommended to estimate future changes at the station scale because this method depends on duration and return period. The mean change method is not reliable as the Δ-method only depends on duration, not on return period.

- Assessing uncertainties is very important to develop adaptation strategies and it helps decision makers in their ranking of adaptation strategies. The CRCM predicts higher precipitation quantiles than the other five simulations from the NARCCAP. The CRCM predicts that in Region 2 for the 24-hr duration, 100-year precipitation events will increase about 30 percent, in Region 3 also around 30 percent and in Region 4 around 18 percent.

8.0.5 Recommendation

Precipitation intensity is used for the design of hydraulic structures. Potential shifts in the distribution of extreme precipitation cause changes in the performance of existing infrastructure and would require changes in the design values for future designs. This study has assessed the change of intensity-duration-frequency (IDF) curves due to climate warming. These changes can be used in the design of sewer systems, hydraulic structures, etc. Areal IDF curves are often required in hydrologic design and in this study areal reduction factors have been estimated. These factors are also useful when simulations are compared to observations.

Regional IDF curves have been developed for Manitoba using the simple scaling GEV model. Information about short duration rainfall is important in the design of hydraulic structures, but data for short durations like 1-hr or 2-hr, etc are not often available. For planning and design of hydraulic structures, the information about extreme rainfall events for a specific return period and for a specific duration is needed. Using one scaling exponent and only 24-hr duration annual extreme rainfall data, rainfall intensity can be determined for a given return period and a given duration. It is also possible to estimate sub-hourly rainfall intensities at partially gauged site.

8.0.6 Future work

- The simple scaling GEV model can be developed for other regions in Canada as an alternative to the traditional quantile estimation technique.
- In this study, ARFs were determined theoretically for the province of Manitoba. It would be useful if ARFs were determined for each region to investigate whether there is variations among regions. This information would be important for estimating design floods and for comparing gridded data with point data.
- Future work should focus on combining more simulations of future climate and

on determining extending the result to the rest of Canada.

Bibliography

Aronica, G., and G. Freni, Estimation of sub-hourly DDF curves using scaling properties of hourly and sub-hourly data at partially gauged site, *Atmospheric Research*, *77*, 114–123, 2005.

Burlando, P., and R. Rosso, Scaling and multiscaling models of depth-duration-frequency curves for storm precipitation, *Journal of Hydrology*, *187*, 45–64, 1996.

Challinor, A. J., J. M. Slingo, T. R. Wheeler, and F. J. Doblas-Reyes, Probabilistic simulations of crop yield over western India using DEMETER seasonal hindcasts ensembles, *Tellus A*, *57*, 498–512, 2005.

Eagleson, P. S., Dynamics of flood frequency, *Water Resources Research.*, *8*(4), 878–898, 1972.

Flato, G. M., and G. Boer, Warming asymmetry in climate change simulations, *Geophysical Research Letters*, *28*(1), 195–198, 2001.

Ghosh, B., Random distances within a rectangle and between two rectangles, *Bulletin Calcutta Mathematical Society*, *43*(1), 17–24, 1951.

Gupta, V. K., and E. Waymire, Multiscaling properties of spatial rainfall and river flow distributions, *Journal of Geophysical Research*, *95*, P. 1999, 1990.

Hebson, C., and E. F. Wood, A study of scale effects in flood frequency response, in: Scale problems in Hydrology, I. Rodriguez-Iturbe and V.K.Gupta and E.F.Wood, *D.Reidel Publishing, Hingham, Mass*, pp. 133–158, 1986.

Houghton, J. T., G. J. Jenkins, and J. J. Ephraums, Climate Change: The IPCC Scientific Assessment, *Cambridge University Press*, 1990.

Ines, V. M. A., and J. W. Hansen, Bias correction of daily GCM rainfall for crop simulation studies, *Agricultural and Forest Meteorology*, *138*, 44–53, 2006.

Kim, S. J., G. Flato, G. Boer, and N. McFarlane, A coupled climate model simulation of the Last Glacial Maximum, part 1: transient multi-decadal response, *Climate Dynamics*, *19*, 515–537, 2002.

Kim, S. J., G. Flato, and G. Boer, A coupled climate model simulation of the Last Glacial Maximum, part 2: approach to equilibrium, *Climate Dynamics*, *20*, 635–661, 2003.

LaPrise, R., D. Caya, M. Giguere, G. Bergeron, H. Ct, J.-P. Blanchet, G. J. Boer, and N. A. McFarlane, Climate and climate change in western Canada as simulated by the Canadian RCM, *American Meteorological Society*, *36*, 1998.

Leclerc, G., and J. C. Schaake, Derivation of hydrologic frequency curves, *Report*

142, Ralph M Parson's Laboratory, Massachusetts Institute of Technology, 151 P., 1972.

Mailhot, A., S. Duchesne, D. Caya, and G. Talbot, Assessment of future change in intensity-duration-frequency (idf) curves for Southern Quebec using Canadian Regional Climate Model (CRCM), *Journal of Hydrology*, *347*, 197–210, 2007.

Mavromatis, T., and P. D. Jones, Evaluation of HADCM2 and direct use of daily GCM data in impact assessment studies, *Climate Change*, *41*, 583–614, 1999.

Mearns, L. O., The North American Regional Climate Change Assessment Program dataset, *National Center for Atmospheric Research, Earth System Grid data portal, Boulder, CO. Data downloaded 2012-07-26.*, 2007, updated 2011.

Menabde, M., A. Seed, and G. Pegram, A simple scaling model for extreme rainfall, *Water Resources Research*, *35*(11), 15–19, 1999.

Nhat, L. M., Y. Tachikawa, T. Sayama, and K. Takara, A simple scaling characteristics of rainfall in the time and space to derive intensity duration frequency relationships, *Annual Journal of Hydraulic Engineering, JSCE*, *51*, 2007.

Roche, M., Hydrologie de surface, *Gauthier-Villars, Paris*, 1963.

Rodriguez-Iturbe, I., and J. Mejia, On the transformation from point rainfall to areal rainfall, *Water Resources Research*, *10*(4), 729–735, 1974.

Sivapalan, M., and G. Bloschl, Transformation of point rainfall to areal rainfall: Intensity-duration-frequency curves, *Journal of Hydrology*, *204*, 150–167, 1998.

Sivapalan, M., and E. F. Wood, A multidimensional model of non-stationary space-time rainfall at the catchment scale, *Water Resources Research*, *23*(7), 1289–2999, 1987.

Sivapalan, M., K. J. Beven, and E. F. Wood, On hydrologic similarity, 3, A dimensionless flood frequency model using a generalized geomorphic unit hydrograph and partial area runoff generation, *Water Resources Research*, *26*(2), 43–58, 1990.

Subramanya, K., *Engineering Hydrology*, Tata McGraw-Hill, New Delhi, 1984.

Walsh, J., Statistical Downscaling, *NOAA Climate Services Meeting*, 2011.

Warrilow, D. A., A. B. Sangster, and A. Slingo, Modeling of land surface processes and their influence on European climate, *Dynamical Climatology Technical Note*, *38*, 92, 1986.

Waymire, E., V. K. Gupta, and I. Rodriguez-Iturbe, A spectral theory of rainfall intensity at the meso-b scale, *Water Resources Research*, *20*(10), 1453–1465, 1984.

Willems, P., and M. Vrac, Statistical precipitation downscaling for small-scale hydrological impact investigations of climate change, *Journal of Hydrology*, *402*, 193–205, 2011.

Wood, E. F., and C. S. Hebson, On hydrologic similarity. 1. Derivation of the dimensionless flood frequency curve, *Water Resources Research*, *22*(11), 1549–1554, 1986.

Yoo, C., and E. Ha, Effect of zero measurements on the spatial correlation structure of rainfall, *Stochastic Environmental Research and Risk Assessment*, *21*(3), 287–297, 2007.

Appendix A

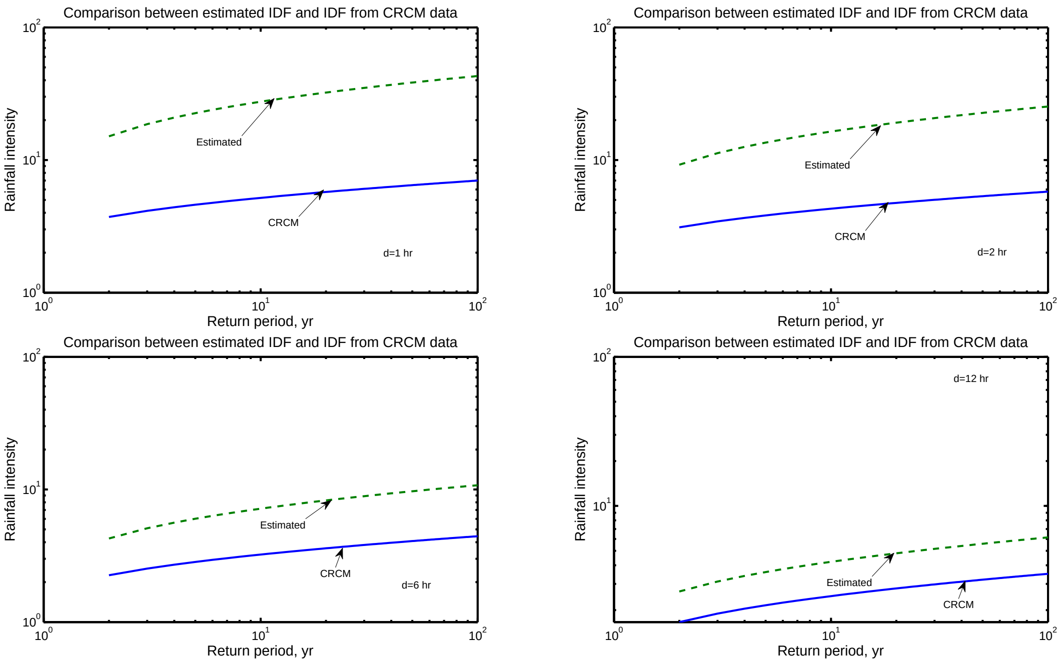

Figure A.1: Comparison of IDF curves of areal and CRCM precipitation for each duration.

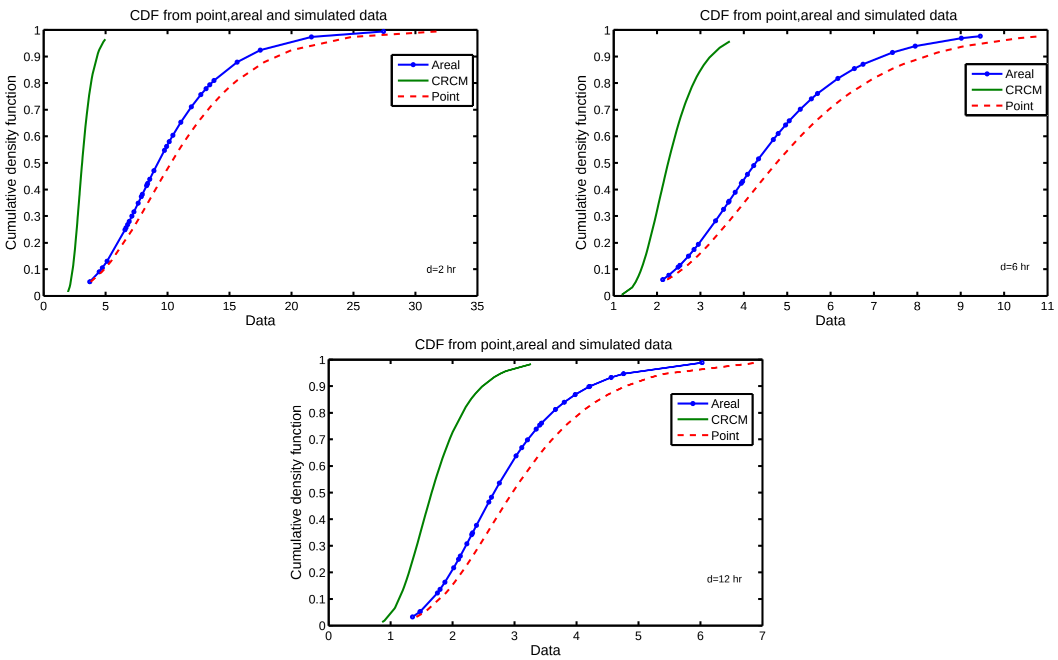

Figure A.2: Cumulative probability curves for each duration.

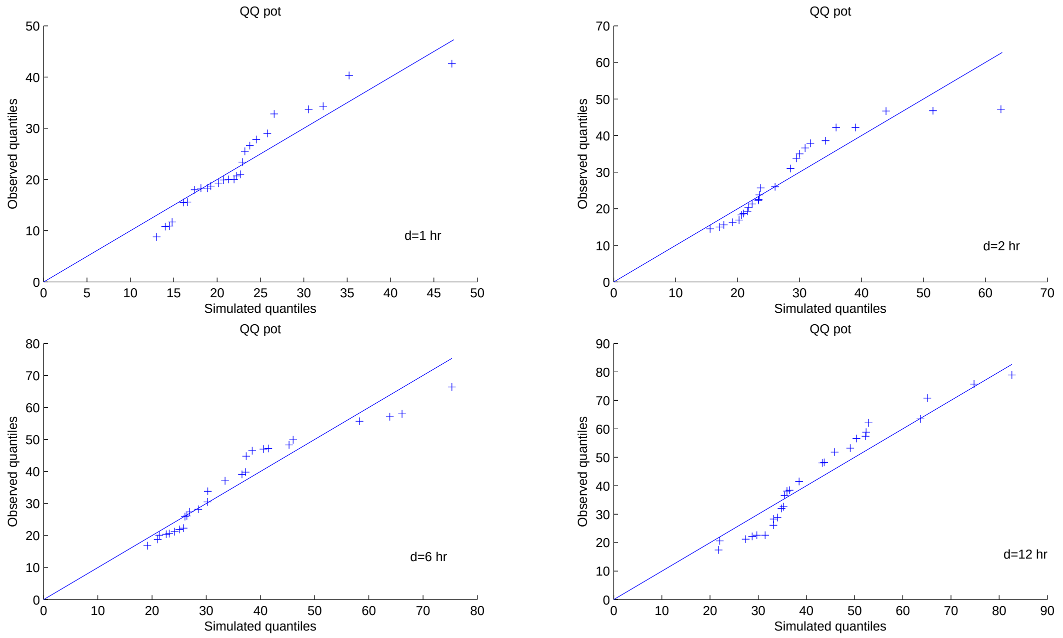

Figure A.3: Quantile-Quantile plot for each duration after correcting the control simulation by the δ-method.

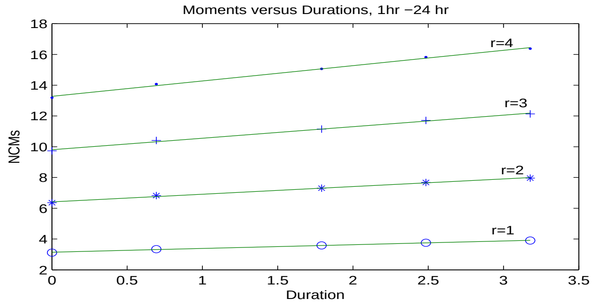

Figure A.4: Moments versus durations for observations.

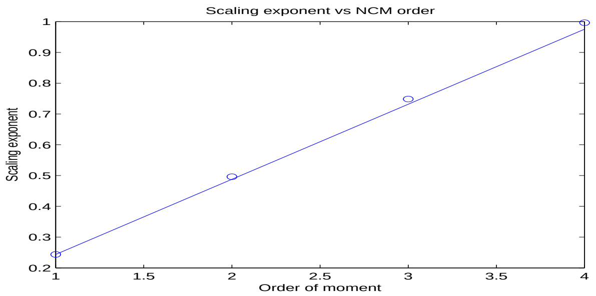

Figure A.5: Scaling exponent versus NCM order for observations.

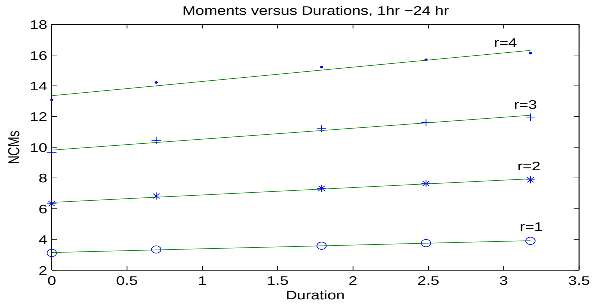

Figure A.6: Moments versus durations for control simulation run.

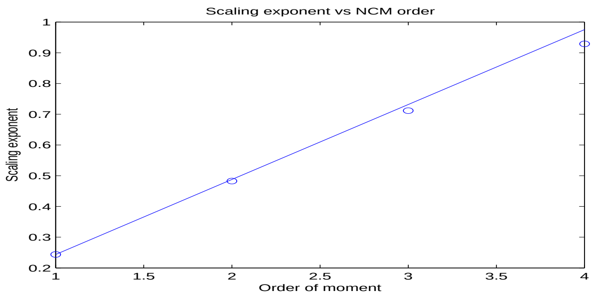

Figure A.7: Scaling exponent versus NCM order for control simulation run.

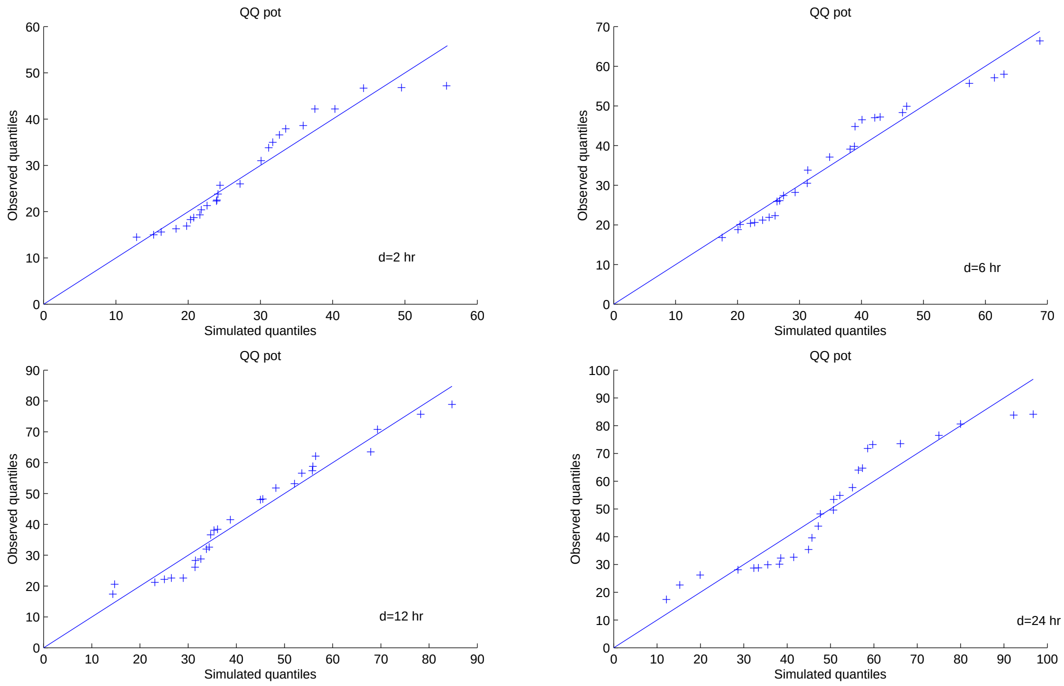

Figure A.8: Quantile-Quantile plot for each duration control climate after mapping the control simulation run by QQ mapping.

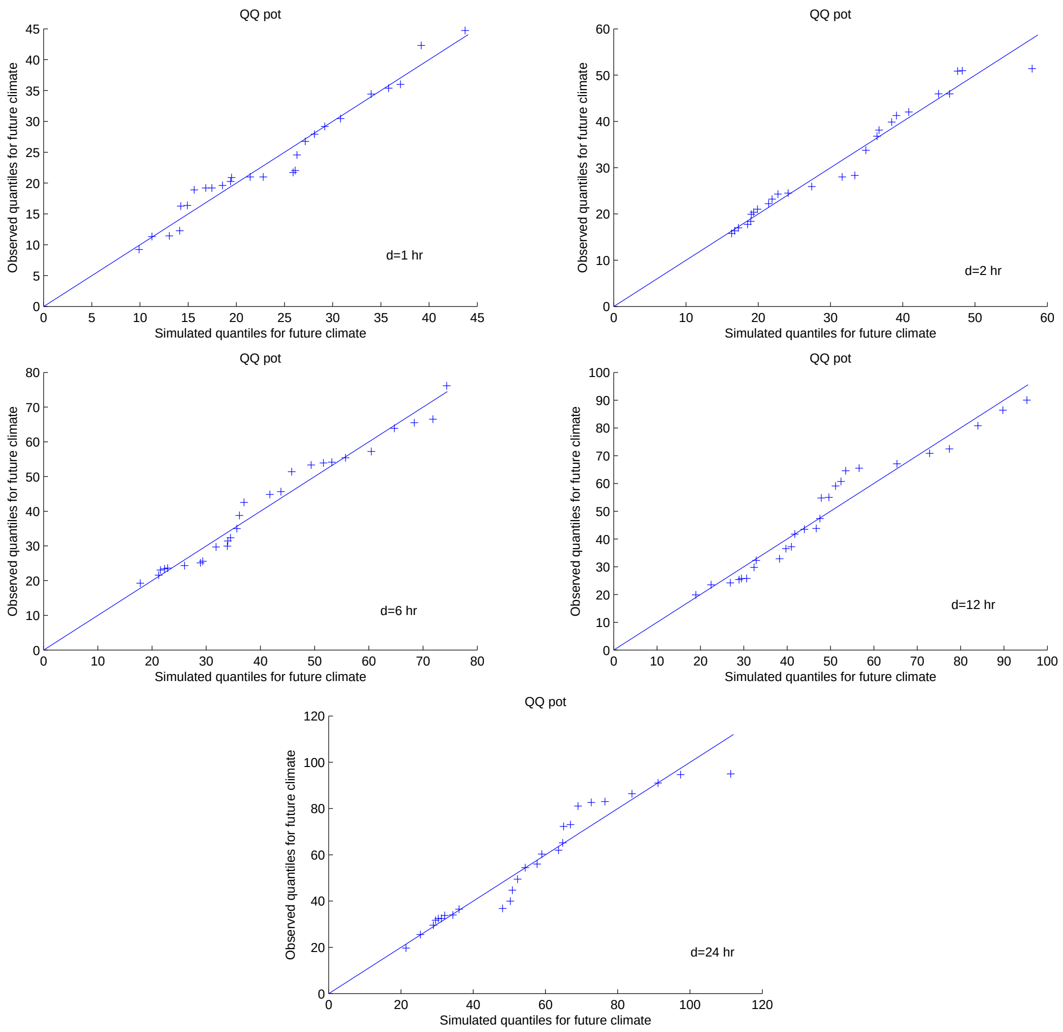

Figure A.9: Quantile-Quantile plot for each duration future climate after mapping the future simulation run based on future observations by QQ mapping. Future observations are determined by multiplying observations by the Δ-factor.

Appendix B

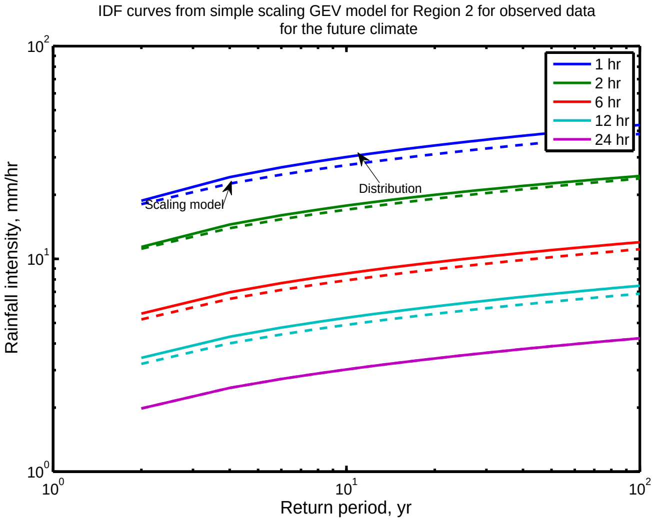

Figure B.1: IDF curves from observed data for the future climate at Region 2.

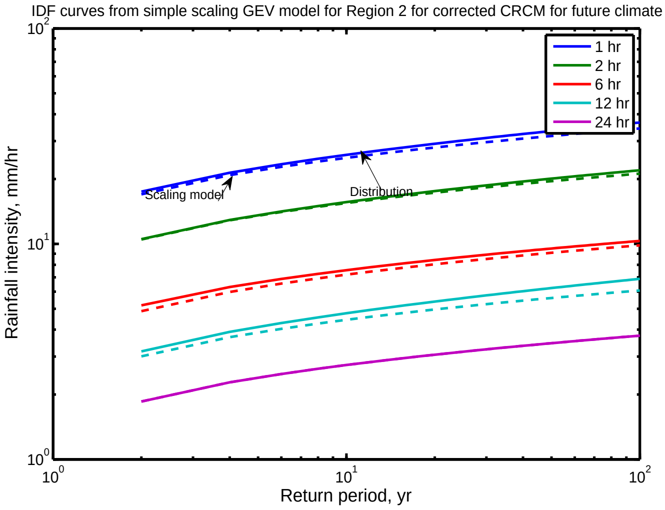

Figure B.2: IDF curves from corrected CRCM data for the future climate at Region 2.

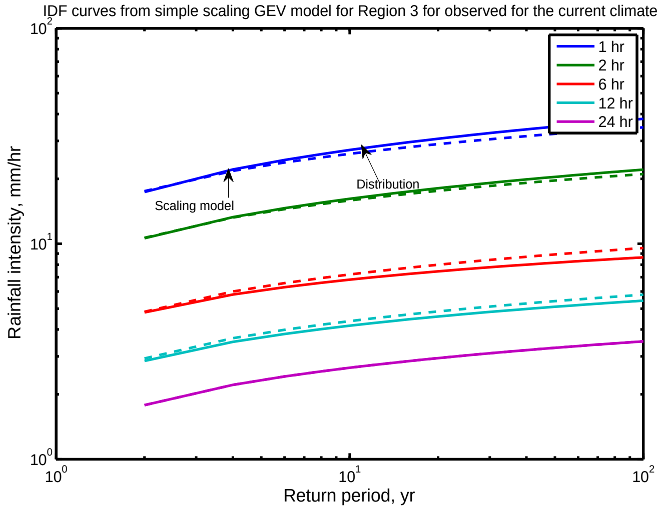

Figure B.3: IDF curves from simple scaling GEV model for observed data for the control climate for Region 3.

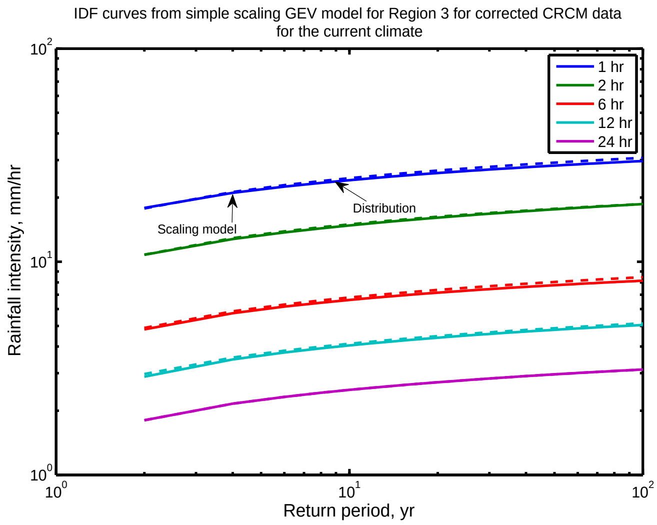

Figure B.4: IDF curves from simple scaling GEV model for corrected CRCM data for the control climate for Region 3.

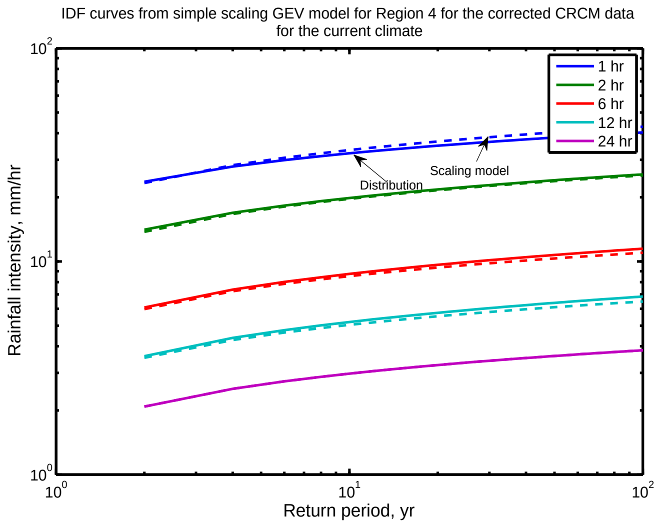

Figure B.5: IDF curves for the corrected CRCM data for Region 4 for the control climate.

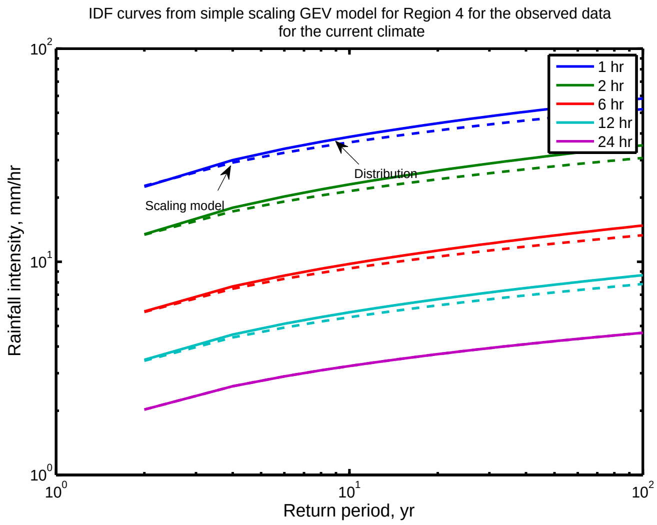

Figure B.6: IDF curves for the observed data for Region 4 for the control climate.

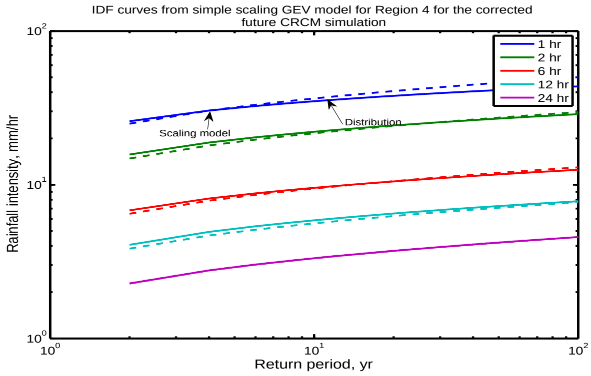

Figure B.7: IDF curves for the corrected CRCM data for Region 4 for the future climate.

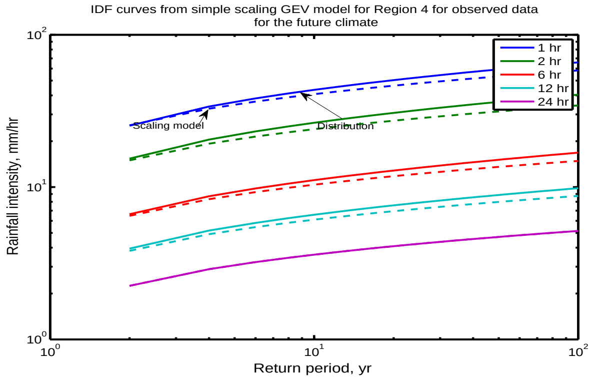

Figure B.8: IDF curves for the observed data for Region 4 for the future climate.

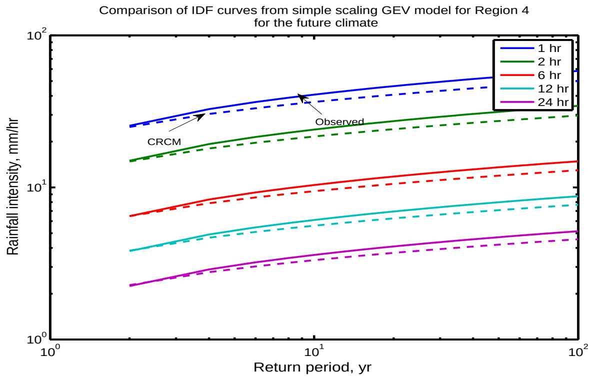

Figure B.9: Comparison of IDF curves for Region 4 for the future climate between observed data and corrected CRCM data.

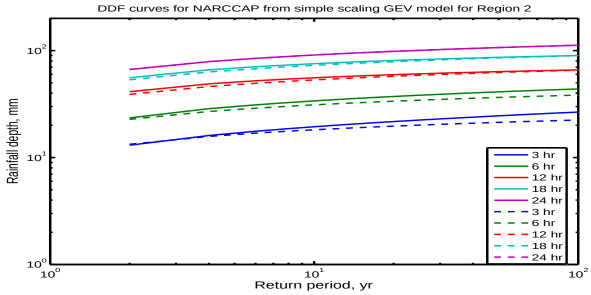

Figure B.10: DDF curves from simple scaling GEV for the CRCM-CCSM for the control climate at Region 2.

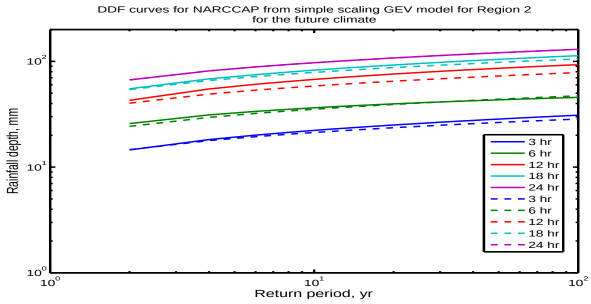

Figure B.11: DDF curves from simple scaling GEV for the CRCM-CCSM for the future climate at Region 2.

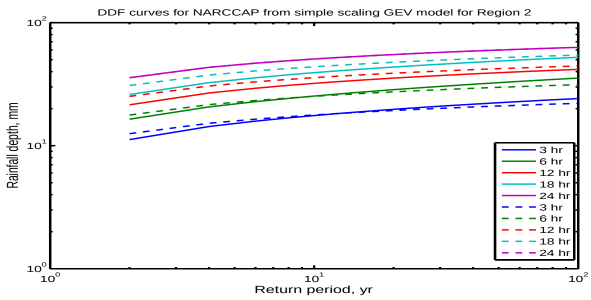

Figure B.12: DDF curves from simple scaling GEV for the MM5I-CCSM for the control climate at Region 2.

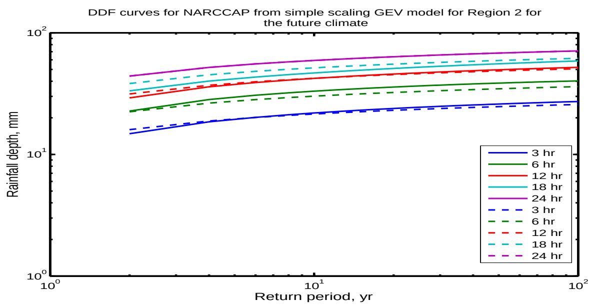

Figure B.13: DDF curves from simple scaling GEV for the MM5I-CCSM for the future climate at Region 2.

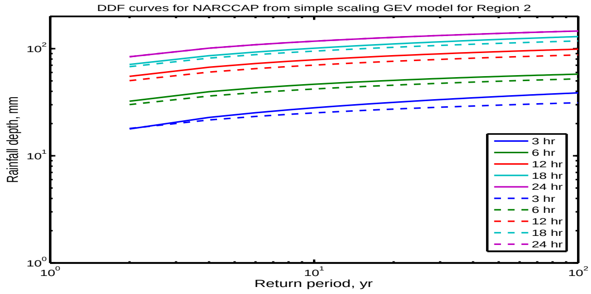

Figure B.14: DDF curves from simple scaling GEV for the HRM3-GFDL for the control climate at Region 2.

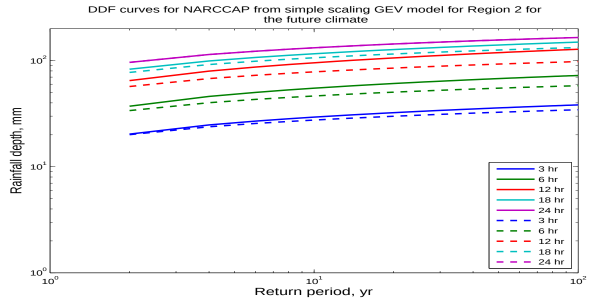

Figure B.15: DDF curves from simple scaling GEV for the HRM3-GFDL for the future climate at Region 2.

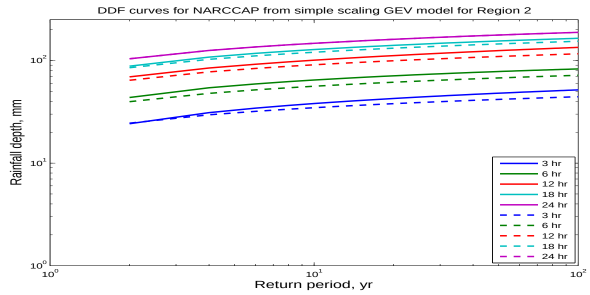

Figure B.16: DDF curves from simple scaling GEV for the HRM3-HADCM3 for the control climate at Region 2.

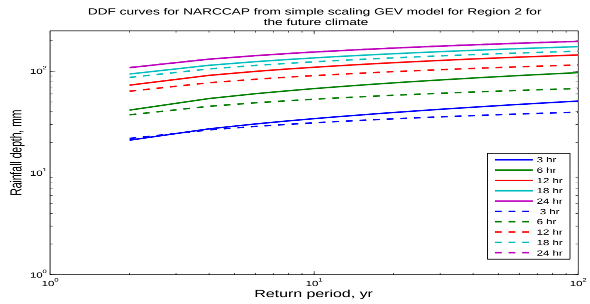

Figure B.17: DDF curves from simple scaling GEV for the HRM3-HADCM3 for the future climate at Region 2.